Title
The localization of magnetite biogenesis proteins in Magnetospirillum magneticum AMB-1

Author
Bickley, Carson Davis

Publication Date
2023

Peer reviewed|Thesis/dissertation

The localization of magnetite biogenesis proteins in *Magnetospirillum magneticum* AMB-1

By

Carson Bickley

A dissertation submitted in partial satisfaction of the

requirements for the degree of

Doctor of Philosophy

in

Microbiology

in the

Graduate Division

of the

University of California, Berkeley

Committee in charge:

Professor Arash Komeili, Chair
Professor Kathleen R. Ryan
Professor Michi E. Taga
Professor Matthew D. Welch

Summer 2023

Abstract

The localization of magnetite shaping proteins in *Magnetospirillum magneticum* AMB-1

by

Carson Bickley

Doctor of Philosophy in Microbiology

University of California, Berkeley

Professor Arash Komeili, Chair

Bacteria make a wide variety of organelles to assist in specific cellular functions (1). How these organelles are assembled is poorly understood. One model for prokaryotic organelle biogenesis is the magnetosome, a lipid-bound compartment that contains a magnetic crystal allowing magnetotactic bacteria (MTB) to navigate along magnetic field lines in their environments (2). To create magnetosomes, MTB localizes many proteins specifically to the developing magnetosome membrane (3,4,5,6,7). How these proteins are sorted is an active area of research. This work explores magnetosome formation and investigates the sorting of a class of magnetosome proteins that are only localized to magnetosomes under magnetite-forming conditions.

The first chapter of this dissertation, an unpublished review article, introduces the topic of magnetosome assembly in magnetotactic bacteria. It explores the selection of *Magnetospirillum magneticum* AMB-1 and *Magnetospirillum gryphiswaldense* MSR-1 as model species for studying magnetosome formation, including early work that created genetic tools enabling molecular characterization. In addition, studies are described that used these tools to identify proteins critical to magnetosome formation. Chapter 1 also describes a working model of magnetosome biogenesis and identifies areas where more research is needed to fill in our understanding of this complex process.

The second chapter of this dissertation, an unpublished primary research article, investigates the localization of magnetite shaping protein Mms6 in AMB-1. Mms6 had previously been shown to localize to magnetosomes after iron is added to iron-starved cells (8). This change in localization suggested that either new Mms6 was produced and targeted to magnetosomes upon addition of iron, or pre-existing Mms6 was able to relocalize after iron addition. Using pulse-chase analysis combined with microscopy, we determine that pre-synthesized Mms6 in the cytoplasm is relocalized to magnetosomes in response to environmental cues. Our findings identify several magnetosome proteins and Mms6 protein domains critical to this dynamic localization behavior.

The third chapter of this dissertation, an unpublished primary research article, identifies another protein, MamD, that is also sorted based on environmental conditions. MamD is a magnetosome protein that has been shown to bind magnetite crystal and inhibit magnetosome membrane growth (9,10). We use fluorescence microscopy to show that MamD, like Mms6, only localizes to magnetosomes when biomineralization of magnetite crystal is possible. In addition, we show

that MamD magnetosome localization requires several of the same magnetosome proteins required for Mms6 localization. Our results suggest that there may be a step in magnetosome assembly where a specific cohort of proteins is conditionally recruited to assist in the nucleation and development of magnetite crystal.

Acknowledgments

Thank you to my thesis committee chair, Professor Arash Komeili, for guidance that was essential during the dissertation process. I would also like to thank the rest of my thesis committee for their assistance and helpful suggestions. This material is based upon work supported by the National Science Foundation Graduate Research Fellowship under Grant No. DGE 1752814. Any opinion, findings, and conclusions or recommendations expressed in this material are those of the authors and do not necessarily reflect the views of the National Science Foundation. Thank you to Dr. Steve Ruzin and Dr. Denise Schichnes of the University of California, Berkeley Biological Imaging Facility for their technical assistance. Research reported in this publication was supported in part by the National Institutes of Health S10 program under award number 1S10OD018136-01. The content is solely the responsibility of the authors and does not necessarily represent the official views of the National Institutes of Health. I also thank the rest of the Komeili lab for their support and advice.

Chapter 1

Development of molecular characterization in model magnetosome-forming bacteria

Carson Bickley and Arash Komeili

Department of Plant and Microbial Biology, University of California, Berkeley, CA, USA

Development of model systems

Magnetotactic bacteria (MTB) were serendipitously discovered in 1975 during an examination of environmental samples from Eel Pond in Woods Hole, Massachusetts (2). During a microscopic examination, Richard Blakemore noticed a morphologically distinct population of bacteria that were uniformly swimming in the same geographic direction. Using a bar magnet, he showed that the swimming behavior of MTB was dependent on alignment to external magnetic fields (2). In the decade and a half following this surprising discovery, MTB were shown to be present in many aquatic environments and to rely on intracellular chains of nanometer-sized magnetic particles for alignment to magnetic fields (11). These features made the study of MTB appealing to a broad range of scientific disciplines ranging from environmental microbiologists to those interested in the biotechnological applications of their magnetic particles (12,13). With this growing interest, it became necessary to examine the assembly of magnetosomes in more detail. However, research into the mechanisms of magnetosome biogenesis was hampered by an incomplete understanding of the underlying genetics. A culturable and genetically tractable MTB model was needed to further explore magnetosome formation.

The first magnetotactic species to be isolated in pure culture was Alphaproteobacterium *Magnetospirillum magnetotacticum* MS-1 (MS-1) (14). Culturing MS-1 allowed for many early characterization experiments, but its use as a model organism was hampered by difficulties growing the organism in lab settings, particularly as colonies on plates. The isolation of Alphaproteobacterial MTB species *Magnetospirillum gryphiswaldense* MSR-1 (MSR-1) and *Magnetospirillum magneticum* AMB-1 (AMB-1) in 1991 provided the field with better candidates for study (15,16). Due to the relative ease of growing these organisms in the laboratory, AMB-1 and MSR-1 became workhorses for molecular characterization of MTB.

Molecular experiments in MTB began in 1988 with magnetosome proteomics. Groundbreaking work by Gorby et al. purified magnetosomes from MS-1 using magnets and found two unidentified proteins unique to the magnetosome fraction at masses of 15 kDa and 33 kDa (17). Later, a study by Okuda et al. examined the proteins present in the MS-1 magnetosome membrane and named three proteins unique to this fraction MAM12, MAM22, and MAM28 (18). MAM22 (also known as MamA) was sequenced and found to contain tetratricopeptide repeat (TPR) domains that are known to mediate protein-protein interactions (18). Up to this point, only a handful of magnetosome proteins had been identified and sequenced. This changed with two groundbreaking studies by Grünberg et al. using MSR-1. The first study, in 2001, identified MamB, MamC, MamD, and MamE as magnetosome proteins and determined the organization of the encoding genes in MSR-1 (4). *mamA, mamB,* and *mamE* were shown to be in the same gene cluster, termed the *mamAB* cluster, whereas *mamC* and *mamD* were organized in a separate cluster (4). Furthermore, versions of the *mamAB* gene cluster were also found in MS-1 and *Magnetococcus marinus* MC-1 (MC-1) (4). Further work by Grünberg et al. showed that MamF, MamG, MamJ, MamM, MamN, MamO, MamQ, MamR, MamS, and MamT were enriched in the magnetosome fraction of MSR-1 (5). A study by Tanaka et al. later found homologs of many of these proteins present in the AMB-1 magnetosome fraction (7). *mamAB* cluster proteins were found even outside of the Alphaproteobacteria, in Deltaproteobacterium *Desulfovibrio magneticus* RS-1 (RS-1) (19). These studies taken together revealed many of the

proteins involved in magnetosome biogenesis and were early indicators of the similarity of magnetosome building blocks across MTB.

In conjunction with proteomic studies, several genetic techniques were adapted to MTB to enable molecular characterization. In 1992, Matsunaga et al. were the first to transfer genes into MTB using the TM5 transposon to insert foreign DNA into the chromosome of AMB-1 (20). In 2003, Schultheiss et al. detailed techniques for electroporation, conjugation, and transpositional insertion of foreign DNA into MSR-1 (21). Another milestone was reached when deletion of an individual MTB gene was performed on *mamA* in AMB-1 using two-step homologous recombination with sucrose selection (22). In *mamA* null mutants, cells made fewer magnetosomes and had a lowered response to magnetic fields, suggesting *mamA* is necessary for normal biomineralization in AMB-1 (22). Schultheiss et al. made a deletion mutant of *flaA*, encoding a subunit that polymerizes to form flagella, in MSR-1 (23). In *flaA* null mutants, cells were unable to make flagella or perform magnetotaxis (23). The development of deletion protocols for MTB genes enabled subsequent reverse genetics studies aimed at determining the function of specific magnetosome genes. To facilitate further study, the genome of AMB-1 was sequenced using whole genome shotgun sequencing (24). The genome was found to have 65.1% GC content and several putative phage insertion regions (24). The MSR-1 genome was sequenced soon after, revealing similar features (25). These sequencing projects provided the groundwork for comparative genomics.

Discovery of MAI genes

Further investigations uncovered the genomic organization of magnetosome genes and their arrangement in operons. The characterization of a spontaneous non-magnetic mutant of MSR-1 revealed an approximately 130kb region encoding many previously identified magnetosome proteins (26,27). This region was shown to rearrange or disappear frequently during stationary growth phase (26, 27). The region was named the magnetosome gene island (MAI) and found to contain multiple pseudogenes, transposons, IS elements, and a different GC content than the rest of the genome. Similarly, the AMB-1 genome was found to contain a 98 kb MAI (28). The AMB-1 MAI is flanked by repeat regions, and recombination of these regions causes the entire MAI to be excised from the genome (28). Magnetosome genes in the MSR-1 MAI are organized transcriptionally into multiple operons, including the *mamAB*, *mamGFDC*, *mamXY*, and *mms6* gene clusters (29) (Fig. 1). Genes from the *mamGFDC*, *mamXY*, and *mms6* clusters appear to be specific to *Alphaproteobacteria* (30,31). However, magnetosome genes from the other clusters have been found in diverse bacterial lineages. Shortly after the discovery of the MAI, a region resembling *mamAB* was found in Deltaproteobacterium RS-1 (30,32). Even magnetotactic bacteria as distantly related from AMB-1 and MSR-1 as *Magnetobacterium bavaricum*, a member of the Nitrospira, were found to have a version of the *mamAB* gene cluster (33). Intriguingly, some key genes from the *mamAB* cluster, including *mamA*, *-B*, *-I*, *-E* (or truncated versions), *-K*, *-M*, *-P* (or *P*-like), and *-Q* have been found in every MTB thoroughly characterized so far, suggesting a common ancestry for magnetosome formation (30,31,34).

One important question is how these conserved magnetosome genes originated and were transferred to disparate MTB species. Given the transferable elements present in the magnetosome gene island, and the tendency of genomic islands to be passed through horizontal

gene transfer (HGT), HGT was accepted as a likely explanation for the widespread nature of magnetosome genes. However, not all characterized MTB have magnetosome genes arranged in a true genomic island. Several bacteria, like AMB-1, MSR-1, and *D. magneticus* RS-1 have magnetosome genes in regions with skewed GC content, IS elements, and other hallmarks of a genomic island (24,25,32). But some species, such as *M. marinus* (35) and *Magnetospira* QH-2 (36) have magnetosome genes clustered together without the features of a genomic island. This may indicate that magnetosome genes have stabilized in these genomes after an ancient acquisition event or that they were inherited vertically. In fact, some evidence that magnetosome genes were passed vertically to many disparate MTB species can be found through comparative genomics. For instance, a study by Lefevre et al. showed that the divergence in 16S rRNA sequences between several MTB in the Alphaproteobacteria, Deltaproteobacteria, Gammaproteobacteria, and Nitrospirae matches the sequence divergence in their Mam proteins (37). This indicates that evolution and drift in 16S and magnetosome genes occurred similarly, suggesting *mamAB* has likely been passed vertically. This finding suggests a common ancestor of Proteobacteria and Nitrospirae was magnetotactic, or that an HGT event occurred soon after the divergence of these lineages. Another possibility is that ancient widespread *mam* genes once served a different function and evolved magnetotactic purpose later. Despite the evidence for genes in most MTB being the subject of vertical transfer, it is likely that magnetosome genes have been horizontally transferred in some cases and are still being transferred today. Kolinko et al. found that non-magnetotactic bacteria can produce magnetosomes when expressing elements of the MSR-1 MAI (38). Transferring the *mamGFDC, mms6, mamAB, mamXY, feoAB1,* and *ftsZm* gene clusters by transposon mutagenesis allowed non-MTB *Rhodospirillum rubrum* to form magnetosomes (38). This intriguing result indicates the viability of horizontal gene transfer into non-magnetic organisms. In addition, this groundbreaking work shows that magnetosome formation could be engineered into other organisms for industrial applications. Further research is needed to determine how magnetosome genes have been transmitted. As more MTB are sequenced, the origin and spread of magnetosome genes may become clearer.

Magnetosome formation

Advancements in MTB molecular genetics enabled deeper study into the mechanisms of magnetosome formation. To assess the roles of individual genes in magnetosome assembly, researchers began to dissect the MAI of AMB-1 and MSR-1. The *mamGFDC* operon, which encodes many of the most abundant magnetosome proteins (4), was deleted in MSR-1 (39). Surprisingly, cells still produced magnetosome membranes and magnetite without this operon, although the crystals produced were smaller (39). Complementation of any combination of genes from the operon partially restored crystal size, but a complementation of the whole operon was needed for full-sized crystal production (39). These results suggest *mamGFDC* genes promote crystal growth. Further exploration of operon function came with groundbreaking work from Murat et al., where large regions were deleted from the AMB-1 MAI (40). Only the *mamAB* operon was found to be essential for magnetosome formation (40). Specifically, AMB-1 requires *mamB, mamI, mamL,* and *mamQ* to form magnetosome membrane compartments and *mamE, mamM, mamN,* and *mamO* to fill magnetosomes with magnetite crystal (40). In addition, *mamP, mamR, mamS,* and *mamT* were linked to crystal maturation (40). Large regions of the MSR-1 MAI were deleted shortly thereafter. As in AMB-1, *mamAB* was found to be critical for magnetosome formation, as smaller, misshapen magnetite crystals were still produced when the

other operons were deleted (41). Further dissection was performed in MSR-1 to determine a minimal gene set necessary for magnetosome biogenesis. Only *mamB, mamL, mamQ, mamO, mamM,* and *mamE* were found to be necessary for the formation of small, weakly magnetic crystals (42,43). Based on the developing understanding of magnetosome gene function, proteins were categorized by their role in magnetosome assembly. These roles were correlated to the several proposed steps of magnetosome biogenesis: magnetosomes invaginate from the inner membrane, invaginations are arranged into chains by cytoskeletal elements, proteins are sorted to magnetosome membranes, and magnetite crystal is grown and shaped (40,43,44) It is unclear what order these steps occur in, and it is possible that many of them happen simultaneously. Although a broad picture of stepwise magnetosome formation had developed, more molecular characterization was required to determine the functions of specific proteins at each step.

Magnetosome assembly requires invagination of the inner membrane, but how this process is coordinated remains unclear. Molecular advancements in AMB-1 and MSR-1 have furthered our understanding of this crucial process. MamB and MamM have homology to cation diffusion facilitator (CDF) proteins, transporters of divalent transition metal cations (4). In a study by Uebe et al., MamB was identified as a protein critical to membrane formation in MSR-1 (45). When MamB was deleted, no magnetosome membranes were formed (45). This deletion had the greatest effect on magnetosome membranes of any tested single gene deletion, suggesting a central role in membrane formation (45,46) Furthermore, MamB was found to be a multifunctional protein with independent roles in membrane formation and biomineralization (47). Point mutants in domains required for MamB transport activity were created that blocked biomineralization but allowed for membrane formation (47). In addition, MamB was found to not require its transport activity to initiate vesicle formation, suggesting that these are separate functions (47). Evidence that MamM may form a heterodimer with MamB indicates it may share a role in membrane formation (45). In MSR-1, MamB was depleted in the absence of MamM, suggesting MamM is needed for MamB stability (45). In addition, null mutants of *mamM* form few, immature magnetosome membranes (43,45). These results demonstrate the importance of MamB and MamM to the first step of magnetosome formation.

Magnetosomes are organized into a chain along the shortest axis of the cell in AMB-1 and MSR-1. During the early history of the field, the mechanisms of creating and organizing magnetosomes were unclear. Scheffel et al. found that *mamJ* is necessary for chain alignment in MSR-1 and suggested that it links magnetosomes to an unknown cytoskeletal scaffold (48). That scaffold was identified by Komeili et al. as MamK, which is necessary for chain alignment in AMB-1 (49). MamK is an actin-like protein conserved in many MTB species (49). In addition, cryo-electron tomography imaging revealed that magnetosomes in AMB-1 invaginate from the inner membrane and stay connected to it as they develop (49). Draper et al. showed that MamK, like some eukaryotic actin proteins, is normally stable but becomes dynamic due to MamJ and LimJ activity (50). Pfeiffer et al. discovered another piece of the cytoskeletal machinery in MSR-1, CcfM, a curvature-inducing coiled-coil protein that may act as a linker between magnetosome organization proteins and other widespread cytoskeletal elements (51). By bacterial two-hybrid assays, CcfM interacts with MreB, MamK, and MamY. It is also necessary for proper cell curvature and the formation of long magnetosome chains (51). An investigation into MamY in MSR-1 revealed it as another critical cytoskeletal element (52). MamY was found to localize along the shortest line through the cell, also known as the geodetic axis. Normally, the

magnetosome chain aligns to the geodetic axis, but in *mamY* null mutants, the MSR-1 magnetosome chain aligns to the opposite axis, the longest path through the cell along the outside edge of a Spirillum. This misalignment causes a drop in the cell magnetic response. Although no direct interactions were found, MamY may work with other cytoskeletal elements like MamK and MamJ to anchor the magnetosome chain to the cell axis best for efficient magnetotaxis. Additional magnetosome-related cytoskeletal components have recently been discovered in AMB-1. In 2022, Wan et al. identified McaA and McaB as critical factors determining the positioning of new magnetosomes and the magnetosome chain (53). McaA localizes as a dashed line in the cell membrane that may regulate the placement of crystal-containing magnetosomes based on unknown interactions involving the magnetosome membrane protein McaB. Together, these results reveal a complex system of cytoskeletal elements that positions magnetosomes within the cell.

Magnetosome membranes contain a set of proteins unique to this cell fraction. How proteins are sorted specifically to magnetosomes has long been unclear. Magnetosome proteins lack a shared signal peptide, suggesting that proteins may be sorted to the magnetosome via protein interactions or other methods (46,54). Many proteins may be localized to the magnetosome during membrane invagination in a process known as protein crowding (8,55). In this model, magnetosome proteins form complexes on the cytoplasmic membrane and the force of their aggregation bends the membrane to form the magnetosome compartment, sorting the proteins to this compartment in the process. In addition, MamA has been theorized to be a landmark that binds several magnetosome proteins due to its structure and interesting localization. The crystal structure of MamA displays open surfaces surrounding TPR motifs (56), structural features associated with protein binding (57). An early study of magnetosome proteomics demonstrated that MamA could be removed from the surface of the magnetosome with an alkaline treatment (58). A fascinating follow-up study by Yamamoto et al. used atomic force microscopy to show a globular protein layer surrounding the cytoplasmic surface of magnetosomes, including the MamA protein (59). Taking these findings together suggests MamA may anchor several proteins to a protein layer on the cytoplasmic surface of the magnetosome membrane. Further research is needed to uncover more factors involved in magnetosome protein recruitment and determine when the sorting step occurs.

To function as a site of biomineralization, magnetosomes must contain a specific ratio of iron ions. Several magnetosome proteins have been identified that may adjust this ratio *in situ* by facilitating redox reactions. Besides its role in membrane formation, MamM may also have a role in biomineralization and redox control. A study of MamM in MSR-1 generated a mutant in which the 50th amino acid, aspartic acid, was replaced with alanine (45). In this mutant, MSR-1 produced crystals made of hematite, a weakly magnetic, oxidized version of magnetite, suggesting deficiencies in redox control (45). Null mutants of *mamX* or *mamZ* were also found to impact crystal synthesis and produce crystals made of hematite in MSR-1 (60). The effect was stronger in double deletions of *mamZ* and its homolog *mamH* (60). The effects of *mamX* and *mamZ* deletions on crystal production were exacerbated when the nitrate reductase gene *nap* was also deleted (60). *nap* is theorized to have an impact on redox control in biomineralization (61), indicating that *mamH*, *mamX* and *mamZ* may be involved in redox control within the magnetosome. Another redox control protein has been identified in the *mamXY* operon. In 2010, a truncated homolog of FtsZ was characterized in MSR-1 (62). Due to the proximity of *ftsZm* to

mamXY genes, it was deleted to determine if it was involved in magnetosome formation or alignment. *ftsZm* null mutants were found to produce smaller magnetite crystals, suggesting a role in biomineralization (62). Further study showed the deletion phenotype disappears in the presence of nitrate, suggesting a possible role in redox control (63). Proteins responsible for redox control have also been identified in AMB-1. Taoka et al. showed that MamP is a membrane-bound cytochrome that enhances magnetite production during exponential growth (64). The amount of MamP increases in the magnetosome relative to MamA and MamK during exponential growth, and overexpressing MamP yields a larger number of magnetite crystals per cell. In addition, mutating the MamP heme c-binding motif results in smaller magnetite crystals during the exponential growth phase, suggesting MamP may work to produce or enlarge crystals during rapid cell growth. A study by Jones et al. supported the role of MamP in redox control and identified MamT as a magnetosome-specific cytochrome also possibly involved in redox control. MamP and MamT both possess magnetochrome domains, double cytochrome-like heme-binding motifs predicted to be involved in controlling the redox state of iron for efficient biomineralization (65). When heme motifs from MamP or MamT magnetochrome domains were deleted, smaller magnetite crystals were produced and cell magnetic response decreased (66).

After magnetite crystals are nucleated, a set of proteins controls their growth and development. Many of which were identified by Arakaki et al. in 2003 (9). Magnetite crystal was extracted from magnetosomes and dissolved using a combination of hydrofluoric acid, SDS, and ultrasonic forces (9). The dissolved solution was enriched for several proteins including MamC, MamD, and Mms6 (9). Therefore, these proteins are thought to bind tightly to magnetite and assist in its maturation. When the *mamGFDC* operon was expressed on a plasmid in WT MSR-1, the diameter of magnetite crystals increased slightly, by 14.7%, suggesting that proteins encoded by these genes enhance crystal size (39). MamD has been shown to inhibit magnetosome membrane growth to facilitate crystal nucleation, suggesting it may have an indirect effect on the size of magnetite (10). Murat et al. identified another magnetosome protein, *mmsF,* as a dominant factor in crystal size and shape control (67). In the absence of the *mamGFDC* and *mms6* operons, AMB-1 forms much smaller crystals, and the magnetic response drops significantly (67). When only *mmsF* was restored to this mutant, crystals were produced that looked almost as large as WT, and the magnetic response was almost entirely recovered (67). These results indicate *mmsF* may have a major role in growing magnetite crystals. While several MAI genes have been linked to enhancing crystal growth, two genes characterized in MSR-1 may inhibit magnetite development. In null mutants of *mms36* or *mms48,* magnetite crystal size increased by 10% or 30% respectively (42). Another protein, Mms6, has been revealed as important to crystal shape. Magnetite is misshapen in *mms6* null mutants (42), and the *mms6* C-terminal domain shapes crystal during magnetite formation *in vitro* (68,69). Mms6 intriguingly has been shown to form protein micelles *in vitro* (70,71), but it is currently unclear whether this behavior affects *in vivo* Mms6 function. Further study of crystal shaping proteins could enable tailoring of magnetic crystals to better serve promising medical and industrial applications.

Molecular investigations of model MTB have enabled a more complete understanding of the complexity of magnetosome assembly. From these many excellent studies, we can construct a hypothetical model of magnetosome formation in AMB-1 and MSR-1 (Fig. 2). These models could productively inform where to direct future research into magnetosome formation in MTB

model organisms. A deeper molecular understanding of magnetosome formation could then enable applications that require modification of magnetosome membranes or magnetite crystals.

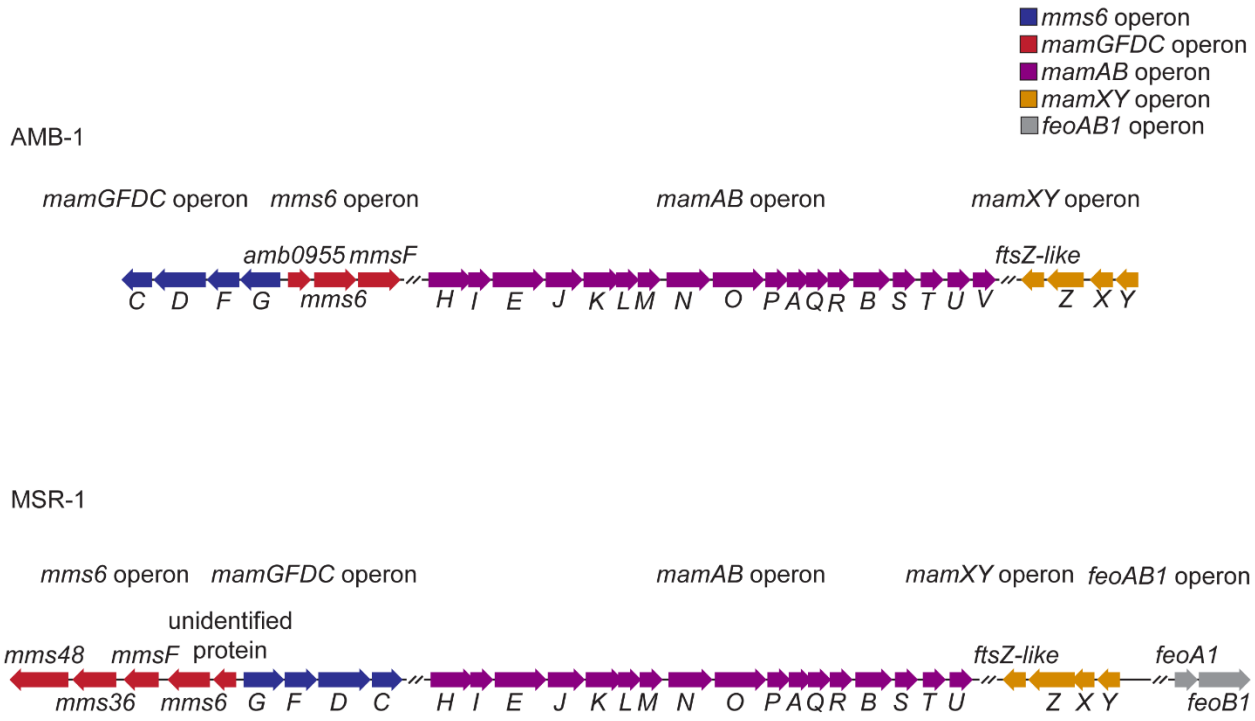

Figure 1. Diagram of magnetosome gene island (MAI) in *Magnetospirillum magneticum* AMB-1 and *Magnetospirillum gryphiswaldense* MSR-1.

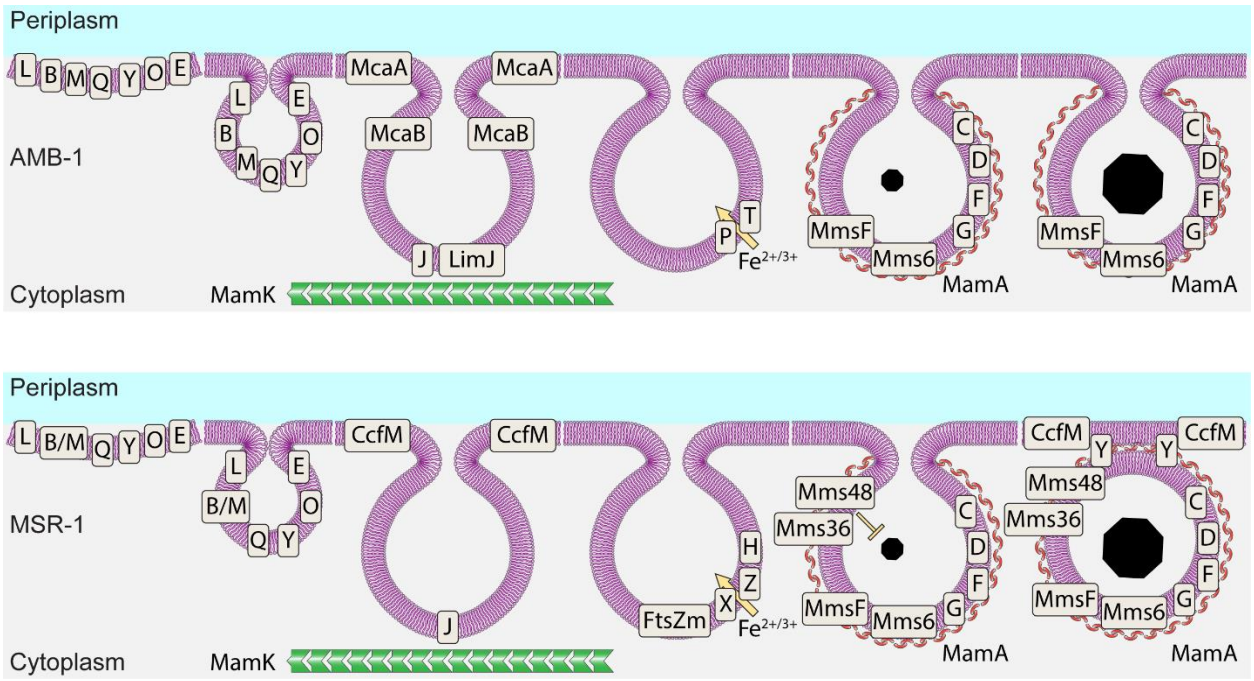

Figure 2. Diagram of magnetosome formation in *Magnetospirillum magneticum* AMB-1 and *Magnetospirillum gryphiswaldense* MSR-1. In AMB-1 and MSR-1, the cellular membrane may be invaginated by the aggregation of magnetosome proteins possibly including MamL, MamB and MamM or a MamB/M dimer, MamQ, MamY, MamO, and MamE. In AMB-1, magnetosomes are positioned along the MamK cytoskeletal filament using at least MamJ and LimJ, and magnetosome spacing is controlled by at least McaA and McaB. In MSR-1, at least MamJ controls orientation along MamK filaments, and CcfM is also involved in positioning. In AMB-1, MamP and MamT are two of the proteins that likely control the redox state of iron inside magnetosomes. In MSR-1, this function is possibly performed by at least MamX, MamZ, MamH, and possibly FtsZm. In AMB-1, the growing magnetite crystal is shaped by MmsF, Mms6, and the MamGFDC proteins, among other likely candidates. These proteins are also likely to shape and enlarge the crystal in MSR-1, while Mms36 and Mms48 may inhibit crystal growth. In MSR-1, magnetosome membranes appear to detach from the cytoplasmic membrane. MamY and CcfM may help position detached membranes. There is still much work to be done to identify the role of each magnetosome protein and to determine whether individual proteins serve the same functions in both bacteria.

Chapter 2

The dynamic localization of magnetosome associated protein Mms6 in *Magnetospirillum magneticum* AMB-1

Carson Bickley and Arash Komeili

Department of Plant and Microbial Biology, University of California, Berkeley, CA, USA

Abstract

Magnetotactic bacteria are a diverse group of bacteria that use intracellular lipid-bounded magnetosome organelles to guide navigation along the geomagnetic field. Construction of magnetosomes in *Magnetospirillum magneticum* AMB-1 and development of the magnetic crystal within require the coordinated action of numerous proteins. Most proteins are thought to localize to magnetosomes during the initial stages of organelle biogenesis regardless of environmental conditions. However, magnetite-shaping protein Mms6 is only found in magnetosomes that contain magnetite, suggesting that it might conditionally localize after the formation of magnetosome membranes. The mechanisms for this unusual mode of localization to magnetosomes are unclear. Here, using pulse-chase labeling, we show that Mms6 translated under non-biomineralization conditions translocates to pre-formed magnetosomes when cells are shifted to biomineralizing conditions. Genes essential for magnetite production, namely *mamE, mamM,* and *mamO* are necessary for Mms6 localization, whereas *mamN* inhibits Mms6 localization. The membrane localization of Mms6 is dependent on a glycine-leucine repeat region, while the N-terminal domain of Mms6 is necessary for retention in the cytosol and impacts conditional localization to magnetosomes. The N-terminal domain is also sufficient to impart conditional magnetosome localization to MmsF, altering its native constitutive magnetosome localization. We therefore propose that Mms6 is kept diffuse in the cytosol by its N-terminal domain and MamN until biomineralization initiates, whereupon it translocates into magnetosome membranes to control the development of growing magnetite crystals. In addition to illuminating an alternative mode of localization to magnetosomes, our findings provide a synthetic route for conditional functionalization of a bacterial organelle.

Introduction

The formation of lipid membrane-bounded organelles in eukaryotes is often a complex task requiring the activity and coordination of many proteins. Several bacteria also create organelles and must localize specific proteins to developing compartments. One of the best-studied bacterial organelles is the magnetosome, produced by magnetotactic bacteria (MTB) (2). MTB are a diverse set of Gram-negative bacteria that synthesize the crystalline magnetic minerals magnetite (Fe_3O_4) or greigite (Fe_3S_4) (37,72,73). The magnetic crystals are produced within a lipid membrane to form a magnetosome, and magnetosomes are aligned into one or more chains across the cell to create a stable magnetic dipole (17,74). MTB may use magnetosome chains to align themselves with the Earth's magnetic field, allowing them to efficiently search for their preferred position in the oxic-anoxic transition zone (2,37).

In the model organisms *Magnetospirillum magneticum* AMB-1 and *Magnetospirillum gryphiswaldense* MSR-1, magnetosome biogenesis is performed mainly by proteins encoded by the magnetosome gene island (MAI) (26). Magnetosome genes identified in the MAI are organized into four clusters (*mamAB, mamGFDC, mamXY,* and *mms6*) which are necessary and sufficient for magnetosome formation (38). Many MAI proteins localize specifically to magnetosome membranes and are depleted in other cellular membranes (3,4,5,6,7). Little is

known about how proteins are sorted to magnetosomes – magnetosome proteins lack a universal signal peptide (46,54) – but it is thought that they may aggregate on the inner membrane at magnetosome development sites in the early stages of magnetosome membrane invagination (8,54). Aggregated proteins would therefore be concentrated into magnetosome membranes as compartments form.

In contrast, some evidence suggests the approximately 14 kDa protein Mms6 may localize to magnetosomes after membrane formation is complete (8). Mms6 was originally isolated in a proteomic study looking for proteins tightly bound to magnetite crystals of magnetosomes. *In vitro* magnetite synthesis done in the presence of the 6 kDa Mms6 peptide (9, 68), and even with just the acidic C-terminal region (68,69) results in cubo-octahedral crystals, like those produced *in vivo* by some magnetotactic bacteria, suggesting that this region shapes developing crystals. Mutations in *mms6* result in the formation of smaller, misshapen crystals, further indicating a role in magnetite crystal shaping (42,67,68). Consistent with the presence of a transmembrane region, Mms6 has been identified in enriched magnetosome membranes (7). The Mms6 N-terminus is thought to either associate with the magnetosome membrane surface or translocate through the membrane, while the C-terminal region contacts the magnetite (75). Magnetite-binding activity has been suggested to be necessary for Mms6 localization (76). A study by Arakaki et al. in AMB-1 used correlated transmission electron microscopy and fluorescence microscopy to show that Mms6 only localizes to magnetosome membranes that contain magnetite (8). When AMB-1 is grown under oxic conditions that do not permit biomineralization, Mms6-GFP localizes diffusely throughout the cell, although whether Mms6-GFP localized either in the inner membrane or cytoplasm was unclear (8). Furthermore, when conditions are changed to permit biomineralization, Mms6 is localized to magnetosome membranes in as few as 2 h (8).

While previous work has determined an unusual localization mode for Mms6, the dynamics of the process, as well as the extrinsic and intrinsic molecular factors governing it, have remained obscure. Therefore, we combined pulse-chase analyses, imaging, and genetic analyses to define the process of Mms6 localization at a molecular level. We show that upon a shift into biomineralization-permissible conditions (BPC), pre-translated Mms6 relocalizes from the cytosol to pre-formed magnetosome membranes, displaying a surprising localization behavior for a protein containing a transmembrane domain. We also identify three genes, *mamE, mamO,* and *mamM*, that are necessary for Mms6 localization. In contrast, *mamN* is implicated in inhibiting Mms6 localization to empty magnetosomes. The N-terminal domain of Mms6 is necessary for retention in the cytosol and can impart conditional localization on a heterologous magnetosome protein. We speculate that AMB-1 responds to BPC by sorting pre-folded Mms6 to magnetosome membranes to help shape the developing crystal, exhibiting a more dynamic and complex strategy of regulating biomineralization than previously hypothesized. Exploiting this strategy in synthetic applications could allow fine-tuning of biocompatible magnetic nanoparticles, which have wide ranging applications including targeted drug delivery (77), MRI contrast enhancement (78), and magnetic hyperthermia therapy (79).

Results

Pre-translated Mms6 relocalizes to pre-existing magnetosomes when biomineralization begins

Mms6-GFP was shown to localize to magnetosome membranes only when conditions favor biomineralization (8). Understanding the dynamics of this process could provide insights into both the mechanism of relocalization and its importance to cells. Previously, Mms6-GFP was imaged after biomineralization was induced in one of two ways, either by moving cells grown under microaerobic conditions to anaerobic conditions, or by adding iron to iron-starved cells (8). Images taken 2 h after iron addition or 8 h following growth in anaerobic conditions revealed that Mms6-GFP had localized to magnetosomes (8). To replicate these results, cells were first grown in iron starvation conditions. Iron was added to cultures to induce biomineralization, and the localization patterns of Mms6-GFP in live cells was grouped into three categories: “Foci”, indicating cells with one or more unaligned fluorescent foci, “Diffuse”, indicating protein diffuse in the cytoplasm, and “Chain”, indicating linear fluorescent patterns representing protein aligned to the magnetosome chain. Mms6-GFP was primarily diffuse in the cytosol in cells grown without added iron (Fig. 1A,B). In line with previous results, Mms6-GFP was localized to magnetosome chains in most cells 1-2 h post induction (Fig. 1A,B).

The change in Mms6-GFP location after iron addition could be the result of two different phenomena. In one model, Mms6 newly synthesized in biomineralization-permissible conditions (BPC) localizes to magnetosomes, while pre-existing Mms6 is diluted by growth and protein turnover. Alternatively, pre-existing Mms6 synthesized under non-biomineralization permissible conditions (NBPC) may relocalize to magnetosomes upon a change in conditions. To differentiate between these possibilities, we used the HaloTag protein fusion tag, which covalently and irreversibly binds to fluorescent ligands, allowing the tracking of a specific protein pool (80). Mms6-Halo expressed in a *Δmms6* background partially restored the cellular magnetic response, assayed by determining the Coefficient of magnetism (Cmag), a measurement dependent on the differential scattering of light by cells moved into different orientations by an external magnetic field (Fig. 1C).

Using HaloTag, we tracked a pool of Mms6-Halo synthesized before iron was added to non-biomineralizing cells. To determine if the old pool of Mms6-Halo relocalized to magnetosomes or if new protein synthesis was necessary, we performed a pulse-chase experiment. Briefly, AMB-1 cultures grown and passaged under iron starvation conditions were labeled. Then, biomineralization was induced in some samples and samples were grown for several hours. To ensure that a representative sample of cells was tracked during the pulse-chase experiment, the percentage of cells containing fluorescent protein was calculated throughout the experiment. The percentage of cells containing fluorescent protein decreased only slightly, from 73% to 68% over 2 h of incubation, suggesting that similar representative samples were captured at each timepoint (Fig. 1D). One confounding factor with the pulse chase experiment could be incomplete saturation of HaloTag with fluorescent ligand. To measure label saturation of HaloTag, cells from 10 ml cultures were incubated with a pulse ligand for 1 h, washed, supplemented with bacteriostatic antibiotics (700 μg/ml kanamycin and 400 μg/ml chloramphenicol) to prevent new

protein synthesis, incubated for 30 min, and finally incubated with a chase ligand containing a different fluorophore for 1 h. Without antibiotic treatment, similar percentages of cells were labelled with the pulse (82%) and chase (73%) ligands. When treated with antibiotics, 84% of cells were labeled with the pulse ligand, whereas only 27% were labeled with chase ligand, indicating that the pulse ligand conditions saturates most Mms6-Halo proteins (Fig. 1E). Culture growth and magnetic response were tracked during the time course. Cell growth measured by OD_{400} increased steadily after iron addition (black arrow) from an average of .050 to .188 9 h later, showing that cells remained healthy during the experiment (Fig. 1F). Cmag increased steadily after addition of iron from a starting non-magnetic Cmag of 1.0 and reaching a magnetic Cmag of 1.5 6 h after iron addition (Fig. 1G). Before induction of biomineralization, Mms6-Halo localized diffusely in the cytoplasm in the majority of cells (Fig. 1H,I). In contrast, 2 h after iron addition, the old pool of Mms6-Halo had relocalized to the magnetosome chain in most cells (Fig. 1H,I). These results indicate that Mms6-Halo synthesized under NBPC can relocalize to magnetosomes.

To confirm that Mms6-Halo relocalization does not require new protein synthesis, the pulse chase experiment was repeated with bacteriostatic antibiotics to prevent protein synthesis (Fig. 2A,B). 700 µg/ml kanamycin and 400 µg/ml chloramphenicol were added simultaneously (white arrow) to half of the cultures 1 h before iron addition (black arrow). The antibiotics slowed cell growth and stopped biomineralization, suggesting they prevented new protein synthesis (Fig. 2A,B). The percentage of cells containing fluorescent protein increased slightly, from 74% to 80%, over 2 h of incubation without antibiotics, and from 74% to 86% with antibiotics, suggesting that similar representative samples were captured at each timepoint (Supplementary Fig. S1). Despite the effects of the antibiotics, Mms6-Halo still relocalized to the magnetosome chain (Fig. 2C,D), confirming that no new protein synthesis is needed for Mms6 localization. Similarly, in samples that did not receive antibiotics, most cells also had chain-aligned patterns of Mms6-Halo 2 h after iron addition, indicating that the pre-synthesized Mms6-Halo had relocalized to the magnetosome chain. Example images of cells captured using super resolution structured illumination microscopy are provided in Supplementary Figure S2. The timing of relocalization and the patterns observed are most consistent with relocalization to pre-existing chains rather than relocalization exclusively via new magnetosome synthesis (see Discussion). Thus, these results indicate that cytoplasmic Mms6 can relocalize to pre-existing magnetosomes when biomineralization conditions change, revealing a surprising mode of magnetosome protein localization in AMB-1.

MAI proteins are necessary for Mms6 magnetosome localization

Despite Mms6 being a magnetosome-associated protein with a predicted transmembrane domain, its localization in the absence of magnetite formation is strikingly different from other magnetosome-associated proteins (8). Therefore, we tested whether Mms6 localization is an inherent feature of the protein or requires other magnetosome proteins. In the absence of genes essential to magnetosome formation, many magnetosome-associated proteins are dispersed throughout the cytoplasmic membrane (40). The localization patterns of Mms6-GFP and

magnetosome membrane protein GFP-MmsF were examined in mutant cells lacking the MAI and a region outside the MAI that also affects magnetosome positioning, called the magnetosome gene islet (MIS) (81). The MAI and MIS contain the majority of known magnetosome proteins in AMB-1, and cells that lack the MAI and MIS are unable to form magnetosome membranes. As expected, GFP-MmsF highlights the cell periphery in this mutant, consistent with localization to the inner cell membrane. In contrast, Mms6-GFP (Fig. 3A,B) has a cytosolic localization in ΔMAI ΔMIS cells, even in BPC. Similarly, Mms6-Halo localizes to the cytosol in ΔMAI cells, which are also unable to form magnetosome membranes (Fig. 4A,B). Therefore, Mms6 association with membranes requires either other magnetosome proteins or a previously formed magnetosome membrane.

To identify MAI proteins involved in Mms6 translocation to magnetosome membranes, Mms6-Halo was expressed in strains deleted for specific MAI genes. Given Mms6 only localizes to magnetosomes that contain magnetite (8), we first focused on four strains in which magnetite synthesis is completely disrupted, Δ*mamO*, Δ*mamM*, Δ*mamE, and* Δ*mamN* (40). As expected, when *mamO*, *mamM*, or *mamE* is deleted, Mms6-Halo only appears in the cytosol, suggesting that either Mms6 is not localizing to magnetosomes because they lack a mineral or that MamM, MamO, and MamE are more directly involved in Mms6 localization (Fig. 4A,B). Unexpectedly, when another protein essential for magnetite synthesis, MamN, is absent, Mms6-Halo localizes to magnetosome membranes regardless of biomineralization conditions and despite the absence of crystal production (Fig. 4A,B). This surprising exception may indicate that MamN inhibits Mms6 localization until biomineralization begins. Additionally, it demonstrates that the presence of magnetite is not necessary for Mms6 localization. A previous study by Nguyen et al. found that Mms6 interacts with MamA (82). Therefore, we examined the localization of Mms6-Halo in a *mamA* deletion mutant. Mms6-Halo localized the same in the Δ*mamA* and WT strains under NBPC. While there is a significant difference between WT and Δ*mamA* cells in the categorical distribution of Mms6-Halo localization under BPC, the effect size is small and the majority of Δ*mamA* cells still show Mms6-Halo aligned to magnetosome chains. These data taken together indicate that *mamA* is not strictly required for Mms6 localization to magnetosomes (Fig. 4A,B). However, it is still possible that MamA is recruited by Mms6, or that the two proteins interact for a purpose other than localization. Due to its genomic proximity to *mms6*, *mmsF* was also tested. We examined the localization of Mms6-Halo in a strain lacking the *mms6* gene cluster, containing *mms6, mmsF,* and uncharacterized protein *amb0955.* Under NBPC, significantly more *mms6* cluster mutant cells have Mms6-Halo localized to the magnetosome chain, but most cells still have diffuse Mms6-Halo (Fig. 4A,B). Under BPC, Mms6-Halo localizes normally, suggesting that other *mms6* cluster proteins are not needed for *mms6* localization to magnetosomes, but could have a small positive effect on Mms6 cytosolic localization. Additionally, it is possible that *mmsF* homologs *amb0956* and/or *amb1013* could serve a redundant function for *mmsF* and mask the effect of its deletion (67). Examples of localization patterns in the above backgrounds imaged with super resolution microscopy are provided in Supplementary Figure S2.

Other deletions that caused at most minor changes in Mms6 localization are shown in Supplementary Figure S3. Some of these small changes may be explained by biological variance

and may register as significant due to increased sensitivity of chi-squared and fisher's exact tests at higher sample sizes. A deletion of AMB-1 MAI region 3, consisting of the *mamGFDC* operon and the *mms6* cluster, resulted in a small but significant increase in Mms6-Halo localized in foci under NBPC, while Mms6-Halo still localized to magnetosomes in most cells grown under BPC. In a deletion of the *mamGFDC* operon comprising *mamG, mamF*, *mamD*, and *mamC*, Mms6-Halo had a significant, slight increase in chain alignment under NBPC, while Mms6-Halo localization was unchanged in BPC. In a strain lacking MamJ and LimJ, genes that regulate the function of cytoskeletal filament MamK (48,50), Mms6-Halo localized normally under NBPC and had significant but small increases in chain alignment and foci localization under BPC compared to WT cells. In a deletion of *mamK,* Mms6-Halo localized as in WT, except for a small, significant increase in foci localization in NBPC. Since MamK, MamJ, and LimJ regulate magnetosome chain organization, the changes observed may be due to variations in chain architecture. In a deletion of *mamD,* Mms6-Halo showed a small, significant increase in foci localization in NBPC and a small, significant increase in diffuse localization in BPC. Finally, in a deletion of *mamP*, Mms6-Halo showed a small, significant increase in foci localization in BPC. In addition to the ΔMAI ΔMIS mutant (Fig. 3), the localization of Mms6-GFP was examined in two other mutants deficient in magnetosome membrane formation, Δ*mamI* and Δ*mamL* (Supplementary Figure S4A,B). As expected, Mms6-GFP was diffuse in these mutants regardless of biomineralization condition.

Defining intrinsic determinants of Mms6 localization

After identifying other MAI proteins that affect Mms6 localization, we looked for Mms6 domains that contribute to localization. Mms6 can be roughly divided into four protein domains: the N-terminal domain (NTD), glycine-leucine repeat segment (GL), transmembrane domain (TM), and the magnetite-interacting component (MIC) (Fig. 5A). The N-terminal domain is a 98 amino acid region that was not identified when Mms6 was originally discovered in magnetite digests (9). Thus, the NTD may be cleaved from Mms6 during or after localization to the magnetosome membrane. The GL repeat domain consists primarily of alternating glycine and leucine residues and is a defining feature of silk fibroin that may mediate protein-protein interactions (83). An approximately 23 amino acid transmembrane domain (TM) is predicted to begin in the middle of the GL repeat domain (7). Consistent with the presence of a transmembrane region, Mms6 has been identified in enriched magnetosome membranes (7). The MIC is a region of acidic amino acids that binds ferrous iron (68,84), ferric iron (9,70,85), magnetite crystal (86,87), and other minerals (9). The MIC has been implicated in iron crystal nucleation (9,68) and protein localization of Mms6 (76). To test the effect of Mms6 domains on its dynamic localization, truncated Mms6 proteins were expressed in a Δ*mms6* background. Because Mms6 only localizes to magnetosomes that contain magnetite, it seemed likely that the MIC would contribute to localization (8). Unexpectedly, the MIC was dispensable for normal Cmag (Fig. 5B). Under NBPC, $Mms6_{1\text{-}139}$-GFP, lacking the MIC, localizes to the cytoplasm like Mms6-GFP. Surprisingly, in the majority of cells $Mms6_{1\text{-}139}$-GFP localizes to magnetosomes

under BPC (Fig. 5C,D), except for a small but significant increase in diffuse localization, suggesting that magnetite-binding activity is not necessary for Mms6 localization.

After finding that the MIC is dispensable for magnetosome localization, we made further truncations of Mms6. One truncation, Mms6$_{107-157}$-GFP consists of the GL repeat region, the transmembrane region, and the MIC. Under BPC, this variant localizes to magnetosome membranes in most cells, with small but significant increases in diffuse and membrane localization compared to full length Mms6-GFP. Under NBPC, where the full length Mms6-GFP is cytoplasmic, Mms6$_{107-157}$-GFP localizes to the cellular membrane (Fig. 5C,D) (Supplementary Figure S5). In contrast, Mms6$_{113-157}$-GFP, which consists of the TM region and MIC, is diffuse in all conditions (Fig. 5C,D), suggesting it is unable to translocate to the membrane or localize to magnetosomes. These results indicate that a factor within the GL repeat region may be necessary for Mms6 membrane localization. A mutant Mms6$_{107-135}$-GFP was made to test if Mms6 localization was possible with only the GL and TM domains, but no GFP signal was seen, likely due to protein instability or protease activity.

Next, we investigated a segment of Mms6 thought to be cleaved from the mature protein. Mms6 was originally discovered in an experiment by Arakaki et al. that dissolved the magnetite crystal and analyzed proteins in the resulting solution. The solution contained a 6 kDa peptide of Mms6, but the gene codes for a larger protein of 12-15kDa (5,9). Both the 6 kDa and 14.5 kDa Mms6 proteins exist in the cell (4). The shorter form of the protein lacks the 99 amino acid N-terminal domain (NTD), which may be cleaved from the mature protein by MamE protease activity (9,10). Previous work by Arakaki et al. found that without the NTD, Mms6 localized diffusely in either the cytoplasm or cellular membrane (8). However, it could not be determined whether Mms6-GFP localized in either the cytoplasm or inner membrane (8). To investigate the effect of the Mms6 NTD on localization, several mutants of Mms6 were expressed. Under NBPC, Mms6$_{99-157}$-GFP appears in the cell membrane instead of the cytosol (Fig. 5C,D). Under BPC, Mms6$_{99-157}$-GFP localizes both to magnetosome chains and to the cell membrane. These localization differences may indicate that the NTD keeps Mms6 diffuse in the cytosol, possibly to prevent it from translocating into membranes before the initiation of magnetite biomineralization. When Mms6$_{99-157}$-Halo is expressed in ΔMAI mutants that lack most magnetosome proteins and are unable to make magnetosome membranes, Mms6$_{99-157}$ localizes to the cellular membrane (Supplementary Fig. S6). This result suggests that Mms6$_{99-157}$, unlike Mms6, does not require other magnetosome proteins or pre-formed magnetosome membranes to associate with membranes. When only the N-terminal domain is expressed, Mms6$_{1-98}$-GFP localizes to the cytosol regardless of biomineralization condition (Fig. 5C,D). To further investigate the NTD, we created Mms6$_{51-157}$-GFP, in which the N-terminal half of the NTD is absent. Interestingly, Mms6$_{51-157}$-GFP localized to magnetosome membranes under both BPC and NBPC (Fig. 5C,D), suggesting that the NTD may also be involved in the conditional localization of Mms6. Super resolution images of example cells expressing the Mms6 mutants discussed above are shown in Supplementary Figure 6.

To test the effect of *mms6* domain fusions with other magnetosome proteins, the N-terminal domain was fused to the N-terminus of *mmsF.* Wild-type MmsF tagged N-terminally with GFP

localizes to magnetosome chains regardless of biomineralization conditions (Fig. 6). Surprisingly, the GFP-Mms6$_{NTD}$MmsF fusion protein localizes to magnetosomes only in BPC, similar to Mms6. Under NBPC, GFP-Mms6$_{NTD}$MmsF localizes to the cellular membrane (Fig. 6). Therefore, the Mms6 N-terminal domain is both necessary and sufficient for conditional localization in magnetosome proteins. Interestingly, under NBPC, the fusion protein appears localized to the cell inner membrane, suggesting that the Mms6 NTD prevents magnetosome localization of MmsF but not its membrane translocation. This may indicate that the Mms6 NTD has two separate functions - keeping proteins cytosolic, and controlling conditional localization - and that perhaps the NTD is only able to maintain Mms6 in a cytosolic location in concert with other structural features of Mms6. These results show that the Mms6 NTD has an important role in regulating localization that is transferrable to other magnetosome proteins, opening future possibilities for modifying magnetosome protein localization.

Biochemical fractionation of AMB-1 to determine Mms6 localization

Due to the contrast between the existence of a transmembrane domain in Mms6 and its cytosolic location under NBPC, we sought to validate microscopic observations of Mms6 using biochemical subcellular fractionation. Briefly, AMB-1 cells were lysed, and ultracentrifugation was used to separate soluble and insoluble cellular contents. Known magnetosome membrane protein MamE was used as an insoluble fraction marker (4). Unfused monomeric HaloTag has a cytoplasmic localization and was used as a soluble fraction marker. Based on the cytosolic pattern of Mms6-Halo in most cells under NBPC, it was expected that Mms6-Halo would appear in the soluble fraction. Surprisingly, Mms6-Halo was only found in the insoluble fraction (Supplementary Fig. S7).

A variety of factors could cause Mms6-Halo to co-fractionate with insoluble proteins, despite having a cytoplasmic location. Mms6 phase separates *in vitro* and forms protein micelles (70,71). Therefore, we attempted to prevent the formation of protein micelles using several conditions, including the addition of 100 ng/mL 1,6-Hexanediol (Spectrum Chemicals Cat #H52023-500GM), which inhibits phase separation in some systems (88,89), the addition of 100 mM KCl, the elimination of salt from the buffer, and 2 10 s rounds of sonication to disperse protein complexes. No condition tested had a noticeable effect on the subcellular fractionation of Mms6-Halo, except for the mild non-ionic detergent Igepal CA-630 (NP-40 substitute). Cellular fractionation performed with Igepal resulted in the solubilization of Mms6-Halo, whereas magnetosome membrane protein MamE was still present primarily in the insoluble fraction (Supplementary Fig. S7). However, Mms6-Halo was also soluble in cells grown in BPC where it was expected to be inside the magnetosome lumen (Supplementary Fig. S7). The greater solubility of Mms6 compared to MamE may suggest that Mms6 is weakly associated with magnetosome membranes or that Mms6 is only surface associated. Together, our results reveal the complexity of magnetosome protein sorting as well as raise new questions about magnetosome protein modification and membrane topology.

Discussion

A previous study suggested that Mms6 may relocalize as cellular conditions change (8). However, it did not distinguish between the relocalization of existing Mms6 and the initial targeting of Mms6 that is newly synthesized after biomineralization begins. By using irreversibly bound HaloTag ligands, we showed that Mms6 made under NBPC relocalizes within 1-2 h from the cytosol to magnetosome membranes. Although the time course showed that pre-existing Mms6 can relocalize, whether Mms6 could relocalize to pre-formed magnetosomes was still unclear. After induction of biomineralization, either Mms6 relocalized to the pre-existing magnetosome chain, or a new chain of magnetosomes was synthesized that included the Mms6-Halo proteins. Previous work by Cornejo et al. used a strain with inducible MamQ to observe the formation of magnetosome membranes (90). Before induction, the cells lacked sufficient MamQ to form magnetosomes. After induction, a chain of new magnetosomes was formed in 6 h (90). Based on this timescale, it is unlikely that a complete chain of new magnetosomes could be formed in the 2 h needed for Mms6 to relocalize. Therefore, the presence of complete chains of Mms6-Halo 2 h after induction suggests that Mms6 can relocalize to pre-existing magnetosomes. In addition, if Mms6 localized only to newly formed magnetosomes within an existing chain, we would expect an intermediate phase of Mms6 relocalization where Mms6 is primarily localized to foci within the cells, representing localization to the first new magnetosomes formed. The absence of this step suggests the Mms6 pool can relocalize to all crystal-containing magnetosomes in the chain at once. These results taken together indicate that cytoplasmic Mms6 can relocalize to pre-existing magnetosomes when biomineralization conditions change, revealing a surprising mode of magnetosome transmembrane protein localization in AMB-1.

We found that several genes required for magnetite synthesis, namely *mamE, mamM, mamN,* and *mamO,* are also essential for conditional localization of Mms6 to magnetosomes. In contrast, in the absence of the magnetite synthesis gene, *mamN,* Mms6 localizes to magnetosomes under all conditions. We hypothesize that MamN, either directly or indirectly, inhibits Mms6 localization under NBPC. In this mutant, magnetosome membranes form but there are no detectable magnetite particles. Therefore, the physical presence of a magnetic crystal is not required for Mms6 localization. The absence of *mamE, mamM,* or *mamO* also leads to the formation of empty magnetosome membranes. MamE and MamO are involved in a previously characterized biomineralization-dependent checkpoint in AMB-1 that prevents a second stage of magnetosome membrane growth until magnetite nucleation has commenced (90). Mms6 was shown not to be necessary to pass the membrane growth checkpoint. It is possible that checkpoint proteins such as MamE and MamO could recruit Mms6 and other magnetite shaping and nucleating proteins after membranes pass the growth checkpoint. Further work on Mms6 protein interactions and recruitment to magnetosomes is needed to create a full picture of Mms6 dynamics.

To investigate the intrinsic determinants of localization, we created several variants of Mms6 lacking previously characterized domains. We find that the C-terminal MIC of Mms6 is not necessary for localization to the magnetosome or to the cytoplasm (Fig. 5C,D). This finding, along with the observations of the *ΔmamN* strain, further demonstrate that magnetite binding is not needed for localization of Mms6 to magnetosomes. We also found the MIC to be dispensable

for normal magnetic response (Fig. 5B). This finding suggests that Mms6 may have other functions that affect magnetic response which are not related to mineral-binding.

A previous study by Arakaki et al. showed that without the NTD, Mms6-GFP localizes diffusely under BPC (8). However, it could not be determined whether Mms6-GFP localized in either the cytoplasm or inner membrane (8). Here, we show that under NBPC, $Mms6_{99\text{-}157}$-GFP localizes to the inner membrane instead of the cytosol (Fig. 5C,D). Under BPC, in contrast to previous results, we find that $Mms6_{99\text{-}157}$-GFP localizes to the inner membrane and to magnetosome chains. This discrepancy could be due to the difficulty at lower resolution in distinguishing proteins aligned to magnetosome chains from proteins aligned to the cellular membrane. We further demonstrated that the N-terminal half of the Mms6 NTD is necessary for Mms6 conditional localization. A truncated Mms6 lacking the NTD produced *in vitro* has been shown to form large micellar homopolymers (70,71). It is unclear if these micelles form *in vivo* or if they relocalize with changing biomineralization conditions. Therefore, the NTD may serve to keep Mms6 monomers free and cytosolic for rapid re-sorting when required. Notably, in some species, such as *Magnetovibrio blakemorei*, Mms6 lacks the NTD, suggesting that it is not necessary for effective biomineralization (91). Further work could identify what sequence more specifically in this region of the NTD is important for conditional localization. Surprisingly, the localization pattern of MmsF became conditional when fused with the Mms6 NTD, suggesting the NTD could be used to direct heterologous proteins to magnetosome membranes under specific conditions. However, the Mms6 NTD-MmsF fusion protein did not become cytoplasmic in NBPC like Mms6, indicating that other properties of Mms6 mediate its retention in the cytoplasm.

Interestingly, Mms6 tagged with GFP fluoresces both when diffusely localized and when localized to the magnetosome membrane (Fig. 5C). GFP fluoresces only when folded (92), indicating that Mms6 may fully fold in the cytosol before translocation into cellular membranes. The translocation of fully folded proteins is poorly understood in bacteria outside of twin-arginine transport (TAT) systems (93). Mms6 lacks a TAT signal peptide, indicating it is unlikely to be transported by the TAT system. The transportation of Mms6 also does not follow the pattern of other known bacterial folded protein transporters such as the Type 3 secretion system (T3SS) and Type 9 secretion system (T9SS), both of which translocate proteins from the cytoplasm across both the inner and outer membranes into the extracellular space (93). These findings suggest that Mms6 may localize through an undiscovered membrane transporter that translocates fully folded proteins, perhaps one specific to magnetosomes.

A study by Yamagishi et al. showed that deletions in the Mms6 magnetite-interacting component resulted in cells with misshapen magnetite crystals (76), suggesting that this domain is needed for Mms6 localization, function, or stability. To test whether localization was affected by these mutations, Yamagishi et al. isolated the magnetosome membrane fraction from the cytoplasm and the inner membrane fraction and performed immunoblotting. Wild-type Mms6-His was found specifically in the magnetosome membrane, whereas His-tagged mutants with deletions in the mineral interacting component were absent from the magnetosome membrane. These results were taken to mean that Mms6 requires the MIC for magnetosome localization. In contrast, our

live cell fluorescence microscopy results show that Mms6 variants lacking the MIC localize to magnetosomes (Fig. 5C). In addition, complementing the *mms6* deletion mutant with $Mms6_{1\text{-}139}$-GFP restores the cellular magnetic response (Fig. 5B). This discrepancy may be due to a difference in methodology. Yamagishi et al. found that the Mms6 MIC mutants were also absent from the other cell fractions, suggesting that they may have been unstable or degraded by proteases. Mutant $Mms6_{107\text{-}135}$-GFP created for our study expressed a similar length of Mms6 as the mutant from Yamagishi et al. and gave too faint a signal to image, likely due to protein degradation or instability. This result suggests that the N- and C-terminal ends of Mms6 may stabilize the protein *in vivo*. Further work will be necessary to determine the minimal protein domains necessary for the magnetosome sorting of Mms6.

Investigating Mms6 localization using cellular fractionation revealed an association with an unknown component of the insoluble fraction and raised new questions about Mms6 topology. Surprisingly, Mms6 in NBPC appears diffuse in the cytoplasm by microscopy but co-fractionates with insoluble membrane proteins (Supplementary Fig. S7). Mms6 elutes in the soluble fraction when a nonionic detergent is added during fractionation, suggesting it may only have a weak association with the magnetosome membrane or micelle. Curiously, Mms6-GFP fluoresces even after localizing to the magnetosome membrane. Because GFP does not fold in the periplasm in a way that enables fluorescence (92), this finding suggests that either Mms6 folds in the cytoplasm before associating with membranes, or that the Mms6 C-terminus is exposed to the cytoplasm. In addition, the interaction shown between Mms6 and MamA, a protein attached to the magnetosome surface, could also indicate the presence of Mms6 domains on the cytoplasmic side of the membrane (82). These findings are most consistent with the Mms6 C-terminus positioned on the cytoplasmic side of the magnetosome membrane, where it perhaps assists iron import into magnetosomes. Further research will need to be done to clarify Mms6 topology.

Based on these results, we propose a model in which Mms6 is synthesized and kept in the cytoplasm by its N-terminal domain and possibly by *mamN* (Fig. 7). Then, at the beginning of biomineralization in a step dependent on *mamE*, *mamO*, *mamM,* Mms6 relocalizes to magnetosomes. Once Mms6 associates with the magnetosome membrane, its N-terminal domain is cleaved by MamE protease activity and Mms6 assists in the development of magnetite. Our findings emphasize the importance of tight cellular control over protein localization in biomineralization. We show that at least one MAI protein is dynamically sorted to magnetosome compartments as biomineralization conditions change. We also demonstrate that the localization of biomineralization proteins can be modified *in vivo* using the Mms6 NTD. Developing further abilities to modify MAI protein localization and target new proteins to the magnetosome membrane could allow finer control over the production of magnetite particles that can be used in medical and biotechnological applications.

Materials and Methods

Bacterial growth and cellular magnetic response

The strains used in this study are described in Table S1. AMB-1 stock cultures were grown as described by picking single colonies and growing in 1.5 mL Magnetospirillum Growth (MG) medium in 1.7 mL microtubes tubes (Genesee Scientific Cat #24-281) at 30 °C for 3-4 d with 15 µl Wolfe's vitamin solution and 20 µM ferric malate. To start larger cultures, stock cultures were diluted 1:100 in 10 mL MG medium in 24 mL capped tubes and grown at 30 °C for 2 d in a 10% oxygen microaerobic chamber. Antibiotic selection was done with 10 µg/mL kanamycin in solid MG medium and 7 µg/mL kanamycin in liquid MG medium.

To record the magnetic response (Cmag) of an AMB-1 culture, the optical density of AMB-1 cells growing in 10 mL MG medium is measured in a UV-vis spectrophotometer. An external magnetic field was applied to the cells to shift magnetic cells from a parallel to perpendicular orientation relative to the light beam, creating a quantifiable difference in optical density used to represent magnetic response. The ratio of measured OD values when the magnetic field is parallel versus perpendicular is recorded.

Escherichia coli cultures were grown in 10 mL lysogeny broth in 24 mL capped tubes on a rotating wheel at 37 °C for about 10 h. Antibiotic selection was done with 50 µg/mL kanamycin. An addition of 300 µM diaminopimelic acid was necessary to grow *E. coli* strain WM3064.

Genetic manipulation

Oligonucleotides were designed in sequence analysis software Geneious using the *Magnetospirillum magneticum* AMB-1 genome sequence NC_007626.1 and were manufactured by Elim Biopharm or Integrated DNA Technologies. DNA fragments were amplified using GoTaq master mix (Promega Cat #M7123). Plasmids were introduced into AMB-1 through conjugation and are listed in supplementary table S2.

Several plasmids were created to express truncated versions of Mms6 with a GFP fusion tag. To create pAK1456 (*mms6*$_{99\text{-}157}$-GFP), pAK1444 (*mms6*$_{1\text{-}98}$-GFP), pAK1445 (*mms6*$_{113\text{-}157}$-GFP), pAK1446 (*mms6*$_{107\text{-}157}$-GFP), pAK1441 (*mms6*$_{51\text{-}157}$-GFP), and pAK1443 (*mms6*$_{1\text{-}139}$-GFP), fragments of mms6 were PCR amplified from AMB-1 genomic DNA using the primers listed in supplementary table S3 and inserted by Gibson assembly into pAK1102 (*mms6*-GFP), following vector digestion with BamHI-HF and EcoRI-HF restriction enzymes (New England Biolabs). To create pAK1447 (GFP-*mms6*$_{NTD}$*mmsF*), fragments of mms6 were PCR amplified from AMB-1 genomic DNA using the primers listed in supplementary table S3 and inserted by Gibson assembly into pAK532 (GFP-*mmsF*), following vector digestion with BamHI-HF and SpeI-HF restriction enzymes (New England Biolabs).

Fluorescence microscopy and localization pattern quantification

To analyze Mms6 localization in AMB-1 cells, cells growing in 10 mL MG medium were collected once reaching an optical density of OD_{400} 0.08-0.15 by centrifugation at 10,000 x g for 3 min. Cell pellets expressing a HaloTag fusion were resuspended in 100 µL MG medium,

incubated with 500 nM HaloTag 549 ligand (Promega Cat #GA1110) for 60 min in the dark at 30 °C in a 10% O_2 microaerobic chamber, and then centrifuged at 10,000 x g for 3 min. All cell pellets were then resuspended in 100 µL fresh MG medium and stained with 1.4 µM 4',6-diamidino-2-phenylindole (DAPI) from Cell Signaling Technology (Cat #4083S) for 15 min in the dark at 30 °C in the microaerobic chamber. FM 1-43 (Life Technologies Corporation Cat #T3163) was applied in the same way when required. Cells were then centrifuged at 10,000 x g for 3 min and washed 3 times with 100 µL fresh MG medium for 10 min in the dark at 30 °C in the microaerobic chamber. After washing, cells were resuspended in 10 µL fresh MG medium and 0.8 µL cell mixture was added to a slide and sealed under a coverslip using nail polish to reduce drying. Slides were imaged at 1000x magnification using the QImaging Retiga 1350ex camera in a Zeiss Axioimager M2 fluorescence microscope. Localization of proteins was quantified using the ImageJ Cell Counter plugin to categorize the localization in each cell into one of several categories including diffuse, foci, membrane, and chain aligned. Image file names were obscured using the ImageJ Randomizer macro for unbiased counting.

3D Structured illumination fluorescence microscopy and image analysis

Cells were prepared as for fluorescence microscopy above and imaged using the Plan-APOCHROMAT 100x/1.46 objective lens of a Carl Zeiss Elyra PS.1 structured illumination microscope. Lasers at 405, 488, 561, and 642 nm wavelengths were used to excite DAPI, GFP, HaloTag ligand JF549, and HaloTag ligand JF646, respectively. Images were acquired using Zeiss ZEN software and processed using Imaris software (Bitplane).

Pulse-chase analysis

To study Mms6 localization under changing iron conditions, we applied pulse-chase analysis using magnetosome proteins fused with HaloTag. HaloTag binds covalently and irreversibly to fluorescent ligands, allowing the tracking of a specific protein pool. For pulse-chase analysis, stock cultures were passaged into 10 mL fresh MG medium and grown in iron starvation conditions for 2 d in tubes washed with oxalic acid to remove residual iron. This process was repeated twice to ensure cells could not biomineralize. Then, 3 tubes of 10 mL AMB-1 cells per strain were grown in MG medium to early exponential phase (OD400 0.05-0.08) under iron starvation conditions. Cmag was assessed as described above for each culture. Cultures were pelleted by centrifugation at 10,000 x g for 3 min in an anaerobic chamber and resuspended with 500 nM HaloTag 549 pulse ligand and incubated in anaerobic MG medium for 60 min in the dark at 30 °C. Cells were centrifuged at 10,000 x g for 3 min. Cells were washed 3 times with 100 µL fresh, anaerobic MG medium for 10 min in the dark at 30 °C. Anaerobic MG medium was used to resuspend the cell pellets and the cell mixtures were inoculated into sealed anaerobic Balch tubes and incubated in the dark at 30 °C. 20µM Ferric malate was added to induce biomineralization, and OD400 and Cmag was tracked. 1 h before time point collection, cultures were centrifuged at 10,000 x g for 3 min. Cell pellets were resuspended with 500 nM HaloTag 646 (Promega Cat #GA1120) chase ligand in anaerobic MG medium for 45 min in the dark at 30

°C. 1.4 µM 4',6-diamidino-2-phenylindole (DAPI) was added to cells, cells were mixed, and incubation continued for an additional 15 min. Cells were then centrifuged at 10,000 x g for 3 min and washed 3 times with 500 µL fresh MG medium. After washing, cells were resuspended in 10 µL fresh MG medium and 0.8 µL cell mixture was added to a slide and sealed under a coverslip using nail polish to reduce drying. Slides were imaged at 1000x magnification using the QImaging Retiga 1350ex camera in a Zeiss Axioimager M2 fluorescence microscope. Localization of proteins was quantified using the ImageJ Cell Counter plugin to categorize the localization in each cell into one of several categories including diffuse, foci, and chain aligned. Image file names were obscured using the ImageJ Randomizer macro for unbiased counting.

Cellular fractionation

AMB-1 cells were grown in 50 mL MG medium at 30 °C in a microaerobic chamber maintaining 10% atmospheric oxygen. Cells were then diluted 1:100 into 1.5 L MG medium and grown for 2 d. The 1.5 L cultures were centrifuged at 8,000 xg for 20 min at 4 °C.

Pellets were resuspended in 1 mL Buffer A (10 mM Tris-HCl, pH 8.0, 50mM NaCl, 1mM EDTA). Pepstatin and Leupeptin were each added to a final concentration of 2 µg/ml and 2 mM PMSF was added. To lyse cells, 0.5 mg/mL lysozyme was added and samples were incubated at room temperature for 15 min. After lysis, 3mL Buffer B (20mM HEPES-KOH pH 7.5, 50mM NaCl, 1.25mM CaCl2) was added along with 2 mM DTT and 5 µg/mL DNAse I and lysates were rocked at 4 °C for 15 min. To separate soluble and insoluble cell fractions, samples were ultracentrifuged at 160,000 xg for 2 h at 4 °C in ultracentrifuge tubes (Beckman Coulter Cat #328874). The resulting pellet contained the insoluble AMB-1 cell fraction and the supernatant contained the soluble fraction. In fractionations done with Igepal CA-630 (Spectrum Chemicals Cat #I1112-100 ML), also known as Nonidet P-40 substitute or NP-40, 0.4% Igepal was added before ultracentrifugation and samples were kept on ice for 2 h and were gently agitated every 30 min to mix.

Cell fractions were analyzed by SDS-PAGE. Briefly, 2x Laemmli Sample Buffer (Bio-Rad) was mixed with each fraction. After heating fractions for 15 min at 95 °C, proteins were resolved by electrophoresis through 12% agarose polyacrylamide gels and then transferred to PVDF membranes (Bio-Rad Cat #1620175) by electroblotting. Protein detection was done using primary antibody anti- HaloTag monoclonal antibody (1:1,000 dilution, Promega), primary antibody anti-MamE polyclonal antibody (1:3,000 dilution, produced by ProSci Inc), secondary antibody F(ab')2-goat anti-mouse IgG (H+L) HRP-conjugate (1:5,000 dilution, Invitrogen), and secondary antibody goat anti-rabbit IgG (H+L)-HRP-conjugate (1:10,000 dilution, Bio-Rad). Image lab (Bio-Rad) software was used to take images of blots.

Statistics and reproducibility

The chi-square test of independence or fisher's exact test were used to assess if biomineralization condition had a significant relation to Mms6 localization. Mann-Whitney U test is a non-

parametric test used to compare outcomes between two independent groups. The statistical tests were performed in RStudio using R version 4.2.2.

Protein structure prediction

SignalP 5.0 was used to detect signal peptides in Mms6 and other magnetosome proteins. TMHMM 2.0 and TMPred were used to detect transmembrane regions. Phyre2 and CCTOP were used for membrane topology predictions.

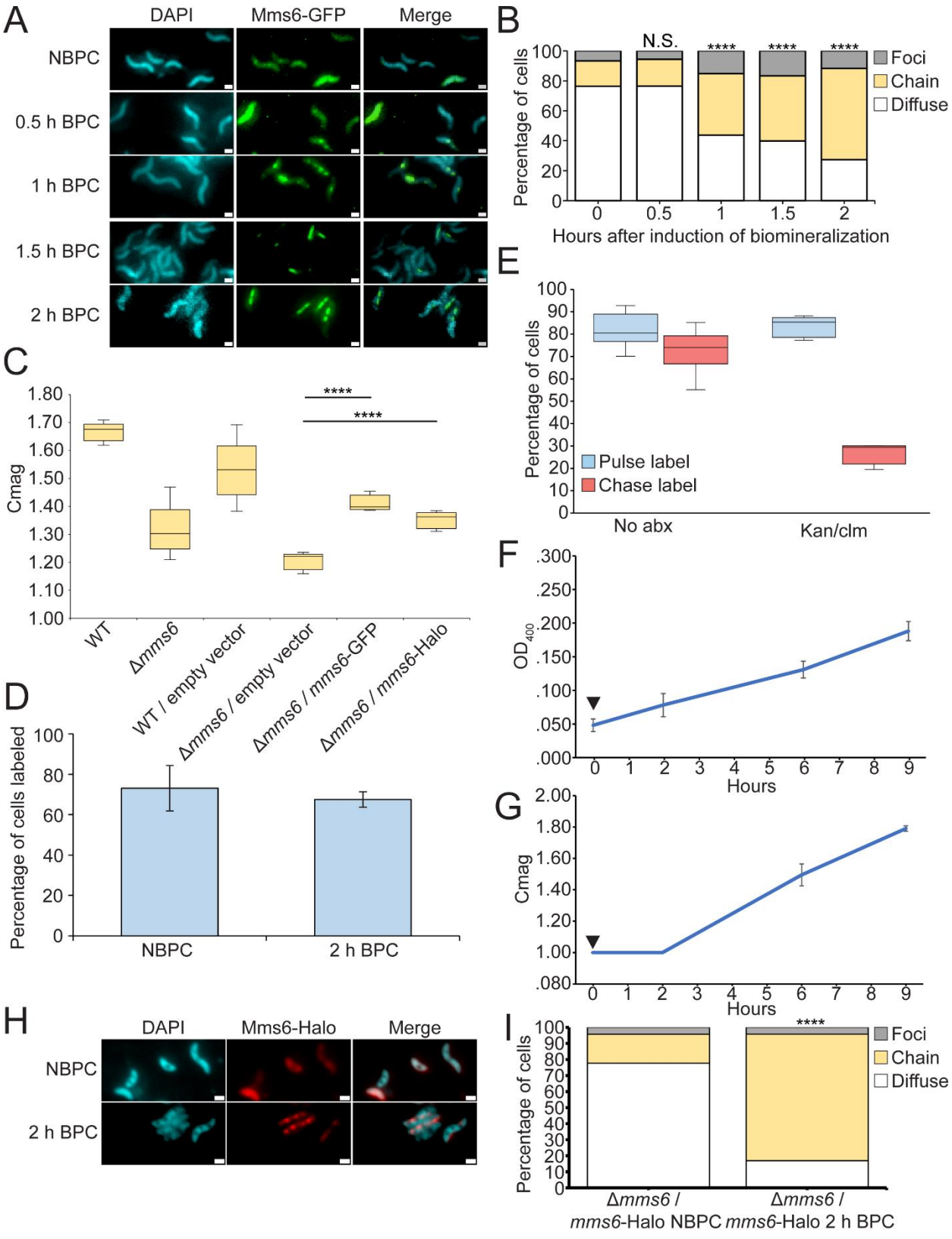

Figure 1. Pre-translated Mms6 is relocalized from the cytoplasm to magnetosomes in response to biomineralization permissible conditions. (A) Representative fluorescence microscopy images

of *Δmms6* expressing Mms6-GFP shown in green. DAPI is shown in blue. Scale bars = 1 μm. (B) Blind quantification of localization patterns of Mms6-GFP during biomineralization time course *in vivo*. Cells were categorized by localization pattern and y-axis represents percentage of cells with Mms6-GFP displaying given localization pattern out of total labeled cells. *P* values were calculated by Chi-squared test of independence comparing given dataset to time 0 (N.S. no significant difference $P > .01$) (**** $P < 10^{-5}$). NBPC $n = 686$ cells, 0.5 h $n = 1147$ cells, 1 h $n = 507$ cells, 1.5 h $n = 1013$ cells, 2 h $n = 1255$ cells. (C) Coefficient of magnetism (Cmag) of strains. *P* values were calculated by Mann-Whitney U test comparing given dataset to Δ*mms6* / empty vector (**** $P < 10^{-5}$). (D) Percentage of cells labeled with Mms6-Halo fluorescence before and during relocalization time course. NBPC $n = 12528$ DAPI labeled cells, 2 h BPC $n = 4268$ DAPI labeled cells. (E) *Δmms6* / *mms6*-Halo cells were incubated with HaloTag pulse and chase ligands to test HaloTag saturation with and without 700 μg/ml kanamycin and 400 μg/ml chloramphenicol to prevent the synthesis of new Mms6-Halo. (F) OD_{400} of 9 cultures of *Δmms6* / *mms6-Halo* grown initially under iron starvation conditions and then given iron to allow biomineralization (black arrow). (G) Coefficient of magnetic response of cultures over time course. (G) Mms6-Halo with J549 ligand shown in red and DAPI shown in blue. (I) Blind quantification of localization patterns of Mms6-Halo during biomineralization time course *in vivo*. Cells were categorized by localization pattern as above. *P* values were calculated by chi-squared test of independence comparing given dataset to NBPC sample (**** $P < 10^{-5}$). NBPC $n = 8432$ labeled cells, BPC $n = 2810$ cells.

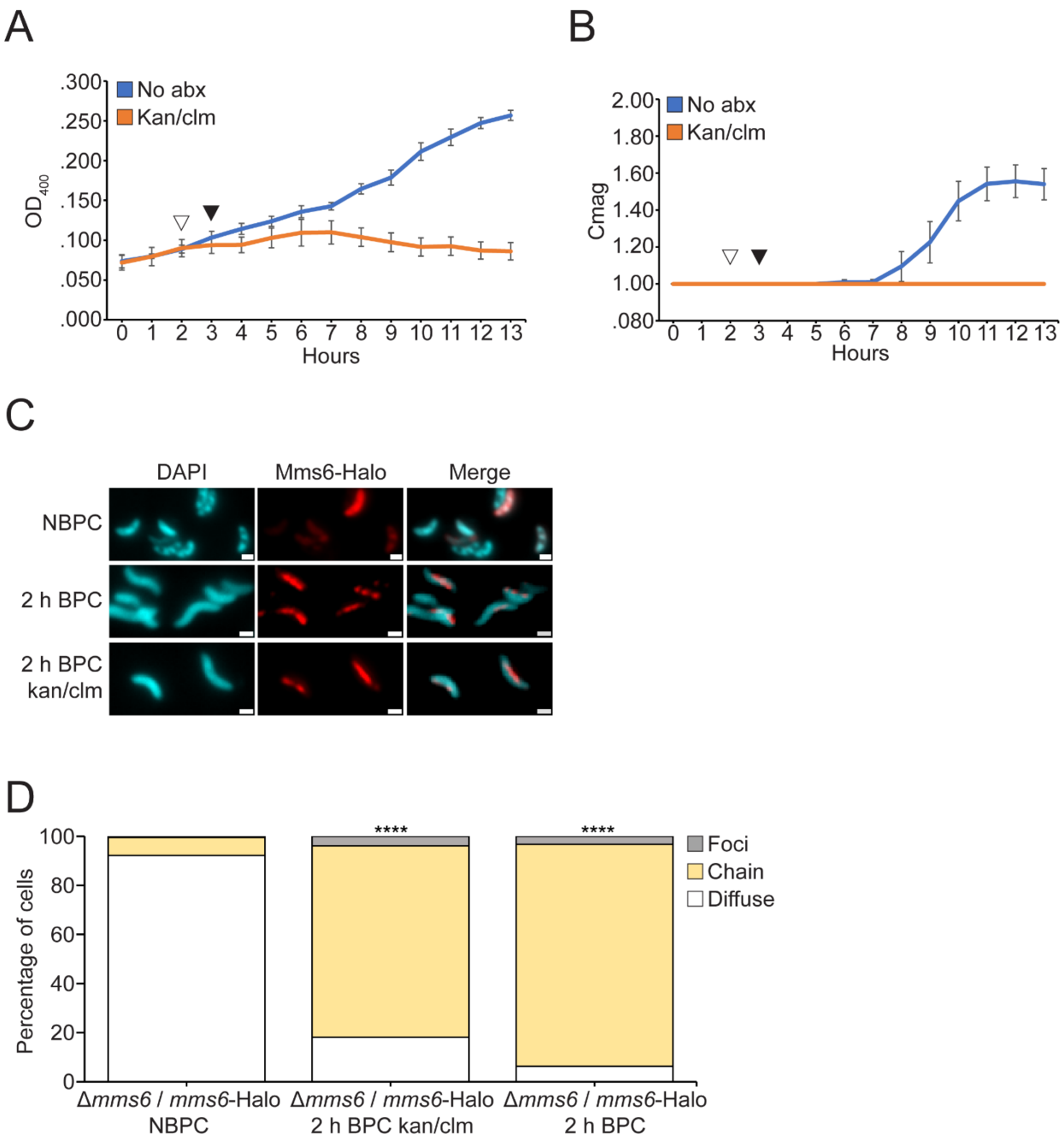

Figure 2. Pre-translated Mms6 relocalizes after iron addition in the absence of new protein synthesis. (A) OD_{400} of *Δmms6* expressing Mms6-Halo grown initially under iron starvation conditions and then given iron to allow biomineralization. 700 µg/ml kanamycin and 400 µg/ml chloramphenicol were added (white arrow) to kan/clm sample to prevent the synthesis of new Mms6 1 h before adding iron (black arrow) to all samples. (B) Coefficient of magnetic response of cultures over time course. (C) Mms6-Halo with J549 ligand shown in red and DAPI shown in blue. (D) Blind quantification of localization patterns of Mms6-GFP during biomineralization time course *in vivo*. Cells were categorized by localization pattern as above. *P* values were

calculated by Fisher's exact test comparing given dataset to NBPC sample (**** $P < 10^{-5}$). NBPC $n = 2112$ cells, 2 h BPC kan/clm $n = 1102$ cells, 2 h BPC $n = 2422$ cells.

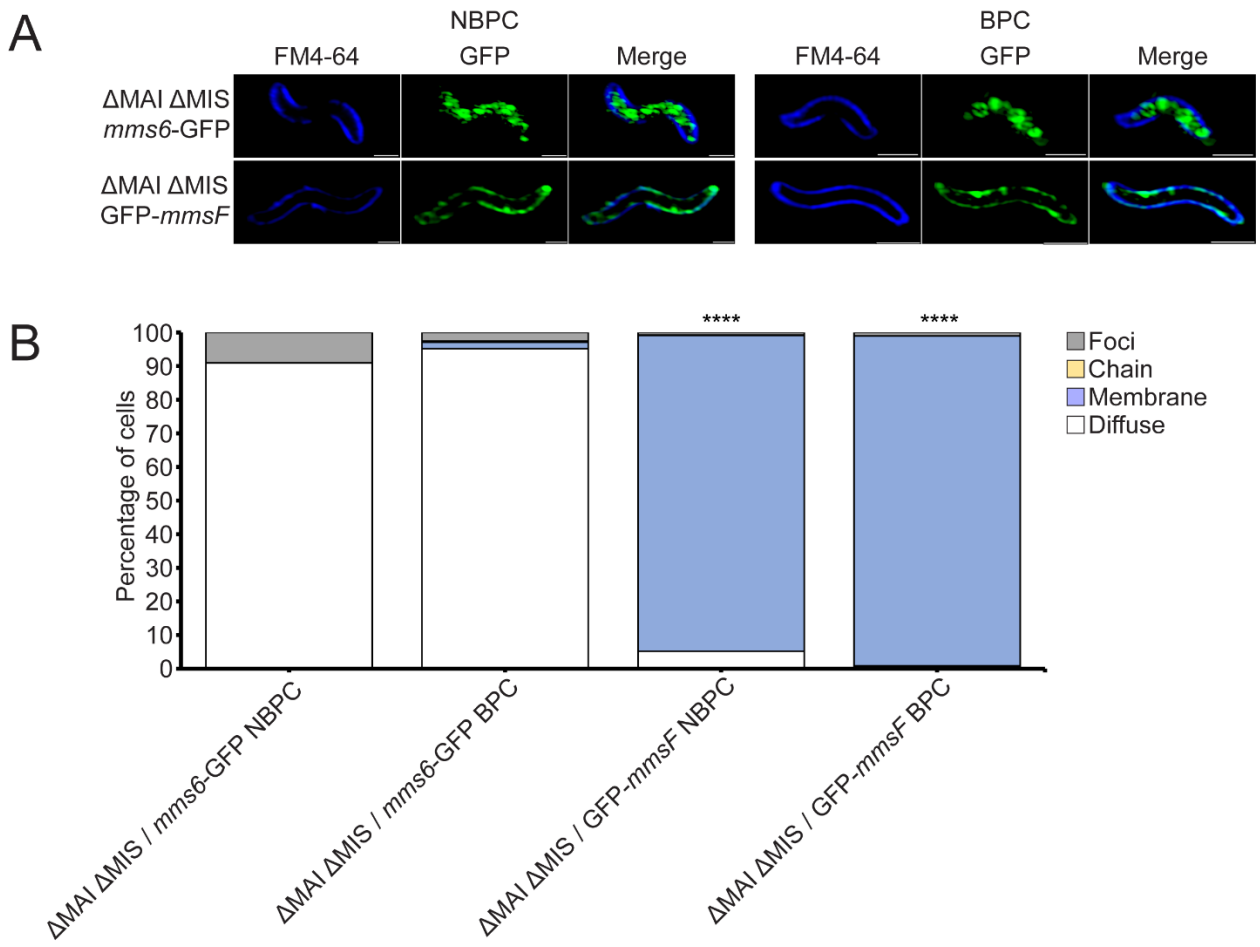

Figure 3. Mms6-GFP is cytoplasmic in the absence of magnetosomes. (A) Representative super resolution 3D Structured Illumination Microscopy (SIM) images of ΔMAI ΔMIS expressing either *mms6*-GFP or GFP-*mmsF* shown in green and membrane stain FM4-64 shown in dark blue. Scale bars = 1 μm. (B) Blind quantification of localization patterns of either *mms6*-GFP or GFP-*mmsF* based on fluorescence microscopy images. Cells were categorized by localization pattern. *P* values were calculated by Fisher's exact test comparing GFP-*mmsF* dataset to *mms6*-GFP dataset of respective biomineralization condition (N.S. no significant difference $P > .01$) (**** $P < 10^{-5}$). ΔMAI ΔMIS / *mms6*-GFP NBPC $n = 624$ cells, ΔMAI ΔMIS / *mms6*-GFP BPC n = 166 cells, ΔMAI ΔMIS / GFP-*mmsF* NBPC n = 588 cells, ΔMAI ΔMIS / GFP-*mmsF* BPC n = 927 cells.

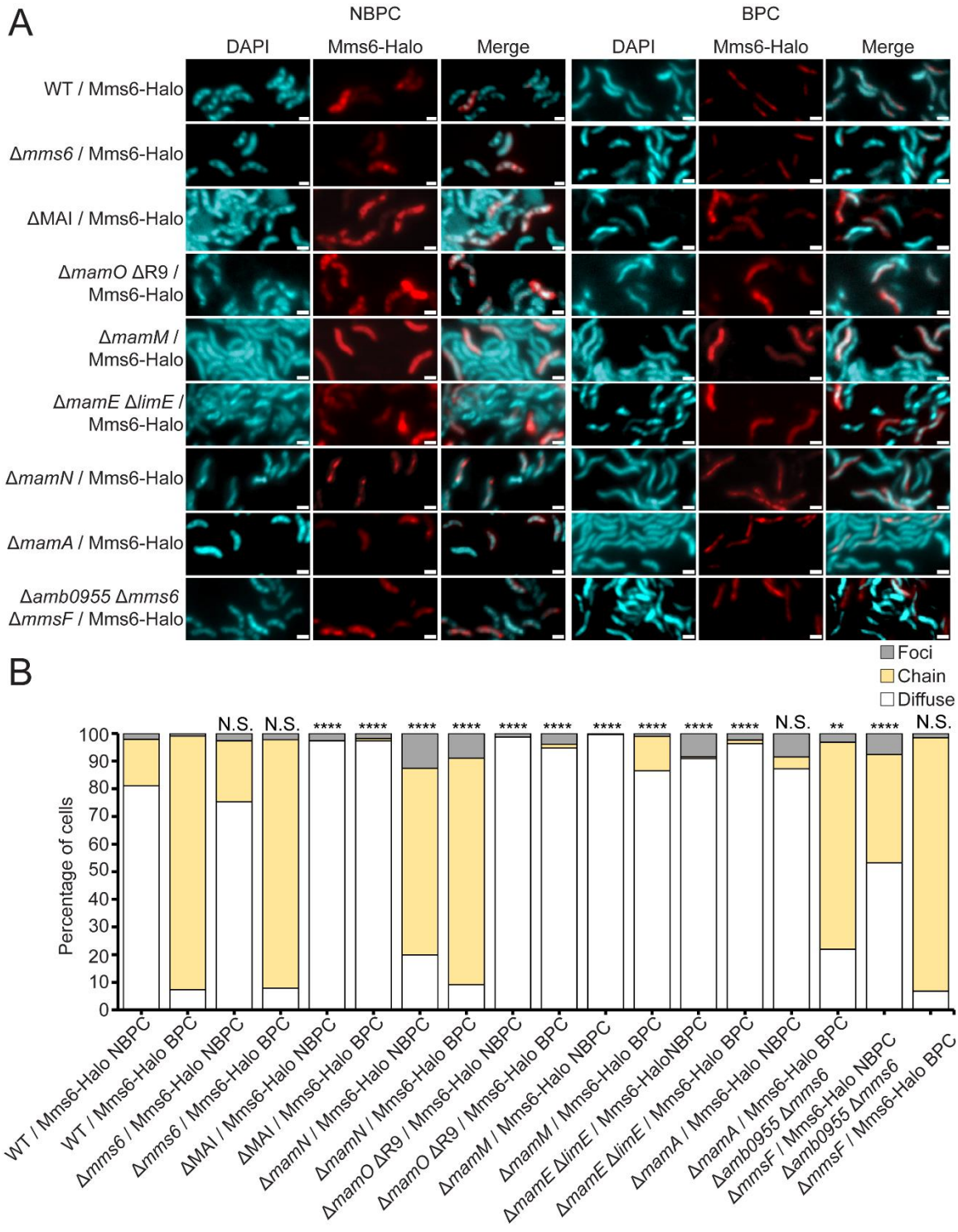

Figure 4. MAI proteins affect Mms6 localization (A) Representative fluorescence microscopy images of AMB-1 with different genetic backgrounds expressing *mms6*-Halo and grown in standard conditions. JF549 HaloTag ligand fluorescence is shown in red and DAPI in blue. Scale bars = 1 µm. (B) Blind quantification of localization patterns of Mms6-Halo. *P* values were calculated by Fisher's exact test comparing given dataset to WT / *mms6*-Halo (N.S. no

significant difference $P > .01$) (**** = $P < 10^{-5}$). WT / *mms6*-Halo NBPC $n = 285$ cells, WT / *mms6*-Halo BPC $n = 436$ cells, ΔMAI / *mms6*-Halo NBPC $n = 496$ cells, ΔMAI / *mms6*-Halo BPC $n = 718$ cells, Δ*mamN* / *mms6*-Halo NBPC $n = 956$ cells, Δ*mamN* / *mms6*-Halo BPC $n = 514$ cells, Δ*mamO* ΔR9 / *mms6*-Halo NBPC $n = 312$ cells, Δ*mamO* ΔR9 / *mms6*-Halo BPC $n = 1199$ cells, Δ*mamM* / *mms6*-Halo NBPC $n = 285$ cells, Δ*mamM* / *mms6*-Halo BPC $n = 401$ cells, Δ*mamE* Δ*limE* / *mms6*-Halo NBPC $n = 154$ cells, Δ*mamE* Δ*limE* / *mms6*-Halo BPC $n = 383$ cells, Δ*mamA* / *mms6*-Halo NBPC $n = 518$ cells, Δ*mamA* / *mms6*-Halo BPC $n = 314$ cells, Δ*amb0955* Δ*mms6* Δ*mmsF* / *mms6*-Halo NBPC $n = 278$ cells, Δ*amb0955* Δ*mms6* Δ*mmsF* / *mms6*-Halo BPC $n = 530$ cells.

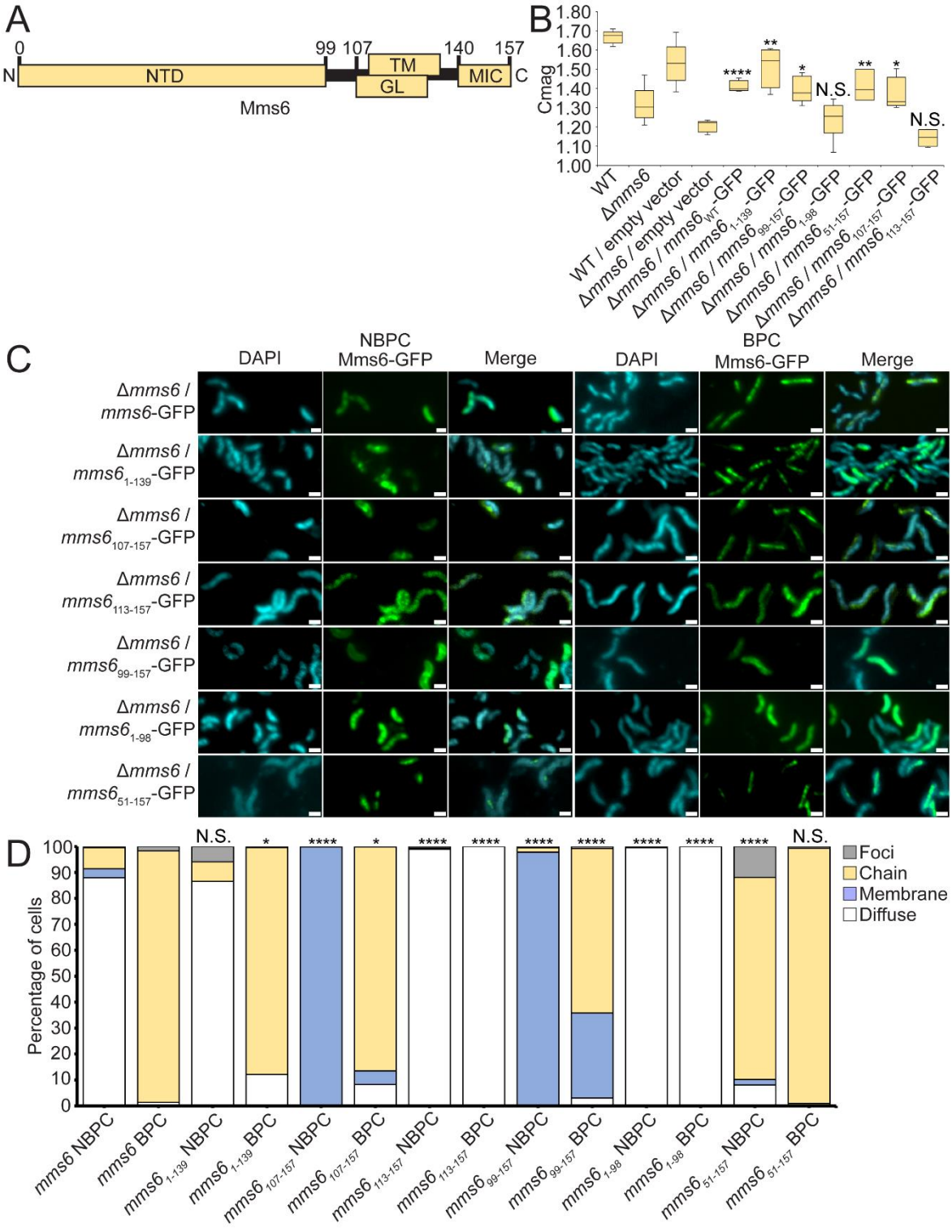

Figure 5. Mms6 protein domains are essential to conditional and diffuse localization. (A) Diagram of Mms6 protein domains (NTD N-terminal domain, TM transmembrane domain, MIC magnetite-interacting component). (B) Coefficient of magnetism (Cmag) of several strains

measured by differential scattering of light by cells moved into different orientations by an external magnetic field. *P* values were calculated by Mann-Whitney U Test comparing given dataset to Δ*mms6* / empty vector (N.S. no significant difference $P > .01$) (* = $P < 10^{-2}$) (** = $P < 10^{-3}$) (**** = $P < 10^{-5}$). (C) Representative fluorescence microscopy images of *Δmms6* expressing WT *mms6* or a mutant version. DAPI counterstain is shown in blue. Scale bars = 1 μm. (D) Blind quantification of localization patterns of WT and mutant versions of Mms6-GFP in *Δmms6. P* values were calculated by Fisher's exact test comparing Mms6 mutant datasets to Δ*mms6* / *mms6*-GFP (N.S. no significant difference $P > .01$) (* = $P < 10^{-2}$) (**** = $P < 10^{-5}$). Δ*mms6* / *mms6*-GFP NBPC *n* = 233 cells, Δ*mms6* / *mms6*-GFP BPC *n* = 812 cells, Δ*mms6* / *mms6*$_{1\text{-}139}$ -GFP NBPC *n* = 128 cells, Δ*mms6* / *mms6*$_{1\text{-}139}$ BPC *n* = 470 cells, Δ*mms6* / *mms6*$_{99\text{-}157}$-GFP NBPC *n* = 411 cells, Δ*mms6* / *mms6*$_{99\text{-}157}$-GFP BPC *n* = 265 cells, Δ*mms6* / *mms6*$_{1\text{-}98}$-GFP NBPC *n* = 437 cells, Δ*mms6* / *mms6*$_{1\text{-}98}$-GFP BPC *n* = 1112 cells, Δ*mms6* / *mms6*$_{51\text{-}157}$-GFP NBPC *n* = 285 cells, Δ*mms6* / *mms6*$_{51\text{-}157}$-GFP BPC *n* = 746 cells, Δ*mms6* / *mms6*$_{107\text{-}157}$-GFP NBPC *n* = 576 cells, Δ*mms6* / *mms6*$_{107\text{-}157}$-GFP BPC *n* = 1095 cells, Δ*mms6* / *mms6*$_{113\text{-}157}$-GFP NBPC *n* = 1152 cells, Δ*mms6* / *mms6*$_{113\text{-}157}$-GFP BPC *n* = 1189 cells.

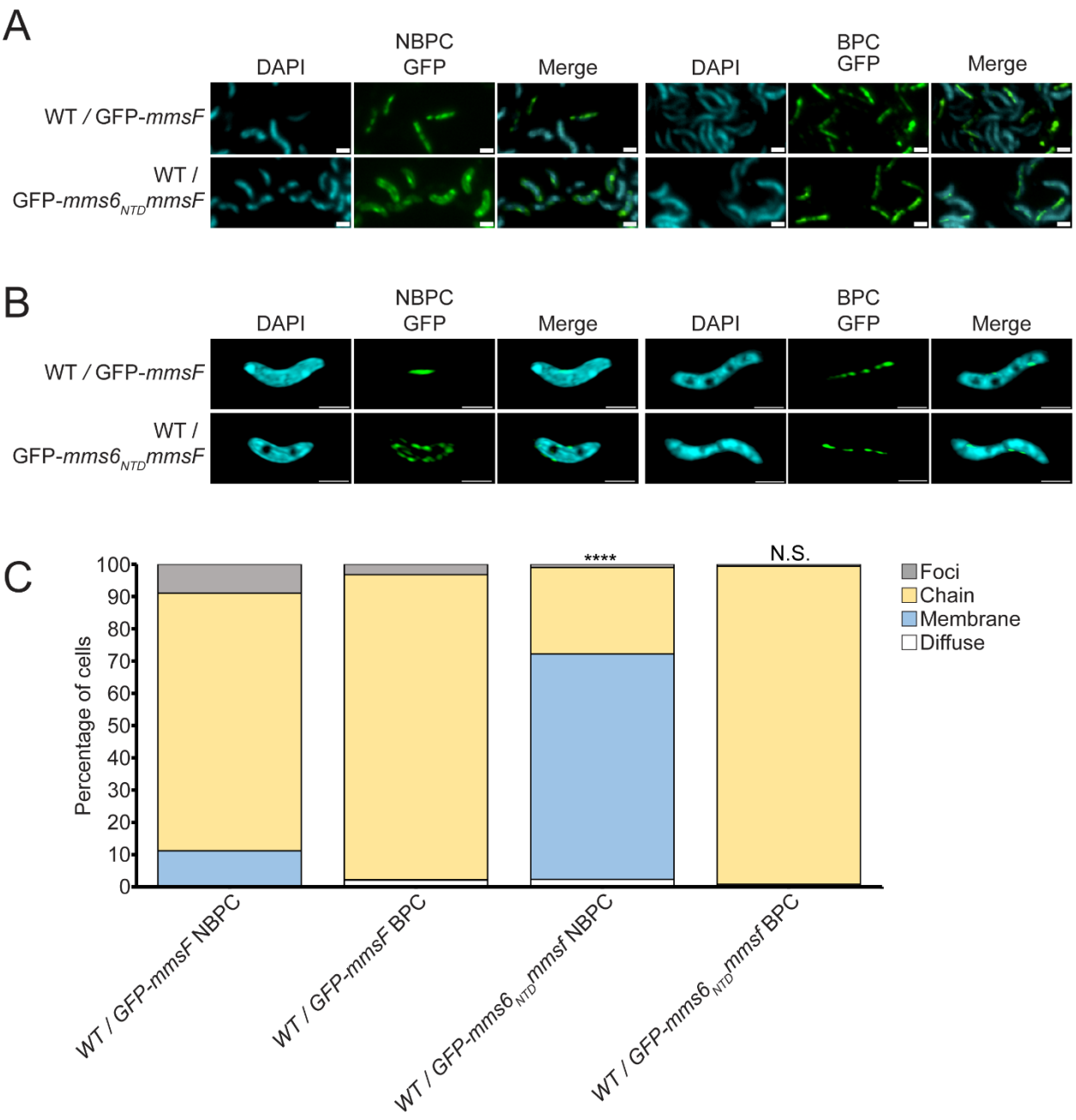

Figure 6. *mms6* N-terminal domain fused to *mmsF* imparts conditional localization. (A) Representative fluorescence microscopy images of WT cells expressing either GFP-*mmsF* or GFP-*mms6*$_{NTD}$*mmsF* shown in green and DAPI shown in blue. (B) Representative super resolution 3D Structured Illumination Microscopy (SIM) images of WT cells expressing either WT / GFP-*mmsF* or WT / GFP-*mms6*$_{NTD}$*mmsF* shown in green and DAPI shown in blue. Scale bars = 1 µm. (C) Blind quantification of localization patterns based on fluorescence microscopy images. *P* values were calculated by Fisher's exact test comparing WT / GFP-*mms6*$_{NTD}$*mmsF* to WT / GFP-*mmsF* dataset of respective biomineralization condition (N.S. no significant difference $P > .01$) (**** $P < 10^{-5}$). WT / GFP-*mmsF* NBPC n = 348 cells, WT / GFP-*mmsF*

BPC n = 802 cells, WT / GFP-*mms6*$_{NTD}$*mmsF* NBPC n = 906 cells, WT / GFP-*mms6*$_{NTD}$*mmsF* BPC n = 625 cells.

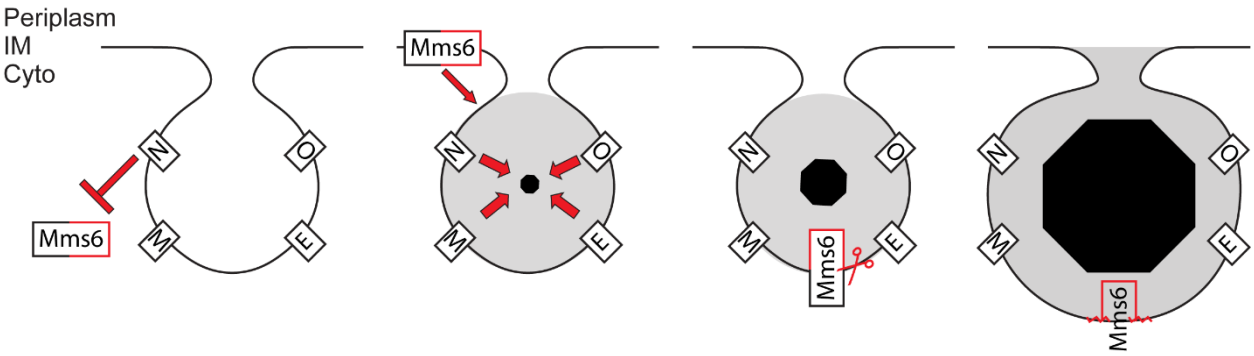

Figure 7. Model of conditional Mms6 sorting. Mms6 is kept in the cytoplasm in NBPC by its N-terminal domain (black outline) and by MamN. Once biomineralization begins, Mms6 is relocalized to the magnetosome, where it likely translocates into the membrane. The N-terminal domain is then cleaved from Mms6 by MamE and Mms6 aids in the nucleation and growth of the magnetite crystal. (IM inner membrane).

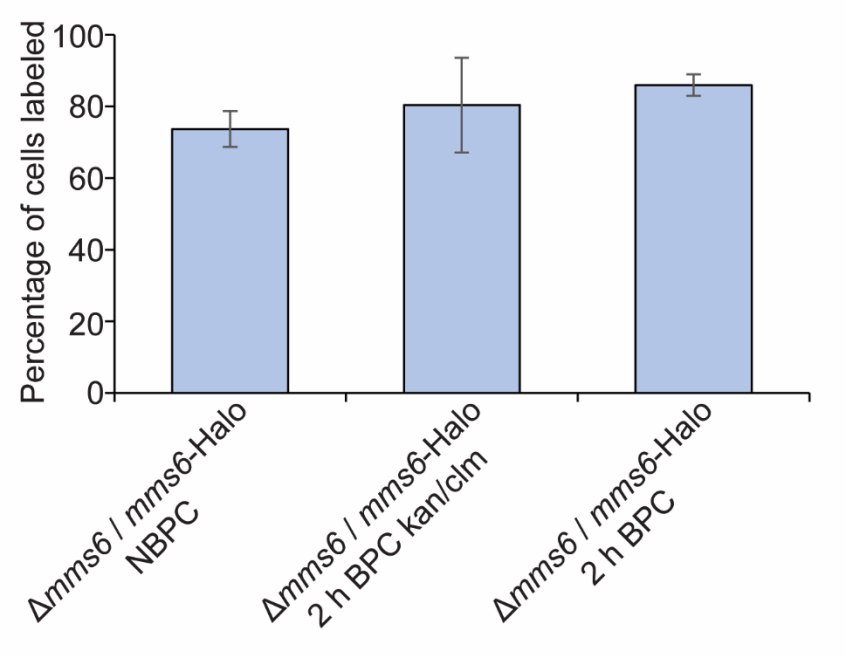

Supplementary Figure 1. Percentage of cells labeled with Mms6-Halo fluorescence before and during relocalization time course with and without antibiotics. NBPC *n* = 2881 DAPI labeled cells, 2 h BPC kan/clm *n* = 1315 DAPI labeled cells, 2 h BPC *n* = 2822 DAPI labeled cells.

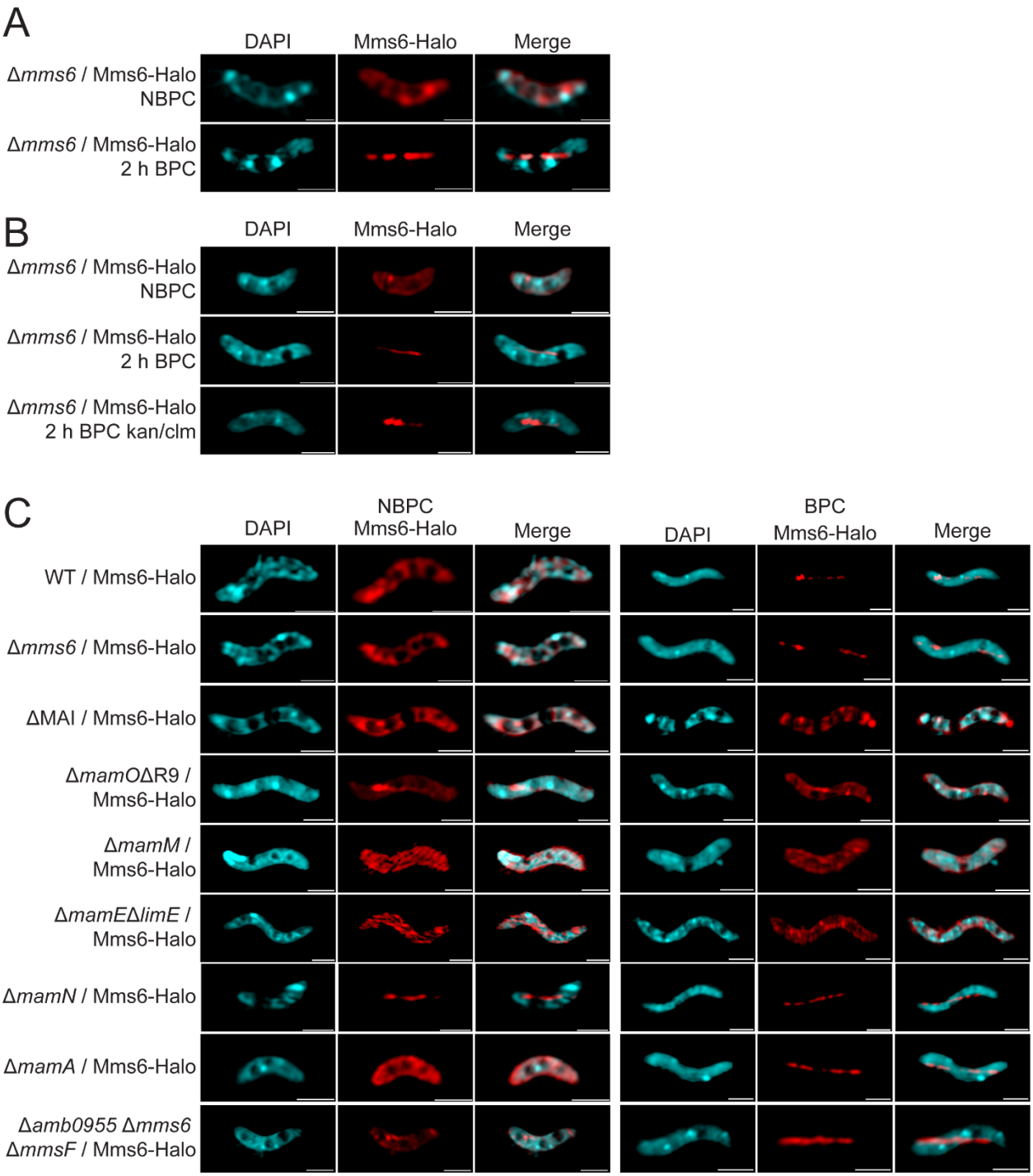

Supplementary Figure 2. Representative super resolution 3D Structured Illumination Microscopy (SIM) images of cells expressing Mms6-Halo. (A) Representative images of WT cells expressing Mms6-Halo from biomineralization time course. WT cells grown under standard growth conditions expressing either GFP-MmsF or GFP-Mms6$_{NTD}$MmsF shown in green and DAPI shown in blue. Sample labeled "kan/clm" was given 700 µg/ml kanamycin and 400 µg/ml chloramphenicol to prevent the synthesis of new Mms6-Halo during and after the one-hour

labeling step. Scale bars = 1 μm. (B) Representative images of cells of different mutant backgrounds expressing Mms6-Halo in red and DAPI shown in blue. Scale bars = 1 μm.

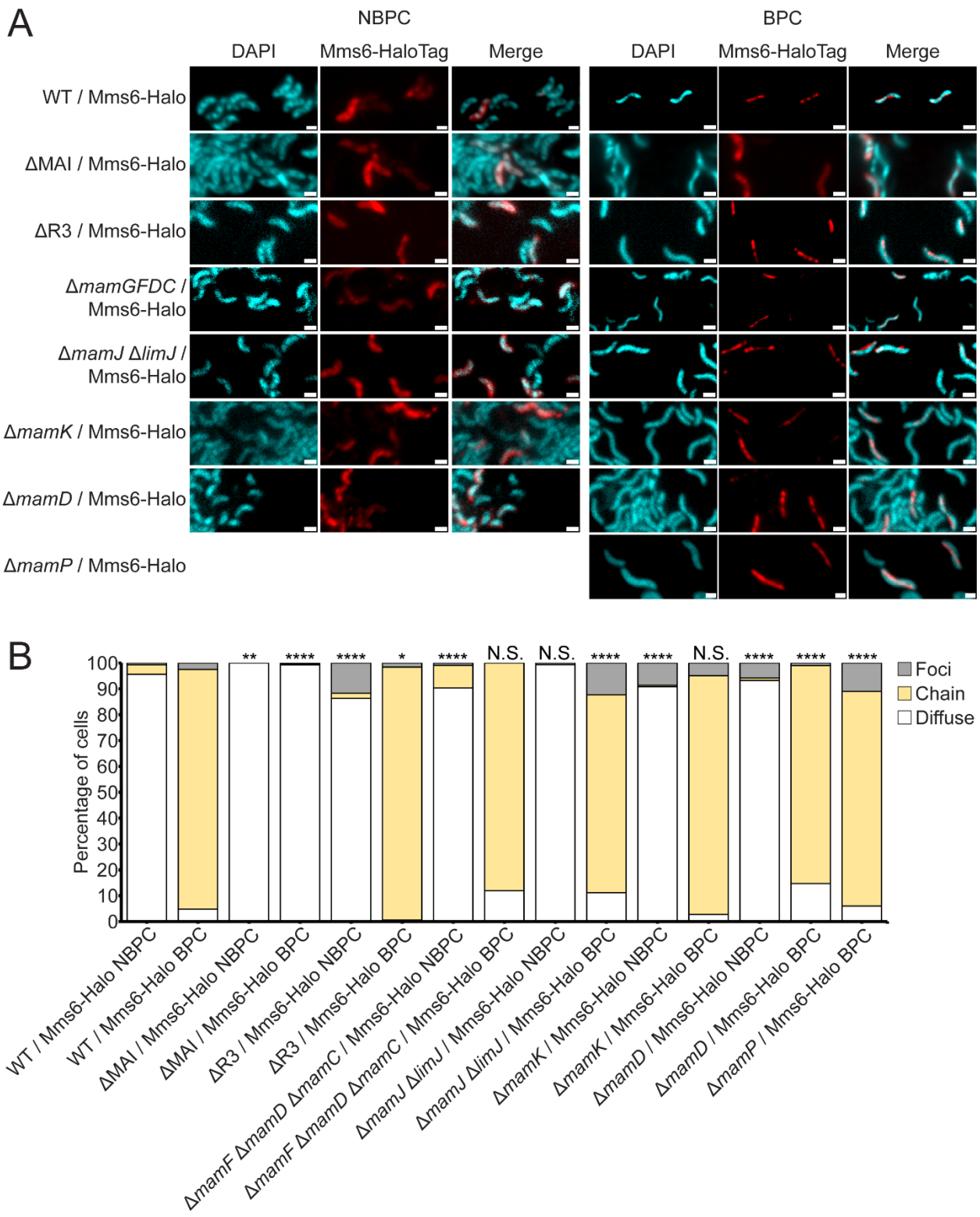

Supplementary Figure 3. Mms6-Halo localization in further MAI protein deletion backgrounds (A) Representative fluorescence microscopy images of AMB-1 with different genetic backgrounds expressing Mms6-Halo and grown in standard conditions. JF549 HaloTag ligand

fluorescence is shown in red and DAPI in blue. Scale bars = 1 μm. (B) Blind quantification of localization patterns of Mms6-Halo. *P* values were calculated by Fisher's exact test comparing given dataset to WT / *mms6*-Halo (N.S. no significant difference $P > .01$) (* = $P < .01$) (** = $P < 10^{-3}$) (**** = $P < 10^{-5}$). WT / *mms6*-Halo NBPC *n* = 1010 cells, WT / *mms6*-Halo BPC *n* = 477 cells, ΔMAI / *mms6*-Halo NBPC *n* = 262 cells, ΔMAI / *mms6*-Halo BPC *n* = 400 cells, ΔR3 / *mms6*-Halo NBPC *n* = 197 cells, ΔR3 / *mms6*-Halo BPC *n* = 316 cells, Δ*mamF* Δ*mamD* Δ*mamC* / *mms6*-Halo NBPC *n* = 996 cells, Δ*mamF* Δ*mamD* Δ*mamC* / *mms6*-Halo BPC *n* = 92 cells, Δ*mamJ* Δ*limJ* / *mms6*-Halo NBPC *n* = 160 cells, Δ*mamJ* Δ*limJ* / *mms6*-Halo BPC *n* = 277 cells, Δ*mamK* / *mms6*-Halo NBPC *n* = 175 cells, Δ*mamK* / *mms6*-Halo BPC *n* = 142 cells, Δ*mamD* / *mms6*-Halo NBPC *n* = 223 cells, Δ*mamD* / *mms6*-Halo BPC *n* = 197 cells.

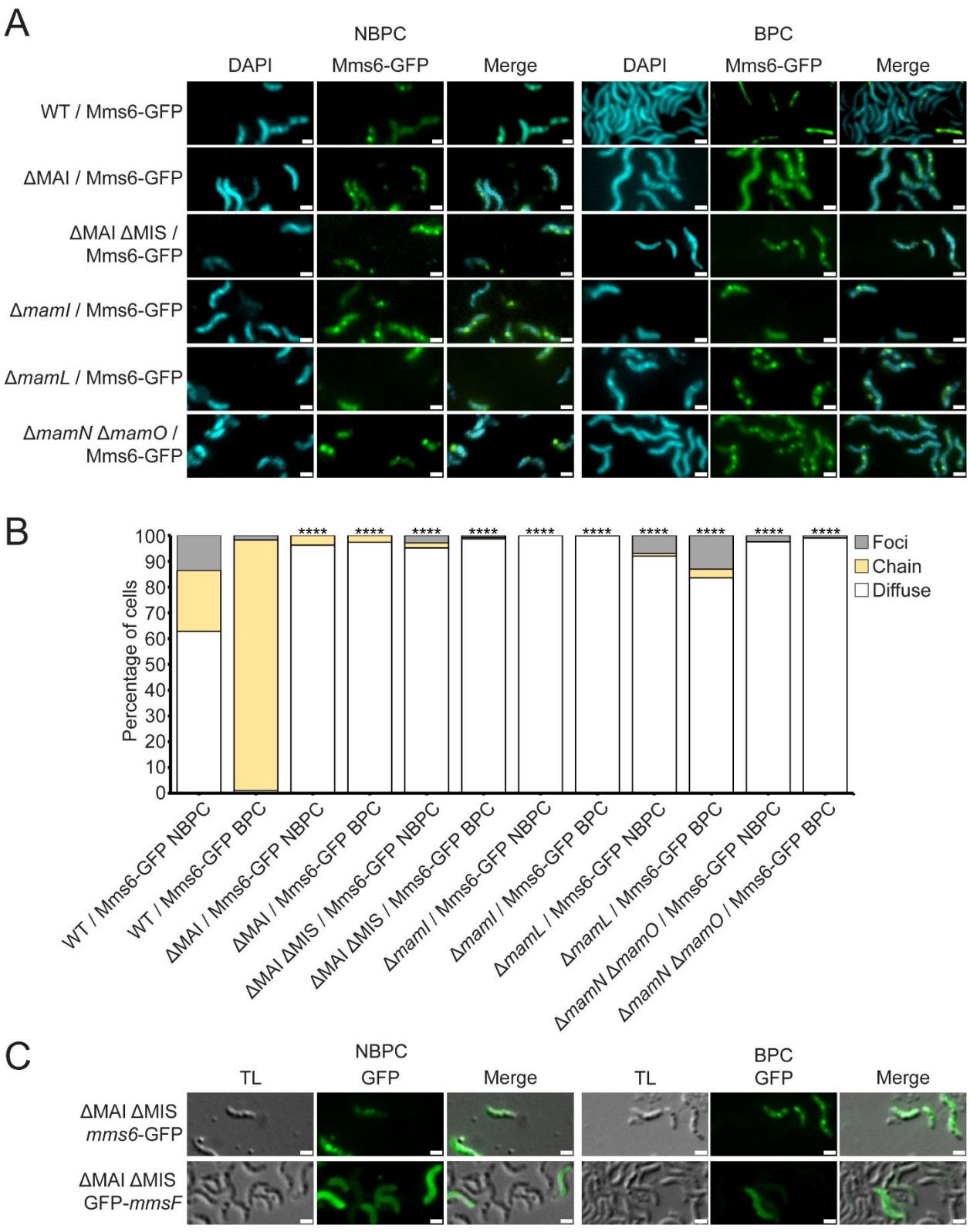

Supplementary Figure 4. Mms6-GFP localization in further MAI protein deletion backgrounds (A) Representative fluorescence microscopy images of AMB-1 with different genetic backgrounds expressing Mms6-GFP and grown in standard conditions. GFP is shown in green

and DAPI in blue. Scale bars = 1 μm. (B) Blind quantification of localization patterns of Mms6-GFP. *P* values were calculated by Fisher's exact test comparing given dataset to WT / *mms6*-GFP (**** = $P < 10^{-5}$). WT / *mms6*-GFP NBPC *n* = 199 cells, WT / *mms6*-GFP BPC *n* = 282 cells, ΔMAI / *mms6*-GFP NBPC *n* = 356 cells, ΔMAI / *mms6*-GFP BPC *n* = 1070 cells, ΔMAI ΔMIS / *mms6*-GFP NBPC *n* = 104 cells, ΔMAI ΔMIS / *mms6*-GFP BPC *n* = 540 cells, Δ*mamI* / *mms6*-GFP NBPC *n* = 72 cells, Δ*mamI* / *mms6*-GFP BPC *n* = 77 cells, Δ*mamL* / *mms6*-GFP NBPC *n* = 487 cells, Δ*mamL* / *mms6*-GFP BPC *n* = 207 cells, Δ*mamN* Δ*mamO* / *mms6*-GFP NBPC *n* = 82 cells, Δ*mamN* Δ*mamO* / *mms6*-GFP BPC *n* = 715 cells. (C) Representative fluorescence microscopy images of ΔMAI ΔMIS grown under standard growth conditions expressing either *mms6*-GFP or GFP-*mmsF* shown in green and transmitted light (TL) shown for contrast.

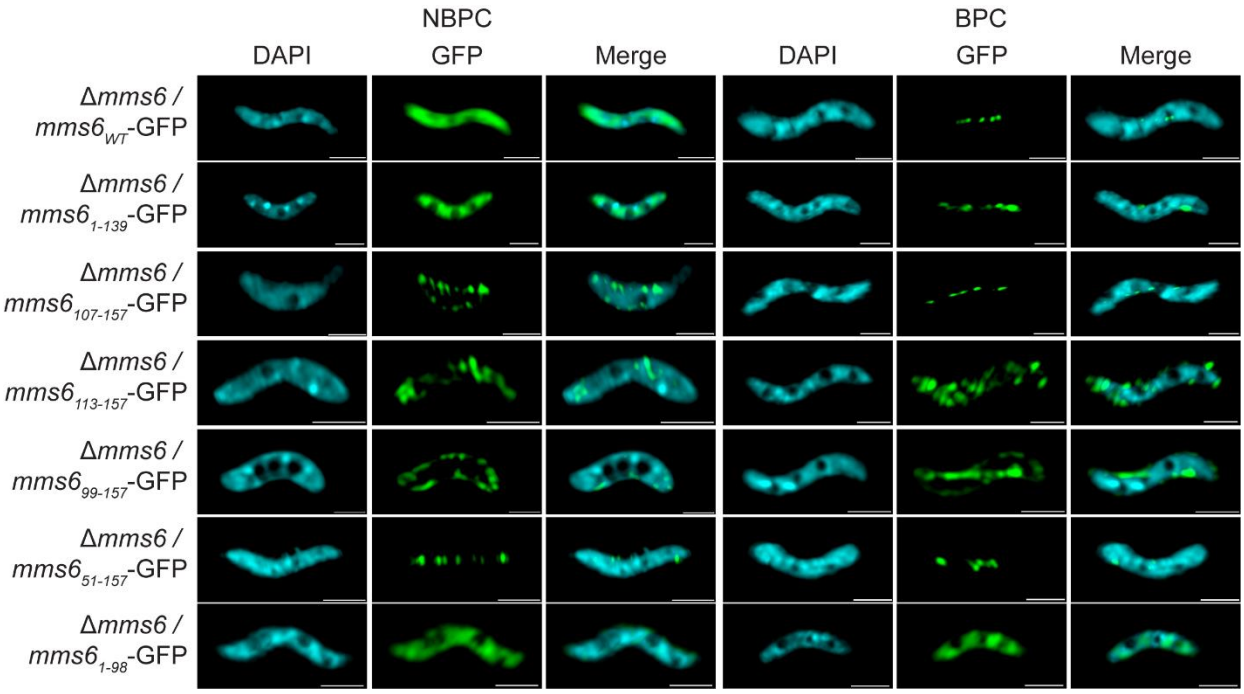

Supplementary Figure 5. Representative super resolution 3D Structured Illumination Microscopy (SIM) images of cells expressing Mms6-GFP. Representative images of Δ*mms6* mutant cells expressing Mms6-GFP or a mutant Mms6 protein tagged C-terminally with GFP. GFP is shown in green and DAPI in blue. Scale bars = 1 µm.

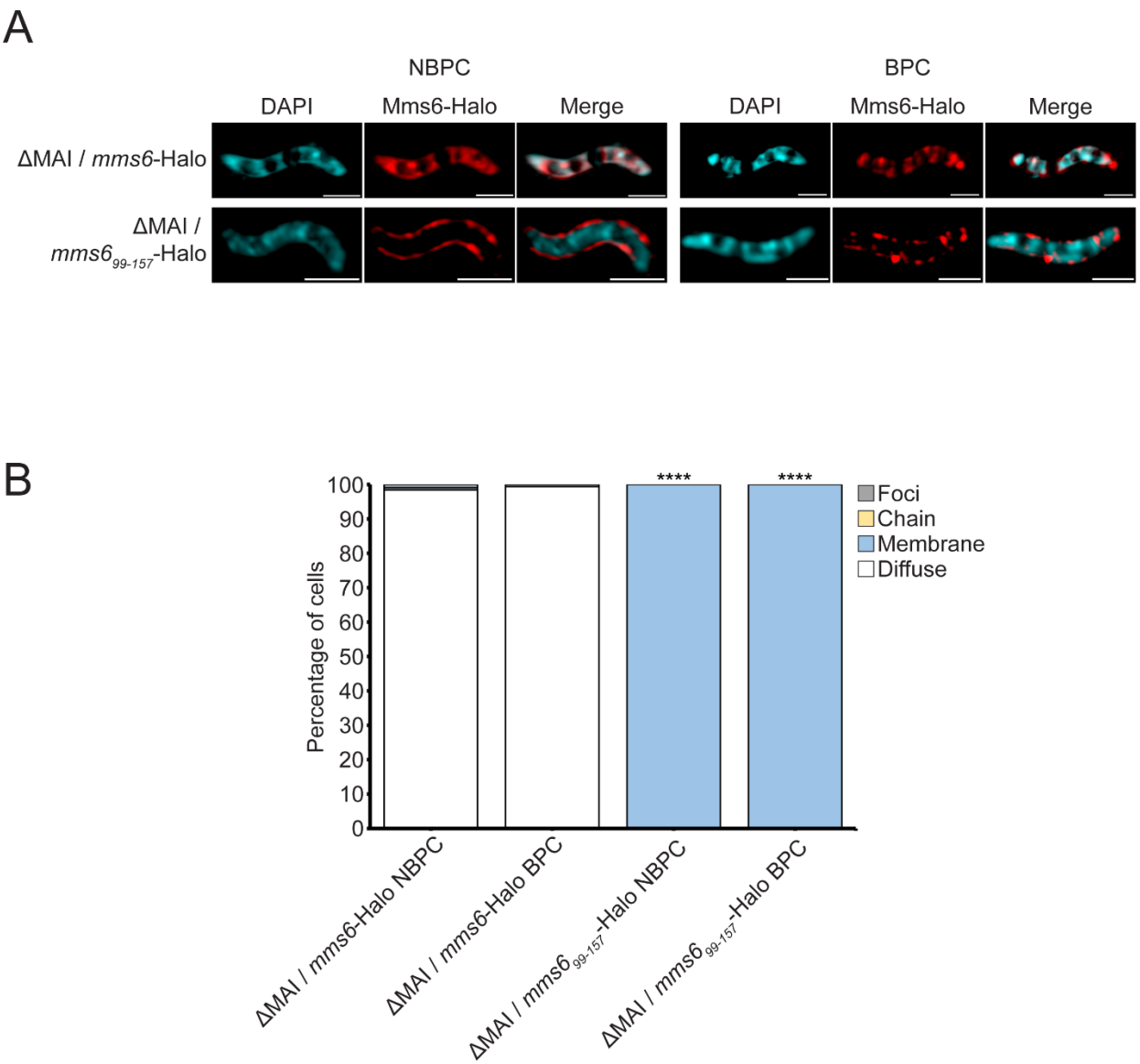

Supplementary Figure 6. Mms6$_{99\text{-}157}$-Halo does not require other magnetosome proteins to translocate into membranes. (A) Representative images of ΔMAI mutant cells expressing Mms6-Halo or Mms6$_{99\text{-}157}$-Halo shown in red. DAPI counterstain is shown in blue. Scale bars = 1 µm. (B) Blind quantification of localization patterns of given protein. *P* values were calculated by Fisher's exact test comparing given dataset to ΔMAI / *mms6*-Halo grown in matching biomineralization condition (**** = $P < 10^{-5}$). ΔMAI / *mms6*-Halo NBPC n = 318 cells, ΔMAI / *mms6*-Halo BPC n = 174 cells, ΔMAI / *mms6*$_{99\text{-}157}$-Halo NBPC n = 82 cells, ΔMAI / *mms6*$_{99\text{-}157}$-Halo BPC n = 23 cells.

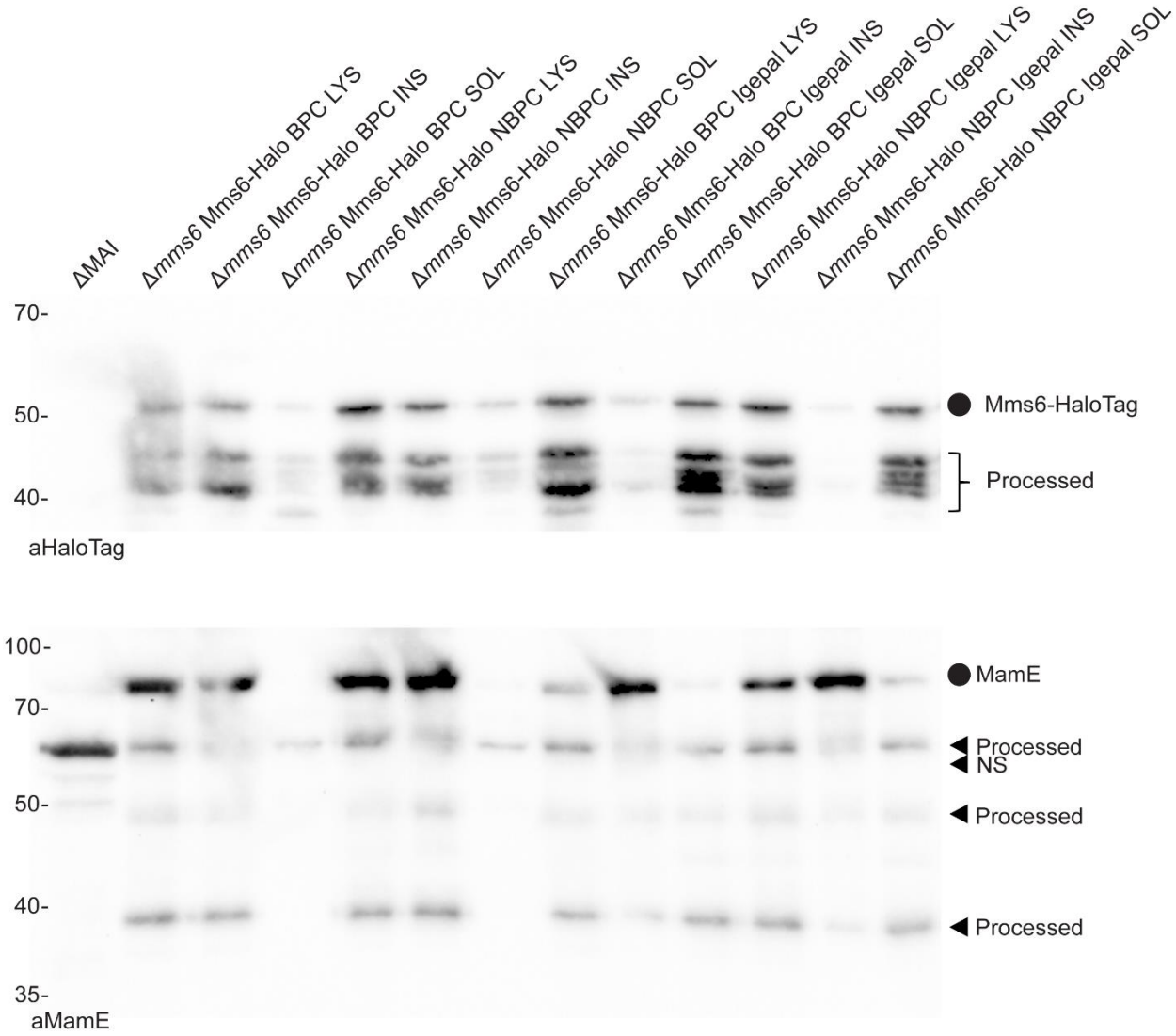

Supplementary Figure 7. Mms6 is weakly associated with insoluble cell contents. Immunoblotting analysis of cell fractions after fractionation of cells expressing Mms6-Halo. HaloTag and MamE were probed for in the whole-cell lysate (LYS) before centrifugation, as well as in insoluble (INS) and soluble (SOL) fractions afterwards. The cell fractionation was performed with and without 0.4% Igepal. Full length protein bands are marked with circles, and both processed fragments and non-specific bands (NS) are marked with arrows.

Strain	Description	Reference
AK30	AMB-1 Wildtype	12
AK31	ΔMAI	37
AK33	Δ*mamL*	37
AK36	ΔR3	37
AK44	Δ*mamM*	37
AK55	Δ*mamN*	37
AK64	Δ*mamI*	37
AK79	Δ*mamA*	19
AK82	Δ*mamK*	46
AK94	Δ*mamO* and deletion of MAI region 9 (R9)	88
AK96	Δ*mamE* Δ*limE*	88
AK103	Δ*mms6*	64
AK104	Δ*mmsF*	64
AK108	Δ*mamJ* Δ*limJ*	47
AK109	Δ*mamF* Δ*mamD* Δ*mamC*	37
AK124	Δ*amb0955* Δ*mms6* Δ*mmsF*	37
AK272	ΔMAI and deletion of magnetosome islet in AMB-1 WT	50
AK329	Δ*mamN* Δ*mamO*	This publication

Supplementary Table 1. Strains used in this study.

Plasmid	Description	Plasmid backbone	Reference
pAK532	Ptac-GFP-*mmsF*	pAK22	64
pAK976	Ptac-mHaloTag	pAK22	84
pAK1101	Ptac-*mms6*-HaloTag	pAK22	50
pAK1102	Ptac-*mms6*-GFP	pAK22	50
pAK1441	Ptac-*mms6* $_{51-157}$-GFP	pAK1102	This publication
pAK1443	Ptac-*mms6* $_{1-139}$-GFP	pAK1102	This publication
pAK1444	Ptac-*mms6* $_{1-98}$-GFP	pAK1102	This publication
pAK1445	Ptac-*mms6* $_{107-157}$-GFP	pAK1102	This publication
pAK1446	Ptac-*mms6* $_{113-157}$-GFP	pAK1102	This publication
pAK1447	Ptac-GFP-*mms6* $_{NTD}$*mmsF*	pAK532	This publication
pAK1456	Ptac-*mms6* $_{99-157}$-GFP	pAK1102	This publication

Supplementary Table 2. Plasmids used in this study.

Primer	Target	Sequence
CB01	pAK-*mms6* $_{1\text{-}98}$-GFP	GATAACAATTTCACACAGGAAACAGAATTCATGCCAGCTCAGATCGCCAACGGAGTTATT
CB02	pAK-*mms6* $_{1\text{-}98}$-GFP	TTCTTCTCCTTTACTCATGGATCCGACGACCTTGGCACCGGCGGC
CB03	pAK-*mms6* $_{99\text{-}157}$-GFP	CAATTTCACACAGGAAACAGAATTCATGGGAACCATCTGGACCGGTAAGGGGCTG
CB04	pAK-*mms6* $_{99\text{-}157}$-GFP	GAAAAGTTCTTCTCCTTTACTCATGGATCCGGCCAGCGCGTCGCGCAGTTCGACTTC
CB05	pAK-*mms6* $_{51\text{-}157}$-GFP	GATAACAATTTCACACAGGAAACAGAATTCATGGTCGCCAAGACCGGCATCGCCGCCAAG
CB06	pAK-*mms6* $_{51\text{-}157}$-GFP	GAAAAGTTCTTCTCCTTTACTCATGGATCCGGCCAGCGCGTCGCGCAGTTCGACTTCCTC
CB07	pAK-*mms6* $_{1\text{-}139}$-GFP	GATAACAATTTCACACAGGAAACAGAATTCATGCCAGCTCAGATCGCCAACGGAGTTATT
CB08	pAK-*mms6* $_{1\text{-}139}$-GFP	GAAAAGTTCTTCTCCTTTACTCATGGATCCACGGCTCTTCATATACGCGTAAACCGCCCC
CB09	pAK-*mms6* $_{107\text{-}157}$-gfp	GATAACAATTTCACACAGGAAACAGAATTCATGGGGCTGGGCCTCGGTCTGGGTCTCGGT
CB10	pAK-*mms6* $_{107\text{-}157}$-gfp	GAAAAGTTCTTCTCCTTTACTCATGGATCCGGCCAGCGCGTCGCGCAGTTCGACTTCCTC
CB11	pAK-*mms6* $_{113\text{-}157}$-gfp	GATAACAATTTCACACAGGAAACAGAATTCATGGGTCTCGGTCTGGGCGCGTGGGGGCCG
CB12	pAK-*mms6* $_{113\text{-}157}$-gfp	GAAAAGTTCTTCTCCTTTACTCATGGATCCATACGCGTAAACCGCCCCGGCGCCAACAAC
CB13	pAK-GFP-mms6$_{NTD}$MmsF	GAAGCGGCGGCCAAAGCAGCAGCGGGATCCCCAGCTCAGATCGCCAACGGAGTTATTTGC
CB14	pAK-GFP-mms6$_{NTD}$MmsF	GCTGCGAAGGATAGCTTCAGTGGATCCGACGACCTTGGCACCGGCGGCGGCCTTG

Supplementary Table 3. Primers used in this study.

Figure	Dataset/strain	Compared datasets/strains	Chi-square test of independence		Cramer's V effect size		
			P-value	Significance	V	df	Effect Size
Figure 1B	NBPC	30 min BPC	0.3517	NS	0.0422	3	Negligible
	NBPC	1 h BPC	$< 10^{-5}$	****	0.3162	3	Large
	NBPC	1.5 h BPC	$< 10^{-5}$	****	0.3496	3	Large
	NBPC	2 h BPC	$< 10^{-5}$	****	0.4602	3	Large
Figure 1I	NBPC	2 h BPC	$< 10^{-5}$	****	0.5654	2	Large
Figure 2E	NBPC	2 h BPC kan/clm	$< 10^{-5}$	****	0.7124	3	Large
	NBPC	2 h BPC	$< 10^{-5}$	****	0.6997	3	Large

Supplementary Table 4. Statistical tests using the Chi-square test of independence. The Chi-square test of independence tests the hypothesis that two variables are unrelated. Cramer's V is an effect size measurement that measures how strongly two categorical fields are associated.

Figure	Dataset/strain	Compared datasets/strains	Mann-Whitney U Test	
			p-value	Significance
Figure 1C	Δ*mms6* / empty vector	Δ*mms6* / *mms6*-GFP	0.000605172	**
	Δ*mms6* / empty vector	Δ*mms6* / *mms6*-Halo	6.92669E-05	***
Figure 5B	Δ*mms6* / empty vector	Δ*mms6* / *mms6*-GFP	0.000605172	**
	Δ*mms6* / empty vector	Δ*mms6* / *mms6*-Halo	6.92669E-05	***
	Δ*mms6* / empty vector	Δ*mms6* / *mms6* $_{1-139}$-GFP	0.000129814	**
	Δ*mms6* / empty vector	Δ*mms6* / *mms6* $_{99-157}$-GFP	0.00125393	*
	Δ*mms6* / empty vector	Δ*mms6* / *mms6* $_{51-157}$-GFP	0.000743289	**
	Δ*mms6* / empty vector	Δ*mms6* / *mms6* $_{1-98}$-GFP	0.518827467	NS
	Δ*mms6* / empty vector	Δ*mms6* / *mms6* $_{113-157}$-GFP	0.00133003	*
	Δ*mms6* / empty vector	Δ*mms6* / *mms6* $_{107-157}$-GFP	0.030961701	NS

Supplementary Table 5. Statistical tests using the Mann Whitney *U* test. The Mann Whitney *U* test is a non-parametric test for the null hypothesis that the means of two populations are equal.

Figure	Dataset/strain	Compared datasets/strains	Fisher's Exact Test		Cramer's V effect size		
			P-value	Significance	V	df	Effect Size
Figure 3C	ΔMAI ΔMIS / *mms6*-GFP NBPC	ΔMAI ΔMIS / GFP-mmsF NBPC	$< 10^{-5}$	****	0.9646	3	Large
	ΔMAI ΔMIS / *mms6*-GFP BPC	ΔMAI ΔMIS / GFP-mmsF BPC	$< 10^{-5}$	****	0.8411	3	Large
Figure 4B	WT / *mms6*-Halo NBPC	Δmms6 / mms6-Halo NBPC	0.1629	NS	0.05754	2	Negligible
	WT / *mms6*-Halo BPC	Δmms6 / mms6-Halo BPC	0.1828	NS	0.03707	2	Negligible
	WT / *mms6*-Halo NBPC	ΔMAI / mms6-Halo NBPC	$< 10^{-5}$	****	0.2387	2	Medium
	WT / *mms6*-Halo BPC	ΔMAI / mms6-Halo BPC	$< 10^{-5}$	****	0.9243	3	Large
	WT / *mms6*-Halo NBPC	ΔmamN / mms6-Halo NBPC	$< 10^{-5}$	****	0.5439	3	Large
	WT / *mms6*-Halo BPC	ΔmamN / mms6-Halo BPC	$< 10^{-5}$	****	0.1856	3	Medium
	WT / *mms6*-Halo NBPC	ΔmamO ΔR9 / mms6-Halo NBPC	$< 10^{-5}$	****	0.3125	2	Medium
	WT / *mms6*-Halo BPC	ΔmamO ΔR9 / mms6-Halo BPC	$< 10^{-5}$	****	0.9166	3	Large
	WT / *mms6*-Halo NBPC	ΔmamM / mms6-Halo NBPC	$< 10^{-5}$	****	0.3163	2	Medium
	WT / *mms6*-Halo BPC	ΔmamM / mms6-Halo BPC	$< 10^{-5}$	****	0.7984	2	Large
	WT / *mms6*-Halo NBPC	ΔmamE ΔlimE / mms6-Halo NBPC	$< 10^{-5}$	****	0.2779	2	Medium
	WT / *mms6*-Halo BPC	ΔmamE ΔlimE / mms6-Halo BPC	$< 10^{-5}$	****	0.9043	2	Large
	WT / *mms6*-Halo NBPC	ΔmamA / mms6-Halo NBPC	0.1676	NS	0.1606	3	Small
	WT / *mms6*-Halo BPC	ΔmamA / mms6-Halo BPC	0.0007271	**	0.2545	2	Medium
	WT / *mms6*-Halo NBPC	Δamb0955 Δmms6 ΔmmsF / mms6-Halo NBPC	$< 10^{-5}$	****	0.4878	3	Large
	WT / *mms6*-Halo BPC	Δamb0955 Δmms6 ΔmmsF / mms6-Halo BPC	0.8531	NS	0.05436	2	Negligible
Figure 5D	Δ*mms6* / *mms6*-GFP NBPC	Δmms6 / mms6$_{1\text{-}139}$-GFP NBPC	0.0208	NS	0.2026	3	Medium
	Δ*mms6* / *mms6*-GFP BPC	Δmms6 / mms6$_{1\text{-}139}$-GFP BPC	0.0010	*	0.2223	2	Medium
	Δ*mms6* / *mms6*-GFP NBPC	Δmms6 / mms6$_{99\text{-}157}$-GFP NBPC	$< 10^{-5}$	****	0.9492	3	Large
	Δ*mms6* / *mms6*-GFP BPC	Δmms6 / mms6$_{99\text{-}157}$-GFP BPC	$< 10^{-5}$	****	0.452	3	Large
	Δ*mms6* / *mms6*-GFP NBPC	Δmms6 / mms6$_{51\text{-}157}$-GFP NBPC	$< 10^{-5}$	****	0.8187	3	Large
	Δ*mms6* / *mms6*-GFP BPC	Δmms6 / mms6$_{51\text{-}157}$-GFP BPC	0.3692	NS	0.0525	2	Negligible
	Δ*mms6* / *mms6*-GFP NBPC	*Δmms6 / mms6 $_{1\text{-}98}$-GFP NBPC*	$< 10^{-5}$	****	0.4793	3	Large
	Δ*mms6* / *mms6*-GFP BPC	*Δmms6 / mms6 $_{1\text{-}98}$-GFP BPC*	$< 10^{-5}$	****	0.9894	2	Large
	Δ*mms6* / *mms6*-GFP NBPC	*Δmms6 / mms6 $_{113\text{-}157}$-GFP NBPC*	$< 10^{-5}$	****	0.4689	3	Large
	Δ*mms6* / *mms6*-GFP BPC	*Δmms6 / mms6 $_{113\text{-}157}$-GFP BPC*	$< 10^{-5}$	****	0.9894	2	Large
	Δ*mms6* / *mms6*-GFP NBPC	*Δmms6 / mms6 $_{107\text{-}157}$-GFP NBPC*	$< 10^{-5}$	****	0.9983	3	Large
	Δ*mms6* / *mms6*-GFP BPC	*Δmms6 / mms6 $_{107\text{-}157}$-GFP BPC*	0.001171	*	0.2525	3	Medium
Figure 6C	WT / GFP-*mmsF* NBPC	WT / GFP-mms6$_{NTD}$mmsF NBPC	$< 10^{-5}$	****	0.7313	3	Large
	WT / GFP-*mmsF* BPC	WT / GFP-mms6$_{NTD}$mmsF BPC	0.4295	NS	0.1129	3	Small

Supplementary Table 6. Statistical tests using the Fisher's exact test. Fisher's exact test tests the same hypothesis as the chi-squared test of independence but is more accurate for sample sizes under 500 and in cases where at least one sample has a value of zero. Cramer's *V* is an effect size measurement that measures how strongly two categorical fields are associated.

Figure	Dataset/strain	Compared datasets/strains	Fisher's Exact Test		Cramer's V effect size		
			P-value	Significance	V	df	Effect Size
Supplementary Figure S1	NBPC	Δmms6 / mms6-Halo 2 h BPC old pool kan/clm	$< 10^{-5}$	****	0.708	2	Large
	NBPC	Δmms6 / mms6-Halo 2 h BPC new pool kan/clm	$< 10^{-5}$	****	0.7224	2	Large
	NBPC	Δmms6 / mms6-Halo 2 h BPC old pool	$< 10^{-5}$	****	0.8382	2	Large
	NBPC	Δmms6 / mms6-Halo 2 h BPC new pool	$< 10^{-5}$	****	0.8116	2	Large
Supplementary Figure S3B	WT / mms6-Halo NBPC	ΔMAI / mms6-Halo NBPC	0.0006087	**	0.09641	3	Small
	WT / mms6-Halo BPC	ΔMAI / mms6-Halo BPC	$< 10^{-5}$	****	0.9416	2	Large
	WT / mms6-Halo NBPC	ΔR3 / mms6-Halo NBPC	$< 10^{-5}$	****	0.2689	3	Medium
	WT / mms6-Halo BPC	ΔR3 / mms6-Halo BPC	0.001183	*	0.1224	2	Small
	WT / mms6-Halo NBPC	ΔmamF ΔmamD ΔmamC / mms6-Halo NBPC	$< 10^{-5}$	****	0.1094	3	Small
	WT / mms6-Halo BPC	ΔmamF ΔmamD ΔmamC / mms6-Halo BPC	0.0159	NS	0.1262	2	Small
	WT / mms6-Halo NBPC	ΔmamJ ΔlimJ / mms6-Halo NBPC	0.03176	NS	0.07292	3	Small
	WT / mms6-Halo BPC	ΔmamJ ΔlimJ / mms6-Halo BPC	$< 10^{-5}$	****	0.2384	3	Medium
	WT / mms6-Halo NBPC	ΔmamK / mms6-Halo NBPC	$< 10^{-5}$	****	0.2223	3	Medium
	WT / mms6-Halo BPC	ΔmamK / mms6-Halo BPC	0.2331	NS	0.07063	2	Small
	WT / mms6-Halo NBPC	ΔmamD / mms6-Halo NBPC	$< 10^{-5}$	****	0.1738	3	Medium
	WT / mms6-Halo BPC	ΔmamD / mms6-Halo BPC	$< 10^{-5}$	****	0.1736	2	Small
	WT / mms6-Halo BPC	ΔmamP / mms6-Halo BPC	$< 10^{-5}$	****	0.1752	2	Small
Supplementary Figure S4B	WT / mms6-GFP NBPC	ΔMAI / mms6-GFP NBPC	$< 10^{-5}$	****	0.5246	2	Large
	WT / mms6-GFP BPC	ΔMAI / mms6-GFP BPC	$< 10^{-5}$	****	0.9888	2	Large
	WT / mms6-GFP NBPC	ΔMAI ΔMIS / mms6-GFP NBPC	$< 10^{-5}$	****	0.3515	2	Large
	WT / mms6-GFP BPC	ΔMAI ΔMIS / mms6-GFP BPC	$< 10^{-5}$	****	0.9777	2	Large
	WT / mms6-GFP NBPC	Δmaml / mms6-GFP NBPC	$< 10^{-5}$	****	0.2313	2	Medium
	WT / mms6-GFP BPC	Δmaml / mms6-GFP BPC	$< 10^{-5}$	****	0.9589	2	Large
	WT / mms6-GFP NBPC	ΔmamL / mms6-GFP NBPC	$< 10^{-5}$	****	0.4136	3	Large
	WT / mms6-GFP BPC	ΔmamL / mms6-GFP BPC	$< 10^{-5}$	****	0.9396	2	Large
	WT / mms6-GFP NBPC	ΔmamN ΔmamO / mms6-GFP NBPC	$< 10^{-5}$	****	0.3577	2	Large
	WT / mms6-GFP BPC	ΔmamN ΔmamO / mms6-GFP BPC	$< 10^{-5}$	****	0.9834	3	Large
Supplementary Figure S6	ΔMAI ΔMIS / mms6-GFP NBPC	ΔMAI ΔMIS / mms6ΔNTD-GFP NBPC	$< 10^{-5}$	****	0.9872	1	Large
	ΔMAI ΔMIS / mms6-GFP BPC	ΔMAI ΔMIS / mms6ΔNTD-GFP BPC	$< 10^{-5}$	****	0.9402	1	Large

Supplementary Table 7. Statistical tests for supplementary figures. Fisher's exact test tests the same hypothesis as the chi-squared test of independence but is more accurate for sample sizes under 500 and in cases where at least one sample has a value of zero. Cramer's *V* is an effect size measurement that measures how strongly two categorical fields are associated.

Chapter 3

MamD is conditionally sorted by magnetosome proteins in a manner similar to Mms6

Carson Bickley and Arash Komeili

Department of Plant and Microbial Biology, University of California, Berkeley, CA, USA

Abstract

Magnetite maturation is a critical step in MTB biomineralization. Once magnetite crystals nucleate inside of magnetosomes, they must be grown and shaped into magnetic particles. A cohort of proteins has been identified as necessary for this process, including MamGFDC, Mms6 and MmsF. These proteins localize to the magnetosome, where they may interact with magnetite crystal directly to guide crystal maturation. How crystal maturation proteins localize to the magnetosome is unclear. Maturation protein Mms6 only localizes to magnetosomes that contain magnetite. Here, we employ fluorescence microscopy to investigate whether the mechanisms that control Mms6 localization are widespread in magnetite maturation proteins. We show that MamD-GFP displays conditional localization similar to Mms6-GFP, but MamF-GFP and MamG-GFP localize to magnetosomes regardless of biomineralization conditions. In addition, we show that the conditional localization of MamD-GFP does not require Mms6. MamN, found to inhibit Mms6 localization also inhibits the localization of MamD-GFP. These results suggest that the mechanisms responsible for Mms6 sorting also coordinate the positioning of MamD. Further work could determine whether MamD can relocalize without new protein synthesis and identify the mechanisms that sort the other crystal maturation proteins.

Introduction

The defining feature of magnetotactic bacteria is their ability to align themselves with magnetic fields. This behavior depends on magnetite crystals that have been grown and shaped into single-domain magnetic nanoparticles. Many MAI proteins have been implicated in growing and shaping developing magnetite crystals. A deletion of the *mamGFDC* operon in *Magnetospirillum gryphiswaldense* MSR-1 (MSR-1) resulted in smaller crystals and lower cellular magnetic response (Cmag) (39). The re-introduction of any single gene from this operon partially restored crystal shape and Cmag, suggesting each gene plays a role in crystal maturation. Another operon in the MAI, the *mms6* operon, is also required for normal crystal growth and shape. MSR-1 and *Magnetospirillum magneticum* AMB-1 (AMB-1) cells lacking Mms6 have misshaped magnetite crystals, resulting in a decrease in cell magnetic response (42,67,68). Purified Mms6 can also shape magnetite crystals forming *in vitro* (9,68). *mmsF*, another gene in the *mms6* operon, is another important crystal growth factor. Expressing only *mmsF* in an AMB-1 strain lacking the entire *mamGFDC* and *mms6* operons almost entirely restores normal crystal size (67).

Past studies have demonstrated that many crystal shaping proteins localize to magnetosomes. MamF, MamC, Mms6, and MmsF all localize to the magnetosome when examined with fluorescence microscopy in AMB-1 (8,67,94). MamD co-fractionates with the magnetosome fraction biochemically, but this result has not yet been corroborated with fluorescence microscopy (9,76). MamG localization in AMB-1 has not been experimentally determined, but it is proposed to localize to magnetosomes similar to its homolog MamG in MSR-1 (6). Some proteins, like Mms6, MamD, and MamC are thought to interact directly with magnetite crystals (9). These three proteins were originally discovered in an assay that extracted and dissolved magnetite crystals with strong acid and SDS, followed by analyzing the protein composition of

the resulting solution (9). Therefore, several magnetite maturation proteins likely interact with magnetite crystals, and would require sorting to the magnetosome to function.

Although magnetosome sorting may be required for the function of crystal-shaping proteins, the mechanism behind their localization is unclear. A study by Arakaki et al. showed that Mms6 only localizes to magnetosomes containing a magnetite crystal (8). In contrast, maturation proteins MamC and MmsF were found to localize to magnetosome membranes even under iron starvation conditions that prevent crystal formation (8). This discrepancy suggests that there may be multiple mechanisms of magnetosome protein localization. Quinlan et al. found that the magnetosome localization of MamC and MamI requires MamE (94). In the previous chapter, the magnetosome localization of Mms6 was found to also depend on MamE. These results suggest that MamE has a role in sorting magnetosome proteins. Past work by Tanaka et al. (68) found that MamC and MamD were depleted from the fraction tightly bound to magnetite crystal in Δ*mms6,* suggesting that Mms6 may also recruit crystal-shaping proteins to the magnetosome.

In related findings, the localization of crystal growth and shaping proteins has been linked to a membrane growth control checkpoint regulated by MamE. Cornejo et al. identified MamE as a key regulator of magnetosome membrane size (90). MamE is a serine protease that has several identified magnetosome protein targets, including Mms6 and MamD (10). MamD was suggested to restrict magnetosome membrane size until the magnetite crystal reaches a size threshold, at which point MamE cleaves MamD and magnetite crystal and membrane growth both continue. MamE is bifunctional, controlling both this membrane checkpoint via protease activity and also controlling protein localization by a different, unknown, mechanism (94). Upstream, MamE protease activity is activated by iron-bound MamO and MamM proteins (10). These results suggest that MamE, MamO, and MamM control an iron-dependent membrane-regulation system which controls the localization of downstream magnetosome assembly proteins. Work shown in the previous chapter suggests that Mms6 localization may be regulated by this checkpoint. In particular, Mms6 localizes in response to iron conditions and requires MamE, MamO, and MamM to localize. Another protein essential for magnetite crystal formation, MamN, was found to inhibit Mms6 localization to empty magnetosomes. In *mamN* deletion mutants, Mms6 was localized to magnetosomes regardless of biomineralization conditions. Therefore, under biomineralization conditions, MamE, activated by MamM and MamO, may inhibit MamN, allowing Mms6 to localize to magnetosomes. Alternatively, MamE may act directly on Mms6, independent of the effects of MamN.

Here, we investigate whether this sorting system controls other magnetite maturation proteins, or if it is unique to Mms6. We determine the locations of several crystal maturation proteins under biomineralization permissible conditions (BPC) and non-biomineralization permissible conditions (NBPC) in wild-type AMB-1 and in several deletion mutants. Tested proteins include those made by the *mamGFDC* and *mms6* operons due to their functions in magnetite development. Using fluorescence microscopy, we identify MamD as a conditionally localizing protein like Mms6. Furthermore, we find that MamD does not require Mms6 for localization and that its magnetosome localization is inhibited by MamN. These findings suggest that the localization of MamD and Mms6 are regulated by the same system, and that both may be

recruited to help nucleate or shape crystals after biomineralization permissible conditions are detected.

Results

MamD localizes conditionally to magnetosomes

To investigate the sorting of magnetite maturation proteins, we compared their localization in biomineralization and non-biomineralization conditions. Mms6 is the only MAI protein known to localize to magnetosomes only in biomineralization permissible conditions. This localization strategy may be the most efficient for crystal shaping proteins because the protein only localizes to magnetosomes when there is a crystal to interact with. Therefore, we investigated whether other crystal maturation proteins, made by the *mms6* and *mamGFDC* operons, were sorted in the same way. The N-terminal domain (NTD) is required to retain Mms6 in a diffuse non-membrane associated-associated condition in NBPC (Fig. 1A). The glycine leucine repeat region (GL) is structurally similar to a protein binding domain found in silk fibroin and may mediate protein-protein interactions (83). The magnetite-interacting component (MIC) is a region of acidic amino acids that can bind ferric iron, ferrous iron, and magnetite (29,68,70,84,86,87), and may help nucleate or directly interact with magnetite crystal.

To investigate protein sorting, WT cells expressing GFP-tagged proteins were grown in either BPC or NBPC. Briefly, WT AMB-1 cultures were grown either in MG media with 20 μM ferric malate to allow biomineralization or were passaged 3 times in oxalic acid washed green cap tubes and grown in MG media without added iron to prevent biomineralization. Cells were imaged using fluorescence microscopy, file names of images were scrambled to ensure blind analysis, and localization patterns of GFP tagged proteins were quantified. Localization was categorized as either “Foci” indicating one or more unaligned bright foci, “Chain” indicating linear pattern representative of alignment to the magnetosome chain, “Membrane” indicating protein throughout the cell membrane, or “Diffuse” indicating protein diffuse in the cytoplasm.

Mms6-GFP, as previously described, was mostly chain aligned under BPC and cytosolic under NBPC (Fig. 1B,C). GFP-MmsF, in contrast, localizes to magnetosomes regardless of biomineralization conditions (Fig. 1B,C). MamG-GFP, MamF-GFP, and MamC-GFP also displayed magnetosome localization in most cells in both conditions (Fig. 1B,C). Although the distribution of protein localization patterns was significantly different between BPC and NBPC for these proteins by Fisher’s exact test, the effect sizes were small, and the majority of cells show chain-aligned protein. This suggests that the proteins localize to magnetosomes under both BPC and NBPC. In contrast to these proteins, MamD displayed conditional localization similar to Mms6 (Fig. 1B,C). MamD-GFP localizes to magnetosomes in most cells only under biomineralization conditions and is distributed on the inner membrane under non-biomineralization conditions. Notably, MamD-GFP was membrane-localized under non-biomineralization conditions, whereas Mms6-GFP appears diffuse in the cytoplasm. This may suggest that the localization of MamD is regulated differently from that of Mms6. Regardless,

the identification of MamD as a conditionally localizing protein suggests the existence of a class of MAI proteins that are localized in response to cell conditions to aid in magnetite development.

Extrinsic factors required for MamD localization

Two possibilities could explain the conditional localization of MamD-GFP to magnetosomes. First, MamD may be recruited directly by Mms6, which itself displays conditional localization. Second, like Mms6, MamD may be sorted to the magnetosome only during biomineralization via the MamEOMN proteins. To differentiate between these possibilities, we examined the localization of magnetite maturation proteins expressed in WT and in mutants lacking *mms6* or other genes found to be important for Mms6 localization. These experiments show that GFP-MmsF, MamF-GFP, MamD-GFP, and MamC-GFP do not require *mms6* for magnetosome localization (Fig. 2A,B). The localization distribution of each fusion protein shows a slight but significant increase in chain alignment in the *Δmms6* background, perhaps due to a decrease in protein mass in the magnetosome membrane.

To explore the possibility that localization of the selected magnetite maturation proteins is controlled by the same factors that control Mms6 localization, the proteins were expressed in various mutant backgrounds. Whereas GFP-MmsF localized to magnetosomes regardless of biomineralization conditions in WT as previously shown, it was distributed around the inner membrane in a strain lacking the MAI and magnetosome gene islet (MIS) (Fig. 3A,B). Similar to Mms6-Halo, GFP-MmsF fails to localize to magnetosomes in Δ*mamO* cells (Fig. 3A,B). However, in contrast to Mms6-Halo, GFP-MmsF does not localize to magnetosomes in the absence of *mamN.* These results show that while MamN inhibits Mms6 localization, it is required for MmsF localization to magnetosomes.

MamD-GFP localized in WT cells to the magnetosomes under biomineralization conditions and was dispersed around the inner membrane under non-biomineralization conditions, as shown in the previous figure (Fig. 3A,B). In ΔMAI ΔMIS or Δ*mamO*, MamD-GFP was dispersed on the inner membrane as it was in the absence of magnetite formation (Fig. 3A,B). In contrast, in a Δ*mamN* background, the majority of cells have MamD-GFP at magnetosomes regardless of biomineralization conditions. This localization pattern is reminiscent of Mms6-Halo expressed in a *ΔmamN* background, suggesting that the magnetosome localization of MamD, like Mms6, is inhibited by MamN (Fig. 3A,B). These findings suggest that there are at least two magnetite maturation protein sorting systems in AMB-1, one that sorts Mms6 and MamD based on biomineralization conditions through inhibition by MamN, and one in which proteins like MamG, MamF, and MamC are sorted to magnetosomes before biomineralization begins. Further work could continue to uncover the components of the system regulating magnetite crystal development.

Discussion

In magnetotactic bacteria, magnetotaxis is thought to be necessary for navigation to favorable growth conditions in the oxic-anoxic transition zone (2,95). Effective magnetotaxis requires the development of magnetic magnetite crystals. It is unclear how the cohort of proteins responsible for crystal development is sorted to the magnetosome membrane. Investigations into Mms6 in the previous chapter revealed an efficient strategy where magnetite development proteins are sorted to magnetosomes only when magnetite is being formed. MmsF, in contrast, was found to localize to magnetosome membranes regardless of biomineralization condition. This discrepancy raised the question of how the other crystal maturation proteins localize, and whether their positioning can be used to learn more about their functions and regulation.

To address this question, we expressed GFP-tagged magnetite development proteins in various conditions and deletion mutants. Our experiments were consistent with previous findings that MamF, MamD, and MamC localize to the magnetosome in AMB-1 (8,9,67,94,96). Furthermore, we performed the first analysis of MamG localization in AMB-1 and show that it localizes to magnetosomes as in MSR-1 (Fig. 1B,C) (6). By analyzing protein localization under different growth conditions, we found that MmsF and MamC localize to magnetosomes whether or not biomineralization is permitted, consistent with previous work done by Arakaki et al. (8). We also identified MamG and MamF as proteins that localize to magnetosomes regardless of biomineralization conditions (Fig. 1B,C). In contrast, we found that MamD-GFP only localizes to magnetosomes when biomineralization can occur, similar to the behavior of Mms6 (8). Past work by Tanaka et al. found that MamC and MamD were depleted from the fraction tightly bound to magnetite crystal in Δ*mms6* (68). In contrast, we found that *mms6* was not needed for the constitutive magnetosome localization of MamC or the conditional localization of MamD, suggesting that they localize independently of Mms6 (Fig. 2A,B). This difference could indicate that Mms6, rather than recruiting these proteins, binds to them once they localize to magnetosomes and increases protein retention at the magnetite crystal. Next, we found that *mamO* was required for both MamD and MmsF localization (Fig. 3A,B). This suggests that MamO, like MamE, may be involved in localizing both sets of maturation proteins. The deletion of *mamN*, however, prevented MmsF magnetosome localization but caused MamD to localize to magnetosomes under any biomineralization condition (Fig. 3A,B). Therefore, MamN may be involved in recruitment of MmsF while it inhibits the localization of MamD. This may suggest that MmsF is required for an earlier stage of magnetosome formation, such as protein recruitment or redox control, while magnetite shaping proteins are recruited once magnetite formation begins.

In the previous chapter, we found that Mms6 localization to magnetosomes is inhibited by MamN. How Mms6 overcomes MamN inhibition is still unknown but could happen during the membrane growth checkpoint (90) or at another uncharacterized step. Magnetosome membranes grow until stalling at a size threshold, when MamE, activated by MamO and MamM, proteolyzes protein targets, allowing further magnetosome growth. Wan et al. determined that MamD inhibits the size of membranes, likely to facilitate the concentration of mineral that allows for magnetite nucleation (10). Once the checkpoint is reached, activated MamE cleaves MamD in a process dependent on the MamE protease domain, and the membrane can resume expansion. For this checkpoint to work as described, MamD must localize to the magnetosome membrane, in

proximity to MamE, prior to the point where the membrane growth stalls. If MamD is localized coincident with the checkpoint and then is immediately processed by MamE, it would be unable to perform its predicted function of delaying membrane growth. Therefore, we propose that conditionally localizing proteins associate with magnetosomes prior to the membrane growth checkpoint. In this model, MmsF and other crystal maturation proteins like MamG and MamF are first recruited to the magnetosome, either during or after magnetosome membrane formation (Fig. 4). This process happens through an unknown mechanism that may depend on MamO and MamN. Until biomineralization permissible conditions are detected, MamN inhibits the magnetosome localization of Mms6 and MamD. Once biomineralization is possible, MamN inhibition is overcome and Mms6 and MamD can then localize to magnetosomes to help nucleate magnetite crystals. MamN inhibition may occur through interaction with MamE, possibly after MamE is activated by MamM and MamO. Once at magnetosomes, MamD keeps membranes under the membrane size threshold until nucleation is complete in order to increase the local iron concentration in the lumen. Once nucleation has begun, the MamE protease domain is activated by MamM and MamO and cleaves MamD, allowing membrane growth.

Further investigation into the localization of MamD could determine which localization dynamics it shares with Mms6. For instance, a HaloTag variant could be used in pulse-chase experiments to determine whether MamD relocalization requires new protein synthesis. Also, truncated MamD variants could be useful to determine the effects of its domains upon function and conditional localization. Overall, these experiments identify MamD as a conditionally sorted magnetite maturation protein that localizes independently of Mms6. This study expands our understanding of localization dynamics and regulation of magnetite shaping proteins and confirms the importance of MamN to protein sorting. Future work on magnetite development proteins could enable greater control over magnetite production and customization for research and industrial applications.

Materials and Methods

Bacterial growth and cellular magnetic response

The strains used in this study are described in Table S1. AMB-1 stock cultures were grown as described by picking single colonies and growing in 1.5 mL Magnetospirillum growth (MG) medium in 1.7 mL microtubes tubes (Genesee Scientific Cat #24-281) at 30 °C for 3 to 4 d with 15 µl Wolfe's vitamin solution and 20 µM ferric malate. To start larger volume cultures, stock cultures were diluted 1:100 in 10 mL MG medium in 24 mL capped tubes and grown at 30 °C for 2 d in a 10% oxygen microaerobic chamber. Antibiotic selection was done with 10 µg/mL kanamycin in MG media plates and 7 µg/mL kanamycin in liquid MG cultures.

Escherichia coli (E. coli) cultures were grown in 10 mL lysogeny broth in 24 mL capped tubes on a rotating wheel at 37 °C for about 10 h. Antibiotic selection was done with 50 µg/mL kanamycin. An addition of 300 µM diaminopimelic acid was necessary to grow E. coli strain WM3064 for conjugation.

Genetic manipulation

Oligonucleotides were designed in sequence analysis software Geneious using the Magnetospirillum magneticum AMB-1 genome sequence NC_007626.1 and were manufactured by Elim Biopharm or Integrated DNA Technologies. DNA fragments were amplified using GoTaq master mix (Promega Cat #M7123). Plasmids were introduced into AMB-1 through conjugation and are listed in supplementary table S2.

Several plasmids were created to express truncated versions of Mms6 with a GFP fusion tag. To create pAK1440 (*mamG*-GFP), *mamG* was amplified from AMB-1 genomic DNA using the primers listed in supplementary table S3 and inserted by Gibson assembly into multiple cloning vector pAK22, following vector digestion with BamHI-HF and EcoRI-HF restriction enzymes (New England Biolabs).

Fluorescence microscopy and localization pattern quantification

To analyze Mms6 localization in AMB-1 cells, cells growing in 10 mL MG medium were collected once reaching an optical density of OD_{400} 0.08-.015 by centrifugation at 10,000 x g for 3 min. Cell pellets expressing a HaloTag fusion were resuspended in 100 µL MG medium, incubated with 500 nM HaloTag 549 (Promega Cat #GA1110) ligand for 60 min in the dark at 30 °C, and centrifuged at 10,000 x g for 3 min. All cell pellets were then resuspended in 100 µL fresh MG medium and stained with 1.4 µM 4’,6-diamidino-2-phenylindole (DAPI) (Cell Signaling Technology Cat #4083S) for 15 min in the dark at 30 °C. Cells were then centrifuged at 10,000 x g for 3 min and washed 3 times with 100 µL fresh MG medium for 10 min in the dark at 30 °C. After washing, cells were resuspended in 10 µL fresh MG medium and 0.8 µL cell mixture was added to a slide and sealed under a coverslip using nail polish to reduce drying. Slides were imaged at 1000x magnification using the QImaging Retiga 1350ex camera in a Zeiss Axioimager M2 fluorescence microscope. Localization of proteins was quantified using the ImageJ Cell Counter plugin to categorize the localization in each cell into one of several categories including diffuse, foci, and chain aligned. Image file names were obscured using the ImageJ Randomizer macro for unbiased counting.

Statistics and reproducibility

The fisher’s exact test was used to assess significant differences in localization pattern distribution between samples. The statistical tests were performed in RStudio using R version 4.2.2. Deep TMHMM was used to detect transmembrane regions.

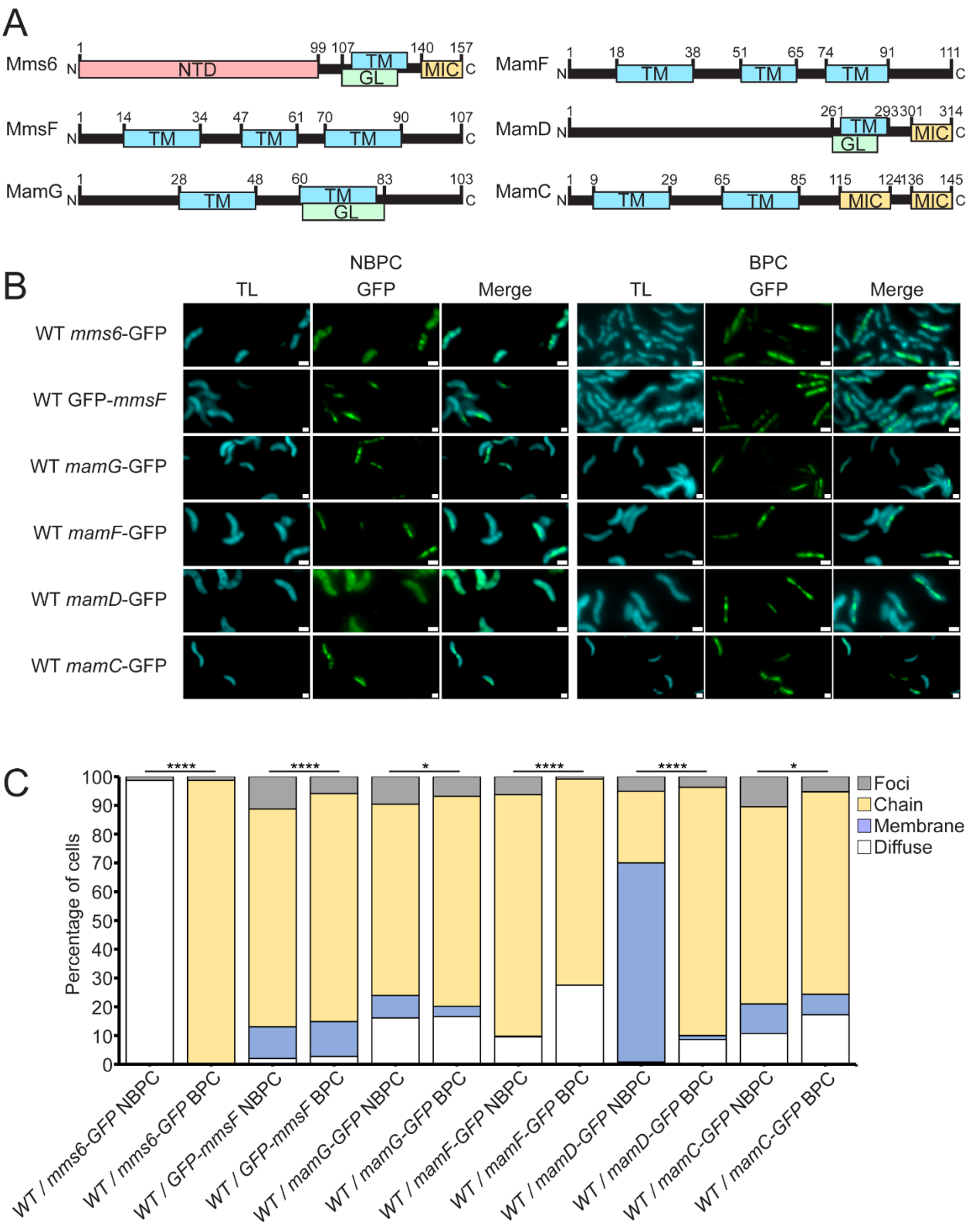

Figure 1. Some magnetosome membrane proteins have localization patterns conditional on biomineralization. (A) Structural features of several magnetosome proteins implicated in crystal

maturation. N-terminal domains (NTD), glycine leucine repeat domains (GL), transmembrane domains (TM), magnetite-binding component (MIC). (B) Representative fluorescence microscopy images of WT AMB-1 cells grown under standard growth conditions expressing magnetosome protein GFP fusions. GFP is shown in green, and transmitted light (TL) is displayed to show outlines of AMB-1 cells. Scale bars = 1 μm. (C) Blind quantification of localization patterns of GFP tagged magnetosome proteins *in vivo*. Cells were categorized by localization pattern. The Y-axis represents percentage of total cell count with indicated protein fluorescence pattern. *P* values were calculated by Fisher's exact test comparing indicated datasets (* $P < .01$) (**** $P < 10^{-5}$). Effect sizes are listed in supplementary table S4. WT / *mms6*-GFP NBPC *n* = 1074 cells, WT / *mms6*-GFP BPC *n* = 1317 cells, WT / GFP-*mmsF* NBPC *n* = 2412 cells, WT / GFP-*mmsF* BPC *n* = 1295 cells, WT / *mamG*-GFP NBPC *n* = 1116 cells, WT / *mamG*-GFP BPC *n* = 367 cells, WT / *mamF*-GFP NBPC *n* = 1238 cells, WT / *mamF*-GFP BPC *n* = 1784 cells, WT / *mamD*-GFP NBPC *n* = 1041 cells, WT / *mamD*-GFP BPC *n* = 971 cells, WT / *mamC*-GFP NBPC *n* = 372 cells, WT / *mamC*-GFP BPC *n* = 1253 cells.

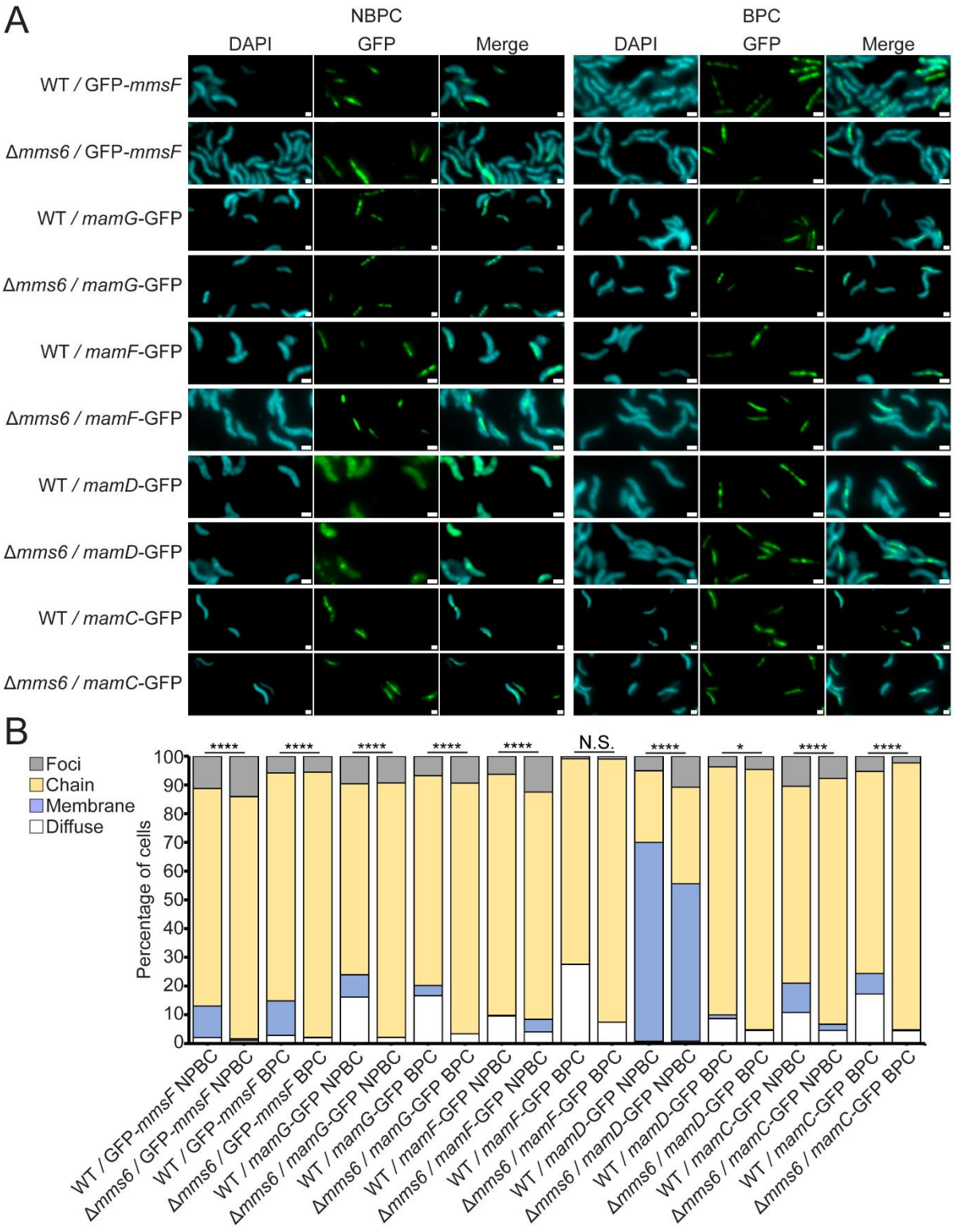

Figure 2. *mms6* is not necessary for magnetite maturation protein localization. (A) Representative fluorescence microscopy images of WT AMB-1 cells grown under standard growth conditions expressing magnetosome protein GFP fusions. GFP is shown in green and 4',6-diamidino-2-phenylindole (DAPI), a DNA-binding fluorescent dye, is shown as a

counterstain in blue. Scale bars = 1 μm. (B) Blind quantification of localization patterns of GFP tagged magnetosome proteins *in vivo* expressed in either WT or *Δmms6* cells. The Y-axis represents percentage of total cell count with indicated protein fluorescence pattern. *P* values were calculated by Fisher's exact test comparing indicated datasets (N.S. no significant difference $P > .01$) (* $P < .01$) (**** $P < 10^{-5}$). WT / GFP-*mmsF* NBPC $n = 2412$ cells, *Δmms6* / GFP-*mmsF* NBPC $n = 497$ cells, WT / GFP-*mmsF* BPC $n = 1295$ cells, *Δmms6* / GFP-*mmsF* BPC $n = 1062$ cells, WT / *mamG*-GFP NBPC $n = 1116$ cells, *Δmms6* / *mamG*-GFP NBPC $n = 1440$ cells, WT / *mamG*-GFP BPC $n = 367$ cells, *Δmms6* / *mamG*-GFP BPC $n = 1560$ cells, WT / *mamF*-GFP NBPC $n = 1238$ cells, *Δmms6* / *mamF*-GFP NBPC $n = 1583$ cells, WT / *mamF*-GFP BPC $n = 1784$ cells, *Δmms6* / *mamF*-GFP BPC $n = 2381$ cells, WT / *mamD*-GFP NBPC $n = 1041$ cells, *Δmms6* / *mamD*-GFP NBPC $n = 1372$ cells, WT / *mamD*-GFP BPC $n = 971$ cells, *Δmms6* / *mamD*-GFP BPC $n = 1660$ cells, WT / *mamC*-GFP NBPC $n = 372$ cells, *Δmms6* / *mamC*-GFP NBPC $n = 793$ cells, WT / *mamC*-GFP BPC $n = 1253$ cells, *Δmms6* / *mamC*-GFP BPC $n = 1881$ cells.

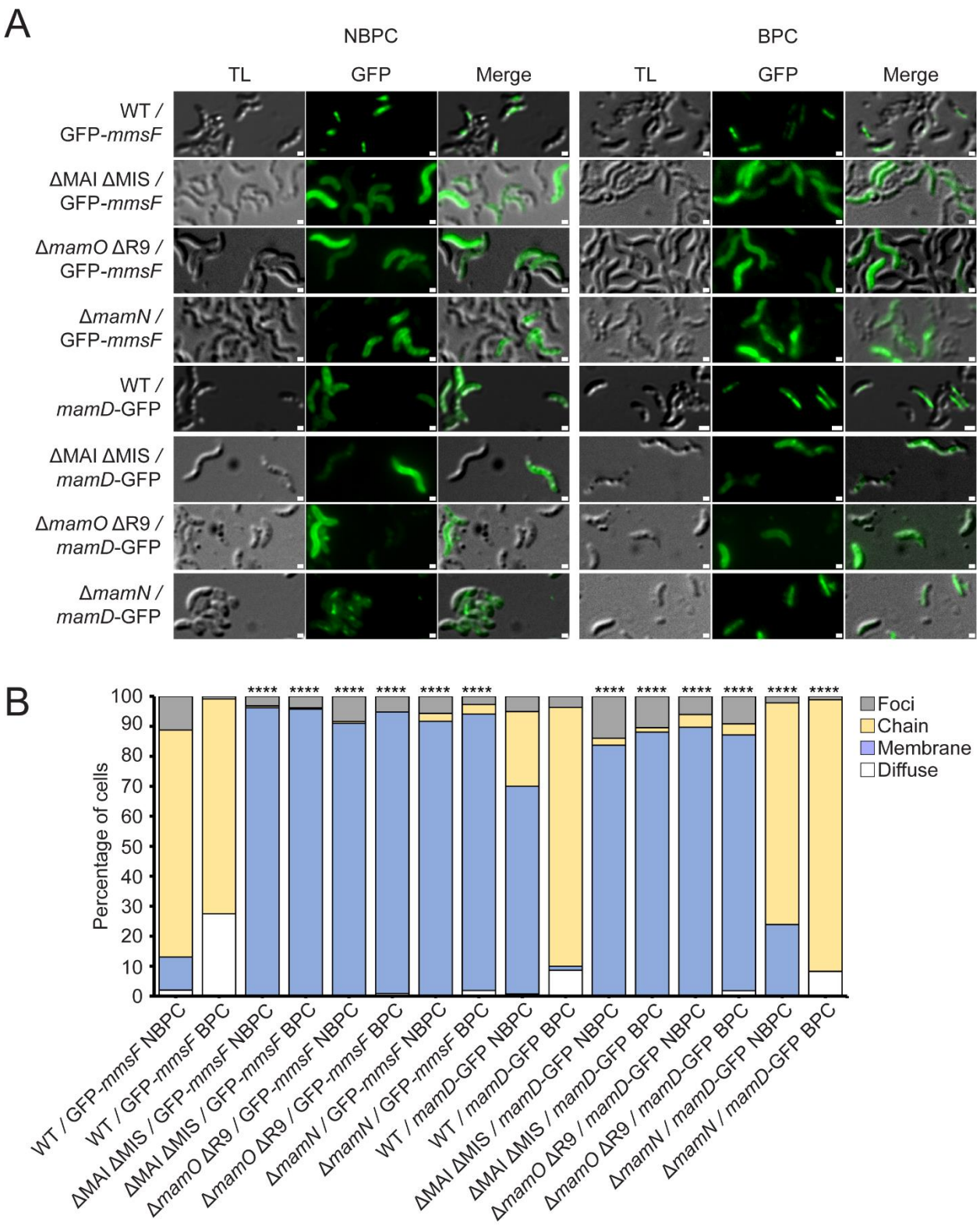

Figure 3. MamN inhibits MamD localization. (A) Representative fluorescence microscopy images of WT AMB-1 cells grown under standard growth conditions expressing magnetosome protein GFP fusions. GFP is shown in green, and TL is displayed to show outlines of AMB-1

cells. Scale bars = 1 μm. (B) Blind quantification of localization patterns of GFP tagged magnetosome proteins *in vivo* expressed in cells with indicated mutant background. The Y-axis represents percentage of total cell count with indicated protein fluorescence pattern. *P* values were calculated by Fisher's exact test comparing indicated datasets to the WT dataset (**** $P < 10^{-5}$). WT / GFP-*mmsF* NBPC *n* = 2412 cells, WT / GFP-*mmsF* BPC *n* = 1295 cells, ΔMAI ΔMIS / GFP-*mmsF* NBPC *n* = 1034 cells, ΔMAI ΔMIS / GFP-*mmsF* BPC *n* = 519 cells, Δ*mamO* ΔR9 / GFP-*mmsF* NBPC *n* = 478 cells, Δ*mamO* ΔR9 / GFP-*mmsF* BPC *n* = 91 cells, Δ*mamN* / GFP-*mmsF* NBPC *n* = 421 cells, Δ*mamN* / GFP-*mmsF* BPC *n* = 524 cells, WT / *mamD*-GFP NBPC *n* = 1041 cells, WT / *mamD*-GFP BPC *n* = 971 cells, ΔMAI ΔMIS / *mamD*-GFP NBPC *n* = 43 cells, ΔMAI ΔMIS / *mamD*-GFP BPC *n* = 67 cells, Δ*mamO* ΔR9 / *mamD*-GFP NBPC *n* = 218 cells, Δ*mamO* ΔR9 / *mamD*-GFP BPC *n* = 165 cells, Δ*mamN* / *mamD*-GFP NBPC *n* = 2599 cells, Δ*mamN* / *mamD*-GFP BPC *n* = 1833 cells.

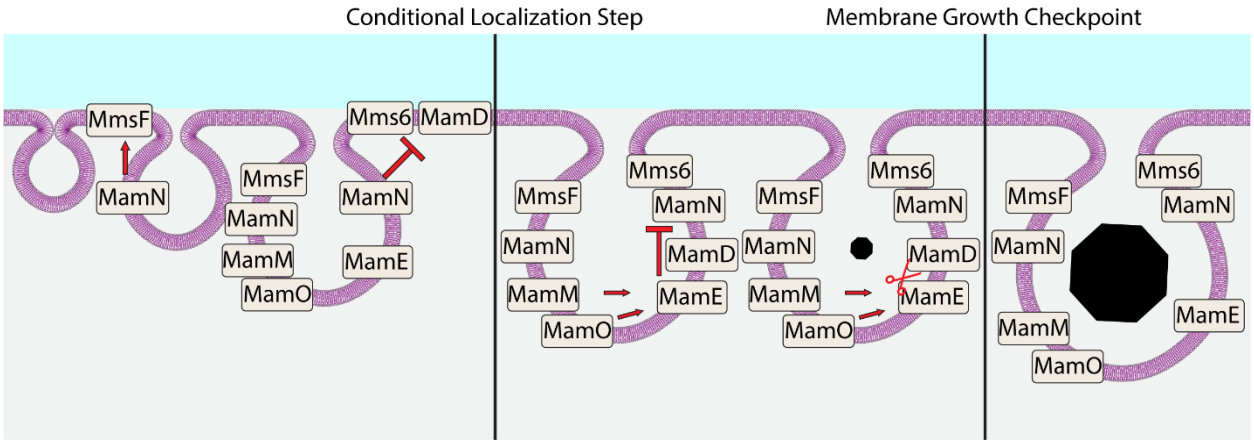

Figure 4. Model of magnetite maturation protein sorting. MamN, MamO, and likely other proteins promote the recruitment of MmsF through an unknown mechanism. After magnetosome membrane formation, but before biomineralization begins, MamN inhibits localization of Mms6 and MamD. Once biomineralization conditions are reached, MamO and MamM activate MamE, which may deactivate MamN, allowing Mms6 and MamD to localize to the magnetosome, where they aid in magnetite nucleation. MamD works to restrict membranes under a size threshold to concentrate mineral, facilitating nucleation. Once magnetite is nucleated, MamE protease domain is activated by MamO and MamM, cleaving MamD and allowing further membrane expansion.

Strain	Description	Reference
AK30	AMB-1 Wildtype	12
AK31	ΔMAI	37
AK55	Δ*mamN*	37
AK94	Δ*mamO* and deletion of MAI region 9 (R9)	88
AK103	Δ*mms6*	64
AK272	ΔMAI and deletion of magnetosome islet in AMB-1 WT	50

Supplementary Table 1. Strains used in this study.

Plasmid	Description	Plasmid backbone	Reference
pAK272	Ptac-*mamI*-GFP	pAK22	50
pAK452	Ptac-*mamC*-GFP	pAK22	88
pAK454	Ptac-*mamF*-GFP	pAK22	88
pAK532	Ptac-GFP-*mmsF*	pAK22	64
pAK976	Ptac-mHaloTag	pAK22	84
pAK1101	Ptac-*mms6*-HaloTag	pAK22	50
pAK1102	Ptac-*mms6*-GFP	pAK22	50
pAK1204	Ptac-*mamD*-GFP	pAK22	This work
pAK1440	Ptac-*mamG*-GFP	pAK22	This work

Supplementary Table 2. Plasmids used in this study.

Primer	Target	Sequence
CB15	Ptac-*mamG*-GFP	GATAACAATTTCACACAGGAAACAGAATTCATGGCCGCTCAGGTTGGAGGGCAGATTTTG
CB16	Ptac-*mamG*-GFP	GAAAAGTTCTTCTCCTTTACTCATGGATCCAGTCGCATCGGCGGCGGCATCAACCTC

Supplementary Table 3. Primers used in this study.

Figure	Compared datasets/strains		Fisher's Exact Test		Cramer's V effect size		
			P-value	Significance	V	df	Effect Size
Figure 1B	WT / mms6-GFP NBPC	WT / mms6-GFP BPC	$< 10^{-5}$	****	0.6677	2	Large
	WT / mmsF-GFP NBPC	WT / mmsF-GFP BPC	$< 10^{-5}$	****	0.08813	3	Small
	WT / mamF-GFP NBPC	WT / mamF-GFP BPC	$< 10^{-5}$	****	0.1553	3	Small
	WT / mamG-GFP NBPC	WT / mamG-GFP BPC	0.00234	*	0.09648	3	Small
	WT / mamD-GFP NBPC	WT / mamD-GFP BPC	$< 10^{-5}$	****	0.7168	3	Large
	WT / mamC-GFP NBPC	WT / mamC-GFP BPC	0.0014	*	0.1003	3	Small
	WT / mamI-GFP NBPC	WT / mamI-GFP BPC	$< 10^{-5}$	****	0.3058	3	Large
Figure 2A	WT / mamG-GFP NBPC	Δmms6 / mamG-GFP NBPC	$< 10^{-5}$	****	0.2454	3	Medium
	WT / mamG-GFP BPC	Δmms6 / mamG-GFP BPC	$< 10^{-5}$	****	0.1891	3	Medium
	WT / mamF-GFP NBPC	Δmms6 / mamF-GFP NBPC	$< 10^{-5}$	****	0.1673	3	Small
	WT / mamF-GFP BPC	Δmms6 / mamF-GFP BPC	0.8683	NS	0.00329	2	Negligible
	WT / mmsD-GFP NBPC	Δmms6 / mmsD-GFP NBPC	$< 10^{-5}$	****	0.1562	3	Small
	WT / mmsD-GFP BPC	Δmms6 / mmsD-GFP BPC	0.0047	*	0.06711	3	Small
	WT / mmsF-GFP NBPC	Δmms6 / mmsF-GFP NBPC	$< 10^{-5}$	****	0.1386	3	Small
	WT / mmsF-GFP BPC	Δmms6 / mmsF-GFP BPC	$< 10^{-5}$	****	0.259	3	Medium
	WT / mamC-GFP NBPC	Δmms6 / mamC-GFP NBPC	$< 10^{-5}$	****	0.2068	3	Medium
	WT / mamC-GFP BPC	Δmms6 / mamC-GFP BPC	$< 10^{-5}$	****	0.1348	3	Small
Figure 3A	WT / mmsF-GFP NBPC	ΔMAI ΔMIS / mmsF-GFP NBPC	$< 10^{-5}$	****	0.8116	3	Large
	WT / mmsF-GFP NBPC	ΔmamO ΔR9 / mmsF-GFP NBPC	$< 10^{-5}$	****	0.5948	3	Large
	WT / mmsF-GFP NBPC	ΔmamN / mmsF-GFP NBPC	$< 10^{-5}$	****	0.6834	3	Large
	WT / mmsF-GFP BPC	ΔMAI ΔMIS / mmsF-GFP BPC	$< 10^{-5}$	****	0.7927	3	Large
	WT / mmsF-GFP BPC	ΔmamO ΔR9 / mmsF-GFP BPC	$< 10^{-5}$	****	0.7644	3	Large
	WT / mmsF-GFP BPC	ΔmamN / mmsF-GFP BPC	$< 10^{-5}$	****	0.7738	3	Large
	WT / mamD-GFP NBPC	ΔMAI ΔMIS / mamD-GFP NBPC	$< 10^{-5}$	****	0.1213	3	Small
	WT / mamD-GFP NBPC	ΔmamO ΔR9 / mamD-GFP NBPC	$< 10^{-5}$	****	0.2007	3	Medium
	WT / mamD-GFP NBPC	ΔmamN / mamD-GFP NBPC	$< 10^{-5}$	****	0.4502	3	Large
	WT / mamD-GFP BPC	ΔMAI ΔMIS / mamD-GFP BPC	$< 10^{-5}$	****	0.8479	3	Large
	WT / mamD-GFP BPC	ΔmamO ΔR9 / mamD-GFP BPC	$< 10^{-5}$	****	0.8989	3	Large
	WT / mamD-GFP BPC	ΔmamN / mamD-GFP BPC	$< 10^{-5}$	****	0.1291	3	Small

Supplementary Table 4. Statistical tests. Fisher's exact test tests the hypothesis that two variables are unrelated and is accurate for sample sizes under 500 and in cases where at least one sample has a value of zero. Cramer's *V* is an effect size measurement that measures how strongly two categorical fields are associated.

Chapter 4

Conclusions and future directions for the localization of Mms6 and other magnetite shaping proteins in *Magnetospirillum magneticum* AMB-1

Carson Bickley

Department of Plant and Microbial Biology, University of California, Berkeley, CA, USA

Abstract

Magnetosome proteins were previously believed to mainly be sorted to newly created membranes in one step during compartment formation. This model has been updated over time to reflect discoveries of dynamic sorting behavior among magnetosome proteins. In this work, we have identified Mms6 as a protein capable of folding in the cytoplasm and then relocalizing to pre-existing magnetosomes in response to environmental conditions. We have also characterized MamD as another possible member of this class of conditionally localizing proteins. Using these results, we have constructed a model of how conditionally localizing proteins are sorted to the magnetosome. We now summarize our results and consider possible next steps that would further explore the complexity of magnetosome assembly.

Sorting of conditionally localizing proteins Mms6 and MamD

In this work, we identified magnetosome proteins involved in controlling a regulation system governing the dynamic positioning of magnetite nucleation and shaping proteins. Mms6 had previously been shown to localize to magnetosomes only when biomineralization was possible (8). However, the proteins controlling this behavior were unclear. We showed that MamO, MamM, and MamE are required for Mms6 localization. However, the mechanism of their function is still uncertain. Previous work indicates MamO and MamM activate MamE activity upon sensing iron (97,98). MamE then carries out its functions including the localization of various proteins and the proteolysis of multiple protein targets including Mms6 and MamD (10). In the model we described in this work, MamE may deactivate MamN to allow Mms6 and MamD localization. Further studies could perform biochemical analysis to investigate this possible interaction. Another mystery is the possible involvement of magnetosome membrane biogenesis proteins MamB, MamL, MamI, and MamQ. Some studies have linked proteins of this class, for example MamI, to magnetite nucleation (39). Due to their related function and localization to the magnetosome, these proteins could have a role in recruiting Mms6 or MamD. However, these proteins proved challenging to study with the methods used in this work. Deletion mutants of MamB, MamL, MamI, or MamQ lack magnetosome membranes, making defects in the localization of Mms6 or MamD undetectable (40). Analysis of these proteins using point mutations or other methods could help create a more complete picture of protein sorting in AMB-1.

The bifunctional N-terminal domain of Mms6

In our work, the Mms6 N-terminal domain was linked to conditional localization and cytoplasmic localization. As suggested previously, Mms6 localizes in the cytoplasm under NBPC (8). However, we found that Mms6 mutants lacking the N-terminal domain localized instead to the cell membrane under NBPC. In addition, these mutants localize to the cell membrane even in the absence of other MAI genes, suggesting no other magnetosome genes are needed for translocation. This result suggests that the Mms6 N-terminal domain somehow blocks Mms6

entry into the cellular membrane. It is unclear how the N-terminal domain performs this function. In addition, an Mms6 mutant lacking the N-terminal half of the N-terminal domain was shown to localize to magnetosome membranes under any biomineralization condition. It is uncertain how the N-terminal domain regulates Mms6 positioning. This result could indicate that MamN interacts with the N-terminal domain to prevent Mms6 magnetosome entry, but more work needs to be done to test this hypothesis. Although more research is needed to understand the mechanisms behind the impact of the Mms6 N-terminal domain on protein sorting, this domain could be useful in research or industrial applications. Several applications for biogenic magnetite have been the subject of recent study. Some of these include the use of magnetosomes as MRI contrast (78) or for hyperthermia treatment for cancerous tumors (79). Being able to control the localization of custom proteins could aid in fine tuning magnetite nanocrystals to better serve these applications. Further work could determine which sections of the Mms6 N-terminal domain are necessary for each of its putative functions, allowing greater understanding of the mechanisms involved and easier use in future applications.

Magnetosome Assembly

Based on our results, we have outlined a step in magnetosome assembly in which conditionally localizing proteins are sorted to the magnetosome to control membrane size and magnetite shape. MamN prevents the magnetosome localization of Mms6 and MamD through an unknown mechanism until deactivated upon a shift to biomineralization permissible conditions. Future work could determine how MamN controls the localization of these proteins and whether any other proteins that affect magnetite are also regulated by this system. In addition, further work could explore the dynamics of MamD. We have shown that Mms6 folds in the cytoplasm and then relocalizes to pre-formed magnetosomes, but whether MamD is also capable of this is unclear. It would also be useful to determine the effect of the conditional proteins on magnetosome assembly. Although both MamD and Mms6 have been linked to magnetite nucleation, neither is necessary for this process (42,67). In addition, the deletion of Mms6 and MamD individually in AMB-1 have been shown to have only minor effects on crystal size and shape (42,67). Creating a deletion mutant of both genes could help determine the cumulative effect of conditionally localizing proteins on biomineralization.

Magnetite nucleation

Despite great progress towards understanding the formation of magnetite in magnetosomes, the mechanisms of magnetite nucleation remain unclear. Previous work showed that MamD restricts magnetosome membrane growth to facilitate nucleation (10). Our work shows how this system might be controlled to efficiently restrict magnetosome membranes only when it is beneficial to biomineralization. Mms6 has also been linked to crystal nucleation (85). However, it is unclear whether Mms6 acts directly on magnetite to shape it throughout its development or if it assists the crystal only in nucleating properly to ensure the correct shape is formed. Our results may indicate that it is brought to magnetosomes to work in tandem with MamD on concentrating iron

into a small region. However, as neither Mms6 nor MamD are necessary for magnetite nucleation, there are likely many other factors working in tandem to complete this essential process. Further research is necessary to uncover the mechanisms of magnetite nucleation in AMB-1.

References

1 Grant, C. R., Wan, J., & Komeili, A. (2018). Organelle Formation in Bacteria and Archaea. *Annual review of cell and developmental biology*, *34*, 217–238. https://doi.org/10.1146/annurev-cellbio-100616-060908

2 Blakemore R. (1975). Magnetotactic bacteria. Science 190:377–379.

3 Okamura Y, Takeyama H, Matsunaga T. (2000). Two-dimensional analysis of proteins specific to the bacterial magnetic particle membrane from Magnetospirillum sp. AMB-1. Appl Biochem Biotechnol 8486:441–446.

4 Grünberg K, Wawer C, Tebo BM, Schüler D. (2001). A large gene cluster encoding several magnetosome proteins is conserved in different species of magnetotactic bacteria. Appl Environ Microbiol 67:4573–4582.

5 Grünberg K, Müller EC, Otto A, Reszka R, Linder D, Kube M, Reinhardt R, Schüler D. (2004). Biochemical and proteomic analysis of the magnetosome membrane in Magnetospirillum gryphiswaldense. Appl Environ Microbiol 70:1040–1050.

6 Lang C, Schüler D. (2008). Expression of green fluorescent protein fused to magnetosome proteins in microaerophilic magnetotactic bacteria. Appl Environ Microbiol 74:4944–4953.

7 Tanaka M., Okamura Y., Arakaki A., Tanaka T., Takeyama H., Matsunaga T. (2006). Origin of magnetosome membrane: proteomic analysis of magnetosome membrane and comparison with cytoplasmic membrane. Proteomics. 6:5234–5247. doi: 10.1002/pmic.200500887.

8 Arakaki A, Kikuchi D, Tanaka M, Yamagishi A, Yoda T, Matsunaga T. (2016). Comparative subcellular localization analysis of magnetosome proteins reveals a unique localization behavior of Mms6 protein onto magnetite crystals. J. Bacteriol. 198:2794–802

9 Arakaki A., Webb J., Matsunaga T. (2003) A novel protein tightly bound to bacterial magnetic particles in Magnetospirillum magneticum strain AMB-1. J. Biol. Chem. 278:8745–8750. doi: 10.1074/jbc.M211729200.

10 Wan, J., Browne, P. J., Hershey, D. M., Montabana, E., Iavarone, A. T., Downing, K. H., & Komeili, A. (2022). A protease-mediated switch regulates the growth of magnetosome organelles in Magnetospirillum magneticum. Proceedings of the National Academy of Sciences of the United States of America, 119(6), e2111745119. https://doi.org/10.1073/pnas.2111745119

11 Lins de Barros, H. G., Esquivel, D. M., & Farina, M. (1990). Magnetotaxis. *Science progress*, *74*(295 Pt 3), 347–359.

12 Spring, S., Amann, R., Ludwig, W., Schleifer, K. H., van Gemerden, H., & Petersen, N. (1993). Dominating role of an unusual magnetotactic bacterium in the microaerobic zone of a freshwater sediment. *Applied and environmental microbiology*, *59*(8), 2397–2403. https://doi.org/10.1128/aem.59.8.2397-2403.1993

13 Schüler, D., & Frankel, R. B. (1999). Bacterial magnetosomes: microbiology, biomineralization and biotechnological applications. *Applied microbiology and biotechnology*, *52*(4), 464–473. https://doi.org/10.1007/s002530051547

14 Blakemore, R. P., Maratea, D., & Wolfe, R. S. (1979). Isolation and pure culture of a freshwater magnetic spirillum in chemically defined medium. *Journal of bacteriology*, *140*(2), 720–729. https://doi.org/10.1128/jb.140.2.720-729.1979

15 Matsunaga T, Sakaguchi T, Tadokoro F. (1991). Magnetite formation by a magnetic bacterium capable of growing aerobically. Applied Microbiology and Biotechnology. 35:651–655.

16 Schleifer KH, Schüler D, Spring S, Weizenegger M, Amann R, Ludwig W, Kohler M. (1991). The genus Magnetospirillum Gen-Nov – Description of Magetospirillum-Gryphiswaldense Sp-Nov and transfer of Aquaspirillum-Magnetotacticum to Magnetospirillum-Magnetotacticum Comb-Nov. Systematic and Applied Microbiology. 14:379–385.

17 Gorby, Y. A., Beveridge, T. J., & Blakemore, R. P. (1988). Characterization of the bacterial magnetosome membrane. *Journal of bacteriology*, *170*(2), 834–841. https://doi.org/10.1128/jb.170.2.834-841.1988

18 Okuda, Y., Denda, K., & Fukumori, Y. (1996). Cloning and sequencing of a gene encoding a new member of the tetratricopeptide protein family from magnetosomes of Magnetospirillum magnetotacticum. *Gene*, *171*(1), 99–102. https://doi.org/10.1016/0378-1119(95)00008-9

19 Matsunaga, T., Nemoto, M., Arakari, A., & Tanaka, M. (2009). Proteomic analysis of irregular, bullet-shaped magnetosomes in the sulphate-reducing magnetotactic bacterium Desulfovibrio magneticus RS-1. *Proteomics*, *9*(12), 3341–3352. https://doi.org/10.1002/pmic.200800881

20 Matsunaga, T., Nakamura, C., Burgess, J. G., & Sode, K. (1992). Gene transfer in magnetic bacteria: transposon mutagenesis and cloning of genomic DNA fragments required for magnetosome synthesis. *Journal of bacteriology*, *174*(9), 2748–2753. https://doi.org/10.1128/jb.174.9.2748-2753.1992

21 Schultheiss, D., & Schüler, D. (2003). Development of a genetic system for Magnetospirillum gryphiswaldense. *Archives of microbiology*, *179*(2), 89–94. https://doi.org/10.1007/s00203-002-0498-z

22 Komeili, A., Vali, H., Beveridge, T. J., & Newman, D. K. (2004). Magnetosome vesicles are present before magnetite formation, and MamA is required for their activation. *Proceedings of the National Academy of Sciences of the United States of America*, *101*(11), 3839–3844. https://doi.org/10.1073/pnas.0400391101

23 Schultheiss, D., Kube, M., & Schüler, D. (2004). Inactivation of the flagellin gene flaA in Magnetospirillum gryphiswaldense results in nonmagnetotactic mutants lacking flagellar filaments. *Applied and environmental microbiology*, *70*(6), 3624–3631. https://doi.org/10.1128/AEM.70.6.3624-3631.2004

24 Matsunaga, T., Okamura, Y., Fukuda, Y., Wahyudi, A. T., Murase, Y., & Takeyama, H. (2005). Complete genome sequence of the facultative anaerobic magnetotactic bacterium Magnetospirillum sp. strain AMB-1. *DNA research : an international journal for rapid publication of reports on genes and genomes*, *12*(3), 157–166. https://doi.org/10.1093/dnares/dsi002

25 Richter, M., Kube, M., Bazylinski, D. A., Lombardot, T., Glöckner, F. O., Reinhardt, R., & Schüler, D. (2007). Comparative genome analysis of four magnetotactic bacteria reveals a complex set of group-specific genes implicated in magnetosome biomineralization and function. *Journal of bacteriology*, *189*(13), 4899–4910. https://doi.org/10.1128/JB.00119-07

26 Schübbe, S., Kube, M., Scheffel, A., Wawer, C., Heyen, U., Meyerdierks, A., Madkour, M. H., Mayer, F., Reinhardt, R., & Schüler, D. (2003). Characterization of a spontaneous nonmagnetic mutant of Magnetospirillum gryphiswaldense reveals a large deletion comprising a putative magnetosome island. *Journal of bacteriology*, *185*(19), 5779–5790. https://doi.org/10.1128/JB.185.19.5779-5790.2003

27 Ullrich, S., Kube, M., Schübbe, S., Reinhardt, R., & Schüler, D. (2005). A hypervariable 130-kilobase genomic region of Magnetospirillum gryphiswaldense comprises a magnetosome island which undergoes frequent rearrangements during stationary growth. *Journal of bacteriology*, *187*(21), 7176–7184. https://doi.org/10.1128/JB.187.21.7176-7184.2005

28 Fukuda, Y., Okamura, Y., Takeyama, H., & Matsunaga, T. (2006). Dynamic analysis of a genomic island in Magnetospirillum sp. strain AMB-1 reveals how magnetosome synthesis developed. *FEBS letters*, *580*(3), 801–812. https://doi.org/10.1016/j.febslet.2006.01.003

29 Schübbe, S., Würdemann, C., Peplies, J., Heyen, U., Wawer, C., Glöckner, F. O., & Schüler, D. (2006). Transcriptional organization and regulation of magnetosome operons in Magnetospirillum gryphiswaldense. *Applied and environmental microbiology*, *72*(9), 5757–5765. https://doi.org/10.1128/AEM.00201-06

30 Lefèvre, C. T., Trubitsyn, D., Abreu, F., Kolinko, S., Jogler, C., de Almeida, L. G., de Vasconcelos, A. T., Kube, M., Reinhardt, R., Lins, U., Pignol, D., Schüler, D., Bazylinski, D. A., & Ginet, N. (2013). Comparative genomic analysis of magnetotactic bacteria from the Deltaproteobacteria provides new insights into magnetite and greigite magnetosome genes required for magnetotaxis. *Environmental microbiology*, *15*(10), 2712–2735. https://doi.org/10.1111/1462-2920.12128

31 Zhang, W., Wang, Y., Liu, L., Pan, Y., & Lin, W. (2021). Identification and Genomic Characterization of Two Previously Unknown Magnetotactic *Nitrospirae*. *Frontiers in microbiology*, *12*, 690052. https://doi.org/10.3389/fmicb.2021.690052

32 Nakazawa, H., Arakaki, A., Narita-Yamada, S., Yashiro, I., Jinno, K., Aoki, N., Tsuruyama, A., Okamura, Y., Tanikawa, S., Fujita, N., Takeyama, H., & Matsunaga, T. (2009). Whole genome sequence of Desulfovibrio magneticus strain RS-1 revealed common gene clusters in magnetotactic bacteria. *Genome research*, *19*(10), 1801–1808. https://doi.org/10.1101/gr.088906.108

33 Jogler, C., Wanner, G., Kolinko, S., Niebler, M., Amann, R., Petersen, N., Kube, M., Reinhardt, R., & Schüler, D. (2011). Conservation of proteobacterial magnetosome genes and structures in an uncultivated member of the deep-branching Nitrospira phylum. *Proceedings of the National Academy of Sciences of the United States of America*, *108*(3), 1134–1139. https://doi.org/10.1073/pnas.1012694108

34 Monteil, C. L., & Lefevre, C. T. (2020). Magnetoreception in Microorganisms. *Trends in microbiology*, *28*(4), 266–275. https://doi.org/10.1016/j.tim.2019.10.012

35 Schübbe, S., Williams, T. J., Xie, G., Kiss, H. E., Brettin, T. S., Martinez, D., Ross, C. A., Schüler, D., Cox, B. L., Nealson, K. H., & Bazylinski, D. A. (2009). Complete genome sequence of the chemolithoautotrophic marine magnetotactic coccus strain MC-1. *Applied and environmental microbiology*, *75*(14), 4835–4852. https://doi.org/10.1128/AEM.02874-08

36 Ji, B., Zhang, S. D., Arnoux, P., Rouy, Z., Alberto, F., Philippe, N., Murat, D., Zhang, W. J., Rioux, J. B., Ginet, N., Sabaty, M., Mangenot, S., Pradel, N., Tian, J., Yang, J., Zhang, L., Zhang, W., Pan, H., Henrissat, B., Coutinho, P. M., … Wu, L. F. (2014). Comparative genomic analysis provides insights into the evolution and niche adaptation of marine Magnetospira sp. QH-2 strain. *Environmental microbiology*, *16*(2), 525–544. https://doi.org/10.1111/1462-2920.12180

37 Lefèvre, C. T., Trubitsyn, D., Abreu, F., Kolinko, S., de Almeida, L. G., de Vasconcelos, A. T., Lins, U., Schüler, D., Ginet, N., Pignol, D., & Bazylinski, D. A. (2013). Monophyletic origin of magnetotaxis and the first magnetosomes. *Environmental microbiology*, *15*(8), 2267–2274. https://doi.org/10.1111/1462-2920.12097

38 Kolinko, I., Lohße, A., Borg, S., Raschdorf, O., Jogler, C., Tu, Q., Pósfai, M., Tompa, E., Plitzko, J. M., Brachmann, A., Wanner, G., Müller, R., Zhang, Y., & Schüler, D. (2014). Biosynthesis of magnetic nanostructures in a foreign organism by transfer of bacterial magnetosome gene clusters. *Nature nanotechnology*, *9*(3), 193–197. https://doi.org/10.1038/nnano.2014.13

39 Scheffel, A., Gärdes, A., Grünberg, K., Wanner, G., & Schüler, D. (2008). The major magnetosome proteins MamGFDC are not essential for magnetite biomineralization in Magnetospirillum gryphiswaldense but regulate the size of magnetosome crystals. *Journal of bacteriology*, *190*(1), 377–386. https://doi.org/10.1128/JB.01371-07

40 Murat, D., Quinlan, A., Vali, H., & Komeili, A. (2010). Comprehensive genetic dissection of the magnetosome gene island reveals the step-wise assembly of a prokaryotic organelle. *Proceedings of the National Academy of Sciences of the United States of America*, *107*(12), 5593–5598. https://doi.org/10.1073/pnas.0914439107

41 Lohße, A., Ullrich, S., Katzmann, E., Borg, S., Wanner, G., Richter, M., Voigt, B., Schweder, T., & Schüler, D. (2011). Functional analysis of the magnetosome island in Magnetospirillum gryphiswaldense: the mamAB operon is sufficient for magnetite biomineralization. *PloS one*, *6*(10), e25561. https://doi.org/10.1371/journal.pone.0025561

42 Lohße, A., Borg, S., Raschdorf, O., Kolinko, I., Tompa, E., Pósfai, M., Faivre, D., Baumgartner, J., & Schüler, D. (2014). Genetic dissection of the mamAB and mms6 operons reveals a gene set essential for magnetosome biogenesis in Magnetospirillum gryphiswaldense. *Journal of bacteriology*, *196*(14), 2658–2669. https://doi.org/10.1128/JB.01716-14

43 Raschdorf, O., Forstner, Y., Kolinko, I., Uebe, R., Plitzko, J. M., & Schüler, D. (2016). Genetic and Ultrastructural Analysis Reveals the Key Players and Initial Steps of Bacterial Magnetosome Membrane Biogenesis. *PLoS genetics*, *12*(6), e1006101. https://doi.org/10.1371/journal.pgen.1006101

44 Matsunaga, T., & Okamura, Y. (2003). Genes and proteins involved in bacterial magnetic particle formation. *Trends in microbiology*, *11*(11), 536–541. https://doi.org/10.1016/j.tim.2003.09.008

45 Uebe, R., Junge, K., Henn, V., Poxleitner, G., Katzmann, E., Plitzko, J. M., Zarivach, R., Kasama, T., Wanner, G., Pósfai, M., Böttger, L., Matzanke, B., & Schüler, D. (2011). The cation diffusion facilitator proteins MamB and MamM of Magnetospirillum gryphiswaldense have distinct and complex functions, and are involved in magnetite biomineralization and magnetosome membrane assembly. *Molecular microbiology*, *82*(4), 818–835. https://doi.org/10.1111/j.1365-2958.2011.07863.x

46 Uebe, R., & Schüler, D. (2016). Magnetosome biogenesis in magnetotactic bacteria. *Nature reviews. Microbiology*, *14*(10), 621–637. https://doi.org/10.1038/nrmicro.2016.99

47 Uebe, R., Keren-Khadmy, N., Zeytuni, N., Katzmann, E., Navon, Y., Davidov, G., Bitton, R., Plitzko, J. M., Schüler, D., & Zarivach, R. (2018). The dual role of MamB in magnetosome membrane assembly and magnetite biomineralization. *Molecular microbiology*, *107*(4), 542–557. https://doi.org/10.1111/mmi.13899

48 Scheffel, A., Gruska, M., Faivre, D., Linaroudis, A., Plitzko, J. M., & Schüler, D. (2006). An acidic protein aligns magnetosomes along a filamentous structure in magnetotactic bacteria. *Nature*, *440*(7080), 110–114. https://doi.org/10.1038/nature04382

49 Komeili, A., Li, Z., Newman, D. K., & Jensen, G. J. (2006). Magnetosomes are cell membrane invaginations organized by the actin-like protein MamK. *Science (New York, N.Y.)*, *311*(5758), 242–245. https://doi.org/10.1126/science.1123231

50 Draper, O., Byrne, M. E., Li, Z., Keyhani, S., Barrozo, J. C., Jensen, G., & Komeili, A. (2011). MamK, a bacterial actin, forms dynamic filaments in vivo that are regulated by the acidic proteins MamJ and LimJ. *Molecular microbiology*, *82*(2), 342–354. https://doi.org/10.1111/j.1365-2958.2011.07815.x

51 Pfeiffer, D., Toro-Nahuelpan, M., Awal, R. P., Müller, F. D., Bramkamp, M., Plitzko, J. M., & Schüler, D. (2020). A bacterial cytolinker couples positioning of magnetic organelles to cell shape control. *Proceedings of the National Academy of Sciences of the United States of America*, *117*(50), 32086–32097. https://doi.org/10.1073/pnas.2014659117

52 Toro-Nahuelpan, M., Giacomelli, G., Raschdorf, O., Borg, S., Plitzko, J. M., Bramkamp, M., Schüler, D., & Müller, F. D. (2019). MamY is a membrane-bound protein that aligns magnetosomes and the motility axis of helical magnetotactic bacteria. *Nature microbiology*, *4*(11), 1978–1989. https://doi.org/10.1038/s41564-019-0512-8

53 Wan J, Monteil CL, Taoka A, Ernie G, Park K, Amor M, Taylor-Cornejo E, Lefevre CT, Komeili A. (2022). McaA and McaB control the dynamic positioning of a bacterial magnetic organelle. Nat Commun. 13(1):5652. doi: 10.1038/s41467-022-32914-9. PMID: 36163114; PMCID: PMC9512821.

54 Schüler, D. (2008). Genetics and cell biology of magnetosome formation in magnetotactic bacteria. FEMS Microbiology Reviews, 32(4), 654–672. doi:10.1111/j.1574-6976.2008.0011

55 Müller, F. D., Schüler, D., & Pfeiffer, D. (2020). A Compass To Boost Navigation: Cell Biology of Bacterial Magnetotaxis. Journal of bacteriology, 202(21), e00398-20. https://doi.org/10.1128/JB.00398-20

56 Zeytuni, N., Ozyamak, E., Ben-Harush, K., Davidov, G., Levin, M., Gat, Y., Moyal, T., Brik, A., Komeili, A., & Zarivach, R. (2011). Self-recognition mechanism of MamA, a magnetosome-associated TPR-containing protein, promotes complex assembly. *Proceedings of the National Academy of Sciences of the United States of America*, *108*(33), E480–E487. https://doi.org/10.1073/pnas.1103367108

57 Allan, R. K., & Ratajczak, T. (2011). Versatile TPR domains accommodate different modes of target protein recognition and function. *Cell stress & chaperones*, *16*(4), 353–367. https://doi.org/10.1007/s12192-010-0248-0

58 Taoka, A., Asada, R., Sasaki, H., Anzawa, K., Wu, L. F., & Fukumori, Y. (2006). Spatial localizations of Mam22 and Mam12 in the magnetosomes of Magnetospirillum magnetotacticum. *Journal of bacteriology*, *188*(11), 3805–3812. https://doi.org/10.1128/JB.00020-06

59 Yamamoto, D., Taoka, A., Uchihashi, T., Sasaki, H., Watanabe, H., Ando, T., & Fukumori, Y. (2010). Visualization and structural analysis of the bacterial magnetic organelle magnetosome using atomic force microscopy. *Proceedings of the National Academy of Sciences of the United States of America*, *107*(20), 9382–9387. https://doi.org/10.1073/pnas.1001870107

60 Raschdorf, O., Müller, F. D., Pósfai, M., Plitzko, J. M., & Schüler, D. (2013). The magnetosome proteins MamX, MamZ and MamH are involved in redox control of magnetite biomineralization in Magnetospirillum gryphiswaldense. *Molecular microbiology*, *89*(5), 872–886. https://doi.org/10.1111/mmi.12317

61 Li, Y., Katzmann, E., Borg, S., & Schüler, D. (2012). The periplasmic nitrate reductase nap is required for anaerobic growth and involved in redox control of magnetite biomineralization in Magnetospirillum gryphiswaldense. *Journal of bacteriology*, *194*(18), 4847–4856. https://doi.org/10.1128/JB.00903-12

62 Ding, Y., Li, J., Liu, J., Yang, J., Jiang, W., Tian, J., Li, Y., Pan, Y., & Li, J. (2010). Deletion of the ftsZ-like gene results in the production of superparamagnetic magnetite magnetosomes in Magnetospirillum gryphiswaldense. *Journal of bacteriology*, *192*(4), 1097–1105. https://doi.org/10.1128/JB.01292-09

63 Müller, F. D., Raschdorf, O., Nudelman, H., Messerer, M., Katzmann, E., Plitzko, J. M., Zarivach, R., & Schüler, D. (2014). The FtsZ-like protein FtsZm of Magnetospirillum gryphiswaldense likely interacts with its generic homolog and is required for biomineralization under nitrate deprivation. *Journal of bacteriology*, *196*(3), 650–659. https://doi.org/10.1128/JB.00804-13

64 Taoka, A., Eguchi, Y., Mise, S., Oestreicher, Z., Uno, F., & Fukumori, Y. (2014). A magnetosome-associated cytochrome MamP is critical for magnetite crystal growth during the exponential growth phase. *FEMS microbiology letters*, *358*(1), 21–29. https://doi.org/10.1111/1574-6968.12541

65 Siponen, M. I., Adryanczyk, G., Ginet, N., Arnoux, P., & Pignol, D. (2012). Magnetochrome: a c-type cytochrome domain specific to magnetotatic bacteria. *Biochemical Society transactions*, *40*(6), 1319–1323. https://doi.org/10.1042/BST20120104

66 Jones, S. R., Wilson, T. D., Brown, M. E., Rahn-Lee, L., Yu, Y., Fredriksen, L. L., Ozyamak, E., Komeili, A., & Chang, M. C. (2015). Genetic and biochemical investigations of the role of MamP in redox control of iron biomineralization in Magnetospirillum magneticum. *Proceedings of the National Academy of Sciences of the United States of America*, *112*(13), 3904–3909. https://doi.org/10.1073/pnas.1417614112

67 Murat, D., Falahati, V., Bertinetti, L., Csencsits, R., Körnig, A., Downing, K., Faivre, D., & Komeili, A. (2012). The magnetosome membrane protein, MmsF, is a major regulator of magnetite biomineralization in Magnetospirillum magneticum AMB-1. *Molecular microbiology*, *85*(4), 684–699. https://doi.org/10.1111/j.1365-2958.2012.08132.x

68 Tanaka M., Mazuyama E., Arakaki A., Matsunaga T. (2011). MMS6 protein regulates crystal morphology during nano-sized magnetite biomineralization *in vivo*. J. Biol. Chem. 286:6386–6392. doi: 10.1074/jbc.M110.183434.

69 Arakaki, A., Masuda, F., Amemiya, Y., Tanaka, T., & Matsunaga, T. (2010). Control of the morphology and size of magnetite particles with peptides mimicking the Mms6 protein from magnetotactic bacteria. Journal of colloid and interface science, 343(1), 65–70. https://doi.org/10.1016/j.jcis.2009.11.043

70 Wang L., Prozorov T., Palo P.E., Liu X., Vaknin D., Prozorov R., Mallapragada S., Nilsen-Hamilton M. (2012). Self-Assembly and Biphasic Iron-Binding Characteristics of Mms6, A Bacterial Protein That Promotes the Formation of Superparamagnetic Magnetite Nanoparticles of Uniform Size and Shape. Biomacromolecules. 13:98–105. doi: 10.1021/bm201278u.

71 Feng, S., Wang, L., Palo, P., Liu, X., Mallapragada, S. K., & Nilsen-Hamilton, M. (2013). Integrated self-assembly of the Mms6 magnetosome protein to form an iron-responsive structure.

International journal of molecular sciences, 14(7), 14594–14606. https://doi.org/10.3390/ijms140714594

72 Mann S, Sparks NHC, Frankel RB, Bazylinski DA, Jannasch HW. (1990). Biomineralization of ferrimagnetic greigite (Fe3S4) and iron pyrite (FeS2) in a magnetotactic bacterium. Nature 343:258–261.

73 Frankel RB, Blakemore RP, Wolfe RS. (1979). Magnetite in freshwater magnetotactic bacteria. Science 203:1355–1356.

74 Balkwill DL, Maratea D, Blakemore RP. (1980). Ultrastructure of a magnetotactic spirillum. J Bacteriol 141:1399–1408.

75 Nudelman, H., Lee, Y. Z., Hung, Y. L., Kolusheva, S., Upcher, A., Chen, Y. C., Chen, J. Y., Sue, S. C., & Zarivach, R. (2018). Understanding the Biomineralization Role of Magnetite-Interacting Components (MICs) From Magnetotactic Bacteria. *Frontiers in microbiology*, *9*, 2480. https://doi.org/10.3389/fmicb.2018.02480

76 Yamagishi, A., Narumiya, K., Tanaka, M., Matsunaga, T., & Arakaki, A. (2016). Core Amino Acid Residues in the Morphology-Regulating Protein, Mms6, for Intracellular Magnetite Biomineralization. Scientific reports, 6, 35670. https://doi.org/10.1038/srep35670

77 Pankhurst Q.A., Connolly J., Jones S.K., Dobson J. (2003). Applications of magnetic nanoparticles in biomedicine. J. Phys. D: Appl. Phys. 36:R167–R181. doi: 10.1088/0022-3727/36/13/201.

78 Reddy L.H., Arias J.L., Nicolas J., Couvreur P. (2012). Magnetic nanoparticles: design and characterization, toxicity and biocompatibility, pharmaceutical and biomedical applications. Chem. Rev. 112:5818–5878. doi: 10.1021/cr300068p.

79 Stephen Z.R., Kievit F.M., Zhang M. (2011). Magnetite nanoparticles for medical MR imaging. Mater. Today. 14:330–338. doi: 10.1016/S1369-7021(11)70163-8.

80 Grimm, J. B., English, B. P., Chen, J., Slaughter, J. P., Zhang, Z., Revyakin, A., Patel, R., Macklin, J. J., Normanno, D., Singer, R. H., Lionnet, T., & Lavis, L. D. (2015). A general method to improve fluorophores for live-cell and single-molecule microscopy. *Nature methods*, *12*(3), 244–250. https://doi.org/10.1038/nmeth.3256

81 Rioux, J. B., Philippe, N., Pereira, S., Pignol, D., Wu, L. F., & Ginet, N. (2010). A second actin-like MamK protein in Magnetospirillum magneticum AMB-1 encoded outside the genomic magnetosome island. PloS one, 5(2), e9151. https://doi.org/10.1371/journal.pone.0009151

82 Nguyen, H. V., Suzuki, E., Oestreicher, Z., Minamide, H., Endoh, H., Fukumori, Y., & Taoka, A. (2016). A protein-protein interaction in magnetosomes: TPR protein MamA interacts with an Mms6 protein. Biochemistry and biophysics reports, 7, 39–44. https://doi.org/10.1016/j.bbrep.2016.05.010

83 Zhou C.-Z., Confalonieri F., Jacquet M., Perasso R., Li Z.-G., Janin J. (2001). Silk fibroin: structural implications of a remarkable amino acid sequence. Proteins. 44:119–122. doi: 10.1002/prot.1078.

84 Rawlings, A. E., Bramble, J. P., Hounslow, A. M., Williamson, M. P., Monnington, A. E., Cooke, D. J., & Staniland, S. S. (2016). Ferrous Iron Binding Key to Mms6 Magnetite Biomineralisation: A Mechanistic Study to Understand Magnetite Formation Using pH Titration and NMR Spectroscopy. Chemistry (Weinheim an der Bergstrasse, Germany), 22(23), 7885–7894. https://doi.org/10.1002/chem.201600322

85 Kashyap S., Woehl T.J., Liu X., Mallapragada S.K., Prozorov T. (2014). Nucleation of iron oxide nanoparticles mediated by Mms6 protein *in situ*. ACS Nano. 8:9097–9106. doi: 10.1021/nn502551y.

86 Bird, S. M., Rawlings, A. E., Galloway, J. M., & Staniland, S. S. (2016). Using a biomimetic membrane surface experiment to investigate the activity of the magnetite biomineralisation protein Mms6. RSC advances, 6(9), 7356–7363. https://doi.org/10.1039/c5ra16469a

87 Arai, K., Murata, S., Wang, T., Yoshimura, W., Oda-Tokuhisa, M., Matsunaga, T., Kisailus, D., & Arakaki, A. (2022). Adsorption of Biomineralization Protein Mms6 on Magnetite (Fe_3O_4) Nanoparticles. International journal of molecular sciences, 23(10), 5554. https://doi.org/10.3390/ijms23105554

88 Ribbeck, K., & Görlich, D. (2002). The permeability barrier of nuclear pore complexes appears to operate via hydrophobic exclusion. *The EMBO journal*, *21*(11), 2664–2671. https://doi.org/10.1093/emboj/21.11.2664

89 Elbaum-Garfinkle S. (2019). Matter over mind: Liquid phase separation and neurodegeneration. *The Journal of biological chemistry*, *294*(18), 7160–7168. https://doi.org/10.1074/jbc.REV118.001188

90 Cornejo, E., Subramanian, P., Li, Z., Jensen, G. J., & Komeili, A. (2016). Dynamic Remodeling of the Magnetosome Membrane Is Triggered by the Initiation of Biomineralization. mBio, 7(1), e01898-15. https://doi.org/10.1128/mBio.01898-15

91 Bazylinski D.A., Williams T.J., Lefevre C.T., Trubitsyn D., Fang J., Beveridge T.J., Moskowitz B.M., Ward B., Schubbe S., Dubbels B.L., Simpson B. (2013). Magnetovibrio blakemorei gen. nov., sp. nov., a magnetotactic bacterium (Alphaproteobacteria: Rhodospirillaceae) isolated from a salt marsh. Int. J. Syst. Evol. Microbiol. 63:1824–1833. doi: 10.1099/ijs.0.044453-0.

92 Feilmeier, B. J., Iseminger, G., Schroeder, D., Webber, H., & Phillips, G. J. (2000). Green fluorescent protein functions as a reporter for protein localization in Escherichia coli. *Journal of bacteriology*, *182*(14), 4068–4076. https://doi.org/10.1128/JB.182.14.4068-4076.2000

93 Pei, D., & Dalbey, R. E. (2022). Membrane translocation of folded proteins. *The Journal of biological chemistry*, *298*(7), 102107. https://doi.org/10.1016/j.jbc.2022.102107

94 A. Quinlan, D. Murat, H. Vali, A. Komeili. (2011). The HtrA/DegP family protease MamE is a bifunctional protein with roles in magnetosome protein localization and magnetite biomineralization. Molecular microbiology 80, 1075-1087.

95 Bazylinski, D., Frankel, R. Magnetosome formation in prokaryotes. (2004). *Nat Rev Microbiol* **2**, 217–230 https://doi.org/10.1038/nrmicro842

96 Yamagishi, A., Tanaka, M., Lenders, J. J., Thiesbrummel, J., Sommerdijk, N. A., Matsunaga, T., & Arakaki, A. (2016). Control of magnetite nanocrystal morphology in magnetotactic bacteria by regulation of mms7 gene expression. *Scientific reports*, *6*, 29785. https://doi.org/10.1038/srep29785

97 Hershey, D. M., Browne, P. J., Iavarone, A. T., Teyra, J., Lee, E. H., Sidhu, S. S., & Komeili, A. (2016). Magnetite Biomineralization in Magnetospirillum magneticum Is Regulated by a Switch-like Behavior in the HtrA Protease MamE. *The Journal of biological chemistry*, *291*(34), 17941–17952. https://doi.org/10.1074/jbc.M116.731000

98 Hershey, D. M., Ren, X., Melnyk, R. A., Browne, P. J., Ozyamak, E., Jones, S. R., Chang, M. C., Hurley, J. H., & Komeili, A. (2016). MamO Is a Repurposed Serine Protease that Promotes Magnetite Biomineralization through Direct Transition Metal Binding in Magnetotactic Bacteria. *PLoS biology*, *14*(3), e1002402. https://doi.org/10.1371/journal.pbio.1002402